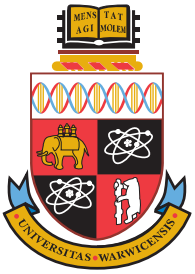

The Self-Assembly of Diphenylalanine Fibres

by

Caroline Beryl Montgomery

Thesis

Submitted to the University of Warwick

for the degree of

Doctor of Philosophy

Supervisors: Dr Giovanni Costantini, Professor Alison Rodger, Professor P. Mark Rodger and Dr Matthew Hicks

MOAC Doctoral Training Centre

November 2015

THE UNIVERSITY OF WARWICK

Contents

List of Figures

Acknowledgements

First and foremost I would like to thank my supervisors, Giovanni Costantini, Alison Rodger, Mark Rodger and Matt Hicks for their endless guidance, support, enthusiasm and patience throughout this project. I would also like to thank Alison in her capacity as MOAC director for allowing me to join the MOAC doctoral training centre and undertake the following project.

I am grateful to Nikola Chmel for teaching me how to use instruments in the lab and for continuous advice and help over the past three years. I would like to thank the other members of the biophysical chemistry group at Warwick: Shirin Jamshidi, Kasra Razmkhah, Vince Hall, Claire Dow, Stephen Norton, Alan Wemyss, Joe Jones, Daniela Lobo, Meropi Sklepari, Vidya Muthukumar, Glen Dorrington and Praveen Amarasinghe, not only for their help in the lab but also for their friendship.

I express my thanks to the members of the Costantini group for their ideas and help, in particular Ben Moreton for helping me to get started with this project as well as Nataliya Kalashnyk, Thomas White, Ada Della Pia and Jonathan Blohm.

I appreciate all of the MOAC community for providing a supportive and friendly environment over the past four years. In particular I thank Chris Smith for allowing me access to and help with the optical microscope. I am grateful to the members of my advisory committee, Ann Dixon, David Quigley and Matt Gibson who provided a new perspective as well as encouragement. I acknowledge the EPSRC for funding my project. I would like to thank Alex Colburn for the custom electronics which made the linear dichroism development possible.

Finally I thank my family and friends for encouraging me to undertake further education and for supporting me throughout: Grandpa, Grandma, Grandad, Gran, Dad, Mum, Nicky, Sarah and Haroon.

Declaration

The following work is entirely my own and was carried out under the supervision of Dr G. Costantini, Professor A. Rodger, Professor P. M. Rodger and Dr M. Hicks. I confirm that it has not been submitted for a degree at another institution. Some of this work is in preparation for future publication.

Abstract

The diphenylalanine (FF) dipeptide is the core recognition motif of the Alzheimer's amyloid beta (Aβ) polypeptide, as well as being important in other amyloidogenic proteins. The Aβ polypeptide self assembles to form fibrils and these fibrils are found in the brains of patients with Alzheimer's disease. FF itself is also known to self-assemble to form fibres and there has been much interest in the FF motif since Reches and Gazit made this observation. The structures it forms are biocompatible and have a high aspect ratio. Under different conditions of humidity and concentration it can form various morphologies such as nanovesicles and ribbons. Despite the great interest in this area, the self-assembly mechanism of these fibres is not known. The motivation throughout this work has been to understand the assembly of the elongated FF fibres in order to be able to control it for the variety of applications that have been suggested.

Several experimental and theoretical techniques were used to this end. Molecular and metadynamics simulations were employed to investigate the early stages of the fibres assembly. Optical spectrocopy was used to investigate their assembly kinetics and mechanism *in situ*. New linear dichroism (LD) methods were developed in order to study the FF fibres which grow into large rigid structures. A new electronic LD sequencer was created which made it possible to automate kinetics measurements over long periods of time, and a new capillary was designed and built which could be cleaned more thoroughly than the previous models. These experiments showed that FF fibres assemble by nucleation driven assembly, with secondary nucleation taking place. They also showed that 40 °C is an important temperature in the onset of fibre formation. Electron and optical microscopy were used to quantify the heterogeneity of the fibres and to observe their growth in real time. It was found that the fibres were more heterogenous than had previously been reported.

The results of these experiments elucidated new information about the characteristics and the self-assembly of FF fibres, as well as developed techniques in order to probe them, and similar biological fibres, further.

List of Abbreviations

AFM	Atomic force microscopy
CD	Circular dichroism
CDF	Cumulative distribution function
CRT	Cathode ray tube
CV	Collective variable
DLS	Dynamic light scattering
DNA	Deoxyribonucleic acid
EM	Electromagnetic
FEGSEM	Field emission gun scanning electron microscope
FF	Diphenylalanine
FTIR	Fourier transform infrafred spectroscopy
GTP	Guanosine triphosphate
HFIP	Hexafluoroisoproranol
LD	Linear dichoism
MC	Monte Carlo
MD	Molecular dynamics
MeOH	Methanol
mRNA	Messenger ribonucleic acid
NA	Numerical aperture
NAMD	Nanoscale molecular dynamics
NPT	Number, pressure and temperature
NVT	Number, volume and temperature
PFM	Piezo-response force microscopy

PME	Particle mesh Ewald
PrP	Mammalian prion protein
RALS	Right angle light scattering
RMSD	Root mean squared deviation
RMSE	Root mean square error
SEM	Scanning electron microscopy
SPM	Scanning probe microscopy
STEM	Scanning tunneling electron microscopy
STM	Scanning tunneling microscopy
TEM	Transmission electron microscopy
TFA	Trifluoroacetic acid
TFE	Trifluoroethanol
UV	Ultraviolet

Standard Amino Acid Abbreviations

The standard amino acid abbreviations are used in the following work.

Amino Acid	Three Letter Abbreviation	One letter Abbreviation
Alanine	Ala	A
Arginine	Arg	R
Asparagine	Asn	N
Aspartic Acid	Asp	D
Cysteine	Cys	C
Glutamine	Gln	Q
Glutamic Acid	Glu	E
Glycine	Gly	G
Histidine	His	H
Isoleucine	Ile	I
Leucine	Leu	L
Lysine	Lys	K
Methionine	Met	M
Phenylalanine	Phe	F
Proline	Pro	P
Serine	Ser	S
Threonine	Thr	T
Trytophan	Trp	W
Tyrosine	Tyr	Y
Valine	Val	V

Chapter 1

Introduction

1. Introduction

Peptides have found a variety of applications in biotechnology, medicine, and nanoscience.[1,2] They are simple, biocompatible and functional molecules which can readily self-assemble. In order to better understand, and ultimately control the self-assembly, this work investigates the simplest model system possible, a dipeptide.

Diphenylalanine (FF) is a dipeptide which is known to self-assemble into fibres with many attractive properties, from biocompatibility to mechanical stability and piezoelectricity.[3,4] This has lead to a plethora of suggested applications in the literature. For example, they have been used to cast metal nanowires,[5] as a supporting matrix in biosensors [6] and as a dry-etching mask for the fabrication of nanostructures.[7] FF is also the core recognition motif of the Alzheimer's amyloid- β polypeptide, so there is consequently a lot of interest surrounding its self-assembly mechanism. Once the assembly of such a small system is understood, it may be applied as a starting point to understand how and why other more complicated fibres form.

Despite the interest in FF fibres, their assembly mechanism has yet to be found. Molecular dynamics simulations have so far failed to recreate the assembly with an adequate number of peptides to create a fibre.[8,9] Until now it has also proved impossible to create a coarse-grained model that mimics the peptides behaviour,[8] and it is impractical to simulate a large number of peptides using molecular dynamics for a time period which is long enough to witness self-assembly. There are also challenges with probing the fibres experimentally as they lack the symmetry of other systems, such as spherical nanomaterials. Therefore standard characterisation techniques such as dynamic light scattering (DLS) cannot be used as easily.

There is an abundance of work on the characterization and applications of FF fibres, however, there is very little on its assembly mechanism. The fibres have

been found to have varying levels of heterogeneity in similar experiments, and this is a problem if the fibres are to be used for the variety of suggested applications. The ideal way to produce homogeneous fibres is to first understand the way they assemble. Once this is known, it may be possible to tune the fibres for the desired purpose. Therefore, in this work a variety of techniques were used and developed, including linear dichroism (LD), in order to contribute to the understanding of the self-assembly of FF fibres. This chapter outlines the previous work on self-assembling peptides in general and FF in particular, the techniques used for fibre characterization, and ends with a summary of the investigation presented in this thesis. First, we start by considering the diseases associated with amyloidogenic proteins and their relationship to peptide self-assembly, as they represent one of the main motivations behind this whole field of research.

1.1 Amyloid Diseases

Amyloid fibrils are elongated insoluble structures made from proteins or peptides that have misfolded and are rich in β-sheets. They result from the self-assembly of these misfolded molecules and play a major role in several diseases and, as such, are of great interest in medicine. However, in many cases, the path from protein misfolding to amyloid formation and toxicity is not well understood. Several of these cases are discussed in the following section.

One example of a protein that is related to amyloid disease is α-synuclein which is considered to be an unstructured protein that typically resists aggregation.[10] In some individuals there is a mutation in the gene which encodes it, resulting in an abnormal form of the protein.[11] In this case, α-synuclein aggregates via self-assembly to create insoluble fibrils, creating an amyloid deposit. These fibrils are found in patients with a class of neurodegenerative conditions called synucleinopathies, which includes Parkinson's disease and dementia with Lewy bodies. The α-synuclein aggregates are thought to be neurotoxic and therefore cause disruption to cellular homeostasis and neuronal death.[12]

A characteristic feature of type two diabetes is the formation of amyloid deposits in the pancreas.[13] These deposits come from a peptide called amylin. β-cells make up a large proportion of the cells in the islets and are responsible for the production of insulin. It is thought that the amylin fibrils are toxic to β-cells and this loss of β-cells leads to a decrease in insulin and therefore an increase in glucose and lipid levels.[14]

Prion proteins are often linked to disease as they are a type of protein that can take on multiple conformations, and pass on that conformation to other prions. Typically, prions have a cross-β amyloid structure and form amyloid plaques which cause cell damage and death. The mammalian prion protein (PrP) is linked to several diseases which are known as transmissible spongiform encephalopathy. Several yeast prion proteins have been discovered and one of them, Sup35, has a fragment that can create fibrils which is used as a model for Sup35.[15] Recently, Langkilde *et al*. have used X-ray diffraction, scattering and electron microscopy to investigate the assembly of this fragment. They were able to find that fibrils grow with no intermediate species. This work highlights the necessity for multiple techniques in the analysis of amyloid fibrils.[15]

Another disease characterized by the build up of amyloid fibrils is Alzheimer's disease. This is a neurodegenerative disease and is the most common form of dementia, affecting more than 520,000 people in the UK alone.[16] Proteinaceous plaques are present in the brains of patients that are made up of a polypeptide called amyloid-β. The protein involved is the amyloid-β precursor peptide which fragments with one of the fragments being amyloid-β. This can self-assemble into soluble oligomers, however if the peptide misfolds in the oligomer assembly it can prompt other amyloid-β molecules to do the same. They then assemble into densely packed amyloid fibres which come together to create insoluble extracellular plaques. It is believed that the misfolded early oligomers may be the toxic species that cause damage and kill neurons.[17] However, the mechanism by which they assemble is currently unknown.

Gazit's group have done much work into the investigation of the self assembly of the amyloid-β polypeptide, some of which is discussed in Section 1.3, as well as other amyloidogenic peptides.[18, 19] They first suggested that π-stacking is important in the formation of amyloid fibrils in 2002 by highlighting the abundance of aromatic amino acids in the basic amyloidogenic units of the peptides and proteins that assemble in to amyloids. For example, a six-residue fragment of amylin (FGAIL) is known to form fibrils *in vitro*. When the aromatic F residue is removed from the sequence the peptide can no longer assemble into fibrils.[20]

Similarly in Alzheimer's disease a short aromatic fragment of amyloid-β (KLVFFAE) was found to assemble into amyloid fibrils.[21] It has also been shown that QKLVFF and LVFFA bind specifically to the full peptide.[22, 23] The FF motif is common amongst amyloid precursor proteins, Table 1.1 shows a list of such proteins contain FF. This induced Gazit and co-workers to suggest that the FF motif is the basic amyloidogenic unit of amyloid-β and that the high directionality and the energetic contribution of the stacking interactions make aromatic molecules ideal for fibre formation.[19]

Disease	**Precursor Protein**
Alzheimer's disease	Amyloid Precursor Protein
Atrial amyloidosis	Atrial natriuretic factor
Injection-localized amyloidosis	Insulin
Secondary systemic amyloidosis	(Apo) serum amyloid A
Finnish hereditary systemic amyloidosis	Gelsolin
Familial amyloidosis	Fibrinogen αA-chain

Table 1.1 Amyloidogeninc proteins containing the diphenylalanine motif and their related diseases. [24, 25]

There are several other examples of aromatic moieties playing an important role in the basic amyloidogenic units of proteins and peptides. For example, in Finnish hereditary amyloidosis the self-assembling protein contains a high

number of phenylalanine residues,[26] as does calcitonin, which is a peptide related to medullary thyroid carcinoma that forms amyloid fibrils.[27] In order to understand the assembly mechanism of many disease-related amyloids, it is thus very pertinent to investigate a simple model peptide system which plays a key part in this process, which, in this case, is FF.

1.2 Self-Assembling Peptides

Self-assembly is the spontaneous formation of a structure due to weak, non-covalent interactions, such as hydrogen bonding and π-stacking, and is a "bottom-up" method for the fabrication of nanostructures. It has many advantages over the traditional "top-down" methods, such as etching followed by lithography.[28] This was first noted by Richard Feynman in his lecture entitled "There's Plenty of Room at the Bottom" in which he highlights the potential for biological materials in creating small-scale structures.[29] Biomolecules are ideally suited to this purpose because they are intrinsically functional and biocompatible. In contrast, typical top-down techniques that start with large objects and make them smaller are much more prone to defects which are intrinsically bound to the removal of material.

Self-assembly is ubiquitous in nature and routinely creates structures with nanoscale precision. Peptides and proteins are synthesised *in vivo* by the translation of a sequence of messenger ribonucleic acid (mRNA) into a chain of covalently bonded amino acids, which constitutes the protein's primary structure. This protein will then undertake self-assembly to form secondary structure motifs, such as α-helices and β-sheets, using noncovalent interactions. Lipid molecules are also known to self-assemble in an aqueous environment. They form micelles when placed into water, and *in vivo* lipid bilayers constitute the basis for the membrane of most living organisms and viruses. They do this because they are amphiphilic – *i.e.* they have a hydrophilic head and a hydrophobic tail – which drives their assembly into a conformation where the tails are shielded from the aqueous environment by the hydrophilic heads, creating a bilayer. The fact that the lipids are not covalently bonded together

means that the membrane is dynamic and can allow transport of substances into and out of the cell.

Naturally occurring peptides are made from a group of about 20 amino acids which covalently bond together to form a chain and these chains can be attracted to each other by weak, noncovalent interactions. This mechanism is exploited by scientists to create rationally designed supramolecular assemblies, and was first implemented by Ghadiri *et al*. in 1993.[30] They used a cyclic peptide with alternating L and D amino acids as they expected this to form a flat ring, with the functional parts of the peptides facing outside. As these rings stack together a hollow nanotube is created. Transmission electron microscopy (TEM) showed that this was indeed the case for the peptide with the following sequence: *cyclo*[-(D-AED-AE-)$_2$] and that these tubes packed together side by side.

Ghadiri's work was followed by Zhang's group who designed and fabricated many self-assembling peptides and proteins. One example is the self-assembly of surfactant-like peptides to make nanotubes and vesicles.[31] The peptides used had a hydrophilic head and a hydrophobic tail, so that when placed in water they formed nanotubes to isolate the hydrophobic tail from the water. Cryo-TEM was used to preserve the structures in their aqueous state and image them. This revealed the networks of nanotubes and vesicles formed by these surfactant-like peptides. The same group also created peptides which self-assemble into a fibrous matrix which can be used as a substrate for mammalian cell growth.[32]

Since then self-assembling peptides have been used to fabricate a variety of structures including fibres, ribbons, micelles and vesicles [33, 34, 35, 36] with potential applications in medicine as well as biotechnology. Some examples from the literature of self-assembling peptides used to create nanostructures are discussed in this section.

For example, Meegan *et al*. used the assembly of MeCO-QQRFQWQFQQQ-NH_2 peptides as templates for silica nanotubes.[37] These nanotubes are of interest in the fields of biocatalysis and bioseparation.[38] This specific sequence was

chosen as the glutamine contains polar side chains which are important for attracting the negatively charged silicate ions. The peptide followed a one-dimensional assembly into an antiparallel β-sheet structure to form amphiphillic tapes which subsequently stacked together in order to shield the hydrophobic moieties. The hydrophilic glutamines were left exposed to hydrogen bond with each other to form fibrils. The silica ions were then added to the solution and they surrounded the fibrils to create a nanotube. The structures were finally calcined to remove the fibrils and the silica nanotubes were left, with an outer diameter of ~20 nm and lengths of under 0.5 μm.

Peptide nanofibres have also been tested for use in *in vitro* neuron cultures.[39] A palmitoyl group was added to a peptide with the sequence GGGAAAKRK. This was done to increase the membrane permeation ability of the nanofibres as peptides are generally hydrophilic in nature so do not mix well with lipid membranes. Positively charged amino acids were chosen as charged nanofibres repel each other and are therefore unlikely to aggregate. They are also attracted to the negative cell membrane. TEM confirmed the existence of the nanofibres that were afterwards fluorescently labelled in order for their degradation to be measured by UV absorbance. The nanofibres degraded by 50 % after 1 week, suggesting that the peptidase enzymes present in blood plasma are able to degrade them. In a separate experiment the nanofibres were incubated with neurons which resulted in them being internalised by the neurons. These qualities make it an ideal candidate as a drug delivery method, if the drug was placed inside the nanotube.

Recently, another type of peptide nanofibre has been shown to have qualities necessary for drug delivery. It is made from a peptide with the sequence Nap-GFFYG-RGD.[40] It has been shown to successfully encapsulate curcumin, which is a hydrophobic drug used in the treatment of cancer, and release it in a sustained manner in an *ex vivo* environment. The RGD group at the end of the peptide sequence makes the nanofibre highly specific to tumour cells as RGD is the binding motif of a protein which is overexpressed in tumours and is

important to the survival of cancer cells.[41] Therefore RGD-containing peptides are promising candidates for cancer drug delivery.

Peptide fibres have recently also been used as a scaffold system for culturing human corneal keratocyte cells, and have shown enhanced results when compared to standards.[42] The cornea can become damaged by disease or trauma which is detrimental to the vision of the patient or can even lead to loss of sight completely. A peptide of sequence YIGSR was designed which mimics laminin, a protein that is essential to cell survival and function. This peptide made nanofibres which assembled into a matrix on which successful corneal cell regeneration was demonstrated.

Dipeptides are the smallest type of peptide and hydrophobic dipeptide assemblies have been most studied because they are the simplest system with a propensity to self-assemble. In particular, the FF motif has been found to create fibres with an unusual structure and attractive properties. In order to be able to realize the full potential of biomolecules for biotechnological applications, it is important to first gain an understanding of their assembly process. To this end, a dipeptide was chosen as a simple model system for this project, which might serve as a starting point to learn how more complicated peptides assemble.

1.3 Potential Mechanisms of Assembly

It is possible to speculate upon possible assembly mechanisms of the FF fibres from previous work done on amyloidogenic and fibrillar proteins. Xue *et al*. have monitored the self-assembly of β2-microglobulin which is a protein that can assemble into amyloid deposits in joints, and is related to a disease called dialysis-related amyloidosis. They suggest that nucleation is the primary process for the assembly of the protein into fibrillar aggregates. This is followed by fragmentation of fibrils which go on to seed further fibril growth.[43] They suggest that this mechanism may be applicable to other amyloid systems and therefore may occur with FF fibres. Indeed, it has recently been shown by Cohen *et al*. that this nucleation and fragmentation mechanism applies to the amyloid-β.[44]

It is possible that diffusion-limited growth plays a role in the self-assembly of FF fibres. This occurs when the Brownian motion of the molecules plays a role in the rate at which the assembly grows. This is opposed to surface-limited growth in which the mechanism of adsorption of the monomers onto the surface of the aggregate limits the growth speed. Collagen is an abundant protein found in human skin, scar tissue and bone and usually exists in the form of fibrils. Parkinson *et al*. have shown that type I collagen assembles *via* a diffusion-limited growth mechanism.[45] It has also been suggested that amyloid-β assembly is governed by diffusion.[46]

1.4 Discovery, Synthesis and Characterization of FF Fibres

In 2003 Reches and Gazit investigated the Alzheimer's amyloid-β polypeptide.[5] The amyloid-β polypeptide is known to assemble into fibres which bundle into plaques in the brains of patients (Figure 1.1). In order to understand the reason for this process, they took a small part of the peptide, FF, and discovered that it self-assembled to form peptide nanotubes. The reason for choosing the FF moiety was to find out whether or not π-stacking interactions played an important role in the assembly of the amyloid-β polypeptide, as assumed.

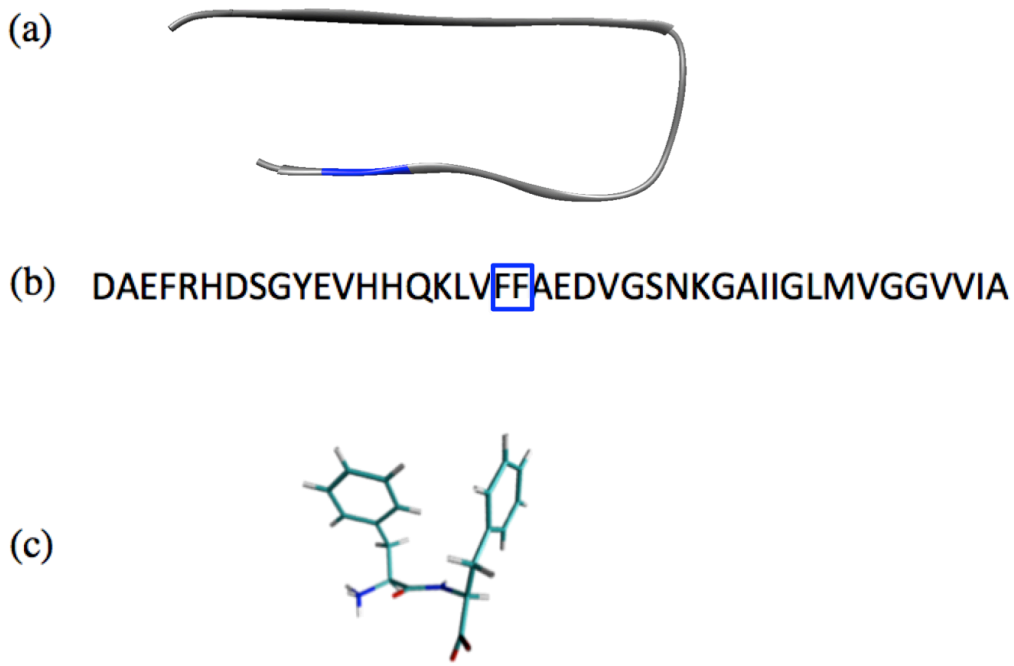

Figure 1.1 *(a) The amyloid-β peptide assembled into a fibril as it would in vivo.*[41] *The diphenylalanine motif is shown in blue. (b) The amino acid sequence of the amyloid-β peptide. The FF motif is present at residues 19 and 20* [47] *(c) The FF molecule, which self-assembles into fibres when dissolved in water.*[48]

Reches and Gazit then dissolved FF at a high concentration in a fluorinated solvent and upon dilution with water nanotubes formed within seconds. DLS and TEM were used to confirm the presence of the fibres and to investigate their size. The diameters of the fibres were found to be around 125 nm with the maximum measuring 300 nm wide. The persistence length was stated to be of the order of microns as observed by microscopy. The same techniques were used with other dipeptides for comparison in the same paper, these were FW, WY and WW which are all aromatic. The only other one to assemble into tubular structures was FW, however there were also a large amount of amorphous aggregates present in the FW sample. This is in contrast to FF, in which primarily tubular structures were observed. This means that FF is unique in its self-assembly process, and the reasons for this can not only be due to its aromaticity, as other aromatic dipeptides do not behave in the same way.[5]

To investigate the structure of the FF nanotubes, Reches and Gazit performed Fourier transform infrared spectroscopy (FTIR) and found a peak at 1640 cm^{-1} which is indicative of the presence of β-sheets. Ionic silver was added to the solution of FF and it was seen by TEM that silver nano wires were formed inside the nanoubes. An enzyme was added to remove the FF and the result was silver nanowires, showing that the fibres can be used to cast metal nanowires.[5]

Reches and Gazit later found a new way of synthesising the nanotubes so that they were aligned.[49] They dissolved the FF in a fluorinated solvent and placed it on a siliconised glass substrate. The solvent then evaporated and a thin layer of aligned FF nanotubes was left pointing upwards from the substrate. The authors suggested that rapid evaporation of the solvent results in a supersaturated environment in which multiple nucleation events occur, which is followed by growth upwards from the substrate in the vapour-liquid-solid system. This work also proposed that these aligned nanotubes had a different structure from the original nanotubes which were formed in solution.[49] However, Görbitz then showed that the structure of the FF nanotubes formed by drying and self-assembly in solution were the same, and also equivalent to the single crystal structure of the fibres by using X-ray diffraction.[48] He also observed nanotubes which had diameters greater than 1 μm and referred to the nanotubes as fibres, which is the nomenclature that will be used in the rest of this work. This structure shows that there is a three-dimensional aromatic stacking between cylinders of hydrogen-bonded molecules (Figure 1.2). He also mentioned that the size of the fibres was less monodisperse than had previously been thought.

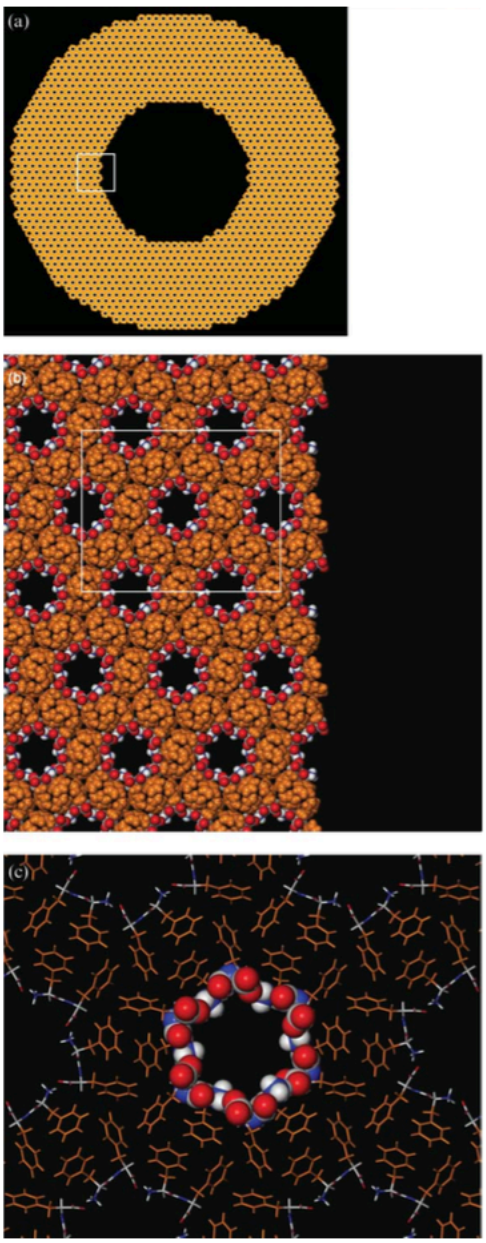

Figure 1.2 *The structure of FF fibres. (a) A cross section of a whole fibre. (b) The square in (a) is shown here. (c) The square in (b) is enlarged in this image. Six peptides use their backbones to create a hexagonal pore.*[48] *The individual FF molecule is shown in Figure 1.1(c).*

Song *et al*. showed an alternative way to synthesise the fibres which excluded the use of a fluorinated solvent.[8] The FF peptides were at a concentration of 2 mg/ml in water and this solution was heated to 65 °C. The peptides dissolved completely at this temperature. The solution was gradually cooled to room temperature and the fibres formed upon cooling. These fibres again had a larger size range with diameters ranging from 100 nm to 2 μm in diameter. This method has the advantage over the method of Reches and Gazit in that it does not require the use of an expensive, harmful solvent.

Kol *et al*. later characterised FF fibres and found them to have several attractive properties.[3] They were found to have a high Young's modulus (19 GPa) by using indentation experiments with atomic force microscopy (AFM). This is many times higher than most other biological materials, and is amongst the stiffest alongside cortical bone. Sedman *et al*. found the fibres to be thermally stable up to 100 °C in an AFM experiment.[50] Hill *et al*. have shown that the FF fibres will align in a 12 T magnetic field.[51] A solution of FF fibres in a 1,1,1,3,3,3-hexafluoro-2-propanol (HFIP)-water solution was dried in a magnetic field and then imaged with AFM with no additional treatment. The main reason for the alignment in a magnetic field is the ordering of the aromatic moieties leading to diamagnetic anisotropy. This alignment is useful for making fibres that can be used in nano devices.

Piezoelectricity is the ability of a material to become electrically charged upon mechanical stress or *vice versa*. This property has been exploited for many applications from sound detection to micro- and nano-positioning and quartz watches. The materials used in these devices are typically inorganic while a biocompatible strongly piezoelectric material has yet to be found.[52] Kholkin *et al*. have shown that FF fibres exhibit this property by using an atomic force microscope (AFM) to perform piezo-response force microscopy (PFM). They found that FF fibres had a piezoelectric coefficient which is three times larger than that of scleral collagen, which was previously the highest known for a biomaterial.[4]

While these properties have led to a great deal of interest in the nano- and microstructures formed by this peptide, it has still not been possible to create a homogenous sample of the FF fibres and their assembly mechanism is not known. Reches and Gazit proposed one mechanism based on the discovery that the introduction of a thiol group to the peptide caused the formation of nanospheres instead of fibres.[53] These spheres are similar to the ones formed by the dipeptide diphenylglycine. They suggest that stacking interactions cause the FF molecules to assemble into a sheet which then curls around into a tube. Their assumption is that when the molecule is thiolated the disulphide interactions cause all edges of the sheet to curl up into a sphere (Figure 1.3). The basic argument is that if the molecule can create a tube or a sphere, then there must be a stage in the assembly process where there is a sheet that can then fold in either one or two dimensions. However, further evidence is needed to prove this hypothesis, as there is no suggestion of a force that would cause the non-thiolated sheet to curl up into a tube.

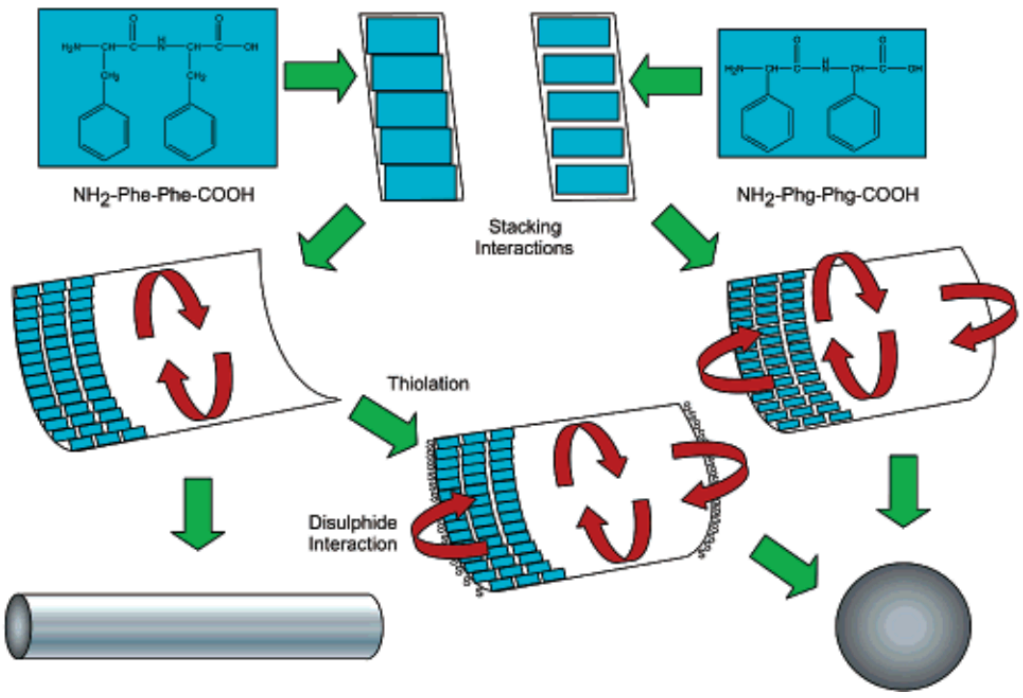

Figure 1.3 The model proposed by Reches and Gazit for the self-assembly of diphenylalanine, thiolated diphenylalanine and diphenylglycine into tubes and spheres.[53]

1.5 Simulations of FF

Computational studies of molecules can allow us to gain a deeper understanding of a system than from experimental work alone. There has been limited computational work into the self-assembly of FF due to the large size of the fibres and the long timescales needed to witness self-assembly. One such work from Song *et al*. overcame this problem by creating a coarse-grained model of the peptide.[8] These simulations demonstrated the self-assembly of a variety of shapes including spheres, tubes and layers. However, all of the structures observed were made up of bilayers, with the hydrophobic parts on the inside and the hydrophilic backbones exposed to the solvent. This is not the structure that the fibres have in reality, and is produced because the coarse-graining of the peptide is too simple. Guo *et al*. performed a similar set of simulations in 2012.[9] They observed the assembly of vesicles and tubes with their coarse-graining but again they consisted of bilayers whereas, in reality, the fibres are thousands of peptides wide.

Recently, a completely new set of simulations was performed on a small number of FF molecules to understand the early stages of self-assembly by Jeon *et al*.[54] The small number of molecules allowed fully atomistic simulations to be performed. Jeon *et al*. compared charged and non-charged versions of the peptide in the simulations and found that the charged peptides produced a more ordered assembly than the neutral ones, suggesting that electrostatics plays an important role in this process. However, the neutral peptides still assembled which means that other interactions must be involved. Similarly Tamamis *et al*. have performed atomistic simulations of 12 FF peptides in water and found that they stated to aggregate over the course of the simulation.[55] In 2013 Rissanou *et al*. simulated 16 FF molecules in water and methanol to compare the self assembling propensity in these solvents, and found that it was much higher in water.[56] These atomistic simulations were limited to 12 or 16 peptides, so that they could be run for long enough to allow self-assembly to take place (in this case 100 ns), whereas at least several hundreds of peptides are needed to simulate structures that might be of some relevance to the experimentally observed fibres.

1.6 Techniques for the Structural Analysis of Fibres

Micro- and nano-scale fibres present several challenges when we try to experimentally characterize their structure and assembly mechanism. As mentioned above, they have a reduced symmetry, implying that some of the most standard techniques cannot be used. Although several types of microscopy can be employed to analyse their morphology – including electron, optical and atomic force microscopy – other methods are needed for a complete characterisation. This section describes some of the specialised experimental techniques that are available for the study of fibres.

Although microscopy cannot probe the molecular structure of a fibre, it has proven useful in their morphological characterization. Scanning electron microscopy (SEM) allows a wide range of sizes to be analysed, and TEM can reveal high resolution images. SEM is widely used in materials science for inspecting the surface of structures and has been employed to observe the fibres formed by phenylalanine.[57] TEM can be used on thin samples and has a higher spatial resolution than SEM. It has been possible to image nanosheets made by the assembly of the peptide A_6R with scanning TEM (STEM).[58] Cryogenic-TEM was used along with STEM on this system and revealed that the nanosheets helically wrap to create tubes at high concentrations. Krysmann *et al*. also used cryo-TEM to observe the fibres formed by KLVFF, which is part of the amyloid-β polypeptide, *in situ*. The use of cryo-TEM eliminates drying effects present in standard TEM.[59] AFM has been used by Zhou *et al*. to examine the fibres formed by Fmoc-RGD.[60] This was coupled with TEM and spectroscopic techniques to determine that they assemble into β-sheets.

Fibre X-ray diffraction has been a particularly successful technique for finding the structure of a variety of fibres. It exploits the 1D symmetry of fibres to produce a 2D diffraction pattern made by radiation shone at the sample. The resulting pattern can be used to obtain information about the arrangement of atoms within the fibre. Fibre diffraction has had a significant impact in the field of structural biology, for example it led to the Watson-Crick model of DNA.[61] More recently it has been used to investigate the structure of several amyloid

fibrils; for example, it has been used to reveal the structure of α-synuclein filaments which play a role in Parkinson's disease.[62] It was also used to find the structure of the disease related peptide, amylin, and a fragment of amyloid-β.[63] This has allowed Jahn *et al*. to elucidate the common architecture of cross-β amyloid.[63]

There are several types of spectroscopy that can be used to probe the structure of rod-shaped systems. For example, Krysmann *et al*. have used UV spectroscopy and circular dichroism coupled with cryo-TEM to find information about the structure of fibres formed by the peptide KLVFF, which is part of the amyloid-β polypeptide.[59]

Linear dichroism (LD) is a technique which is particularly well suited to the study of fibres. It is a polarized light spectroscopy technique which gives information about the orientation of transition moments within a molecule as well as their energy. This technique is particularly useful when monitoring the assembly of fibres. This is because molecules with a similar width and height do not produce an LD signal whereas structures with a high aspect ratio, such as fibres, do (see Section 2.3.2). Therefore, during fibre formation, an LD signal will start to appear as the fibres increase in length. Dafforn *et al*. demonstrated this by monitoring the polymerization of actin with LD.[64] First the LD spectrum of F-actin (fibrous actin) was measured and there was a peak at 205 nm. They then monitored the LD signal at a single wavelength (205 nm) whilst the actin monomers assembled into polymers which resulted in a kinetics plot. The LD signal increased over a period of 500 seconds with an initial lag time and an increase to saturation. This experiment highlights the advantage of LD over other techniques for investigating the assembly of fibres in particular, which is that only the fibres are detected and not their building blocks.

Another example of the use of LD to monitor fibre formation is the work of Marrington *et al*.[65] They used rapid injection LD to monitor the polymerization of the bacterial cell division protein FtsZ, and Hicks *et al*. observed the digestion of DNA by DNase.[66] This shows that LD is an ideal technique for investigating

the assembly and disassembly of biological fibres and therefore could be used in the case of FF fibres.

1.7 Conclusion

FF is an ideal model system for studying peptide self-assembly as it is simple yet capable of forming fibres. It is also of interest in relation to its role in Alzheimer's disease as well as to the field of biotechnology because of its many attractive properties. Therefore in this work FF fibres and their self-assembly mechanism are studied. The literature shows that microscopy coupled with spectroscopy is an effective way to approach this problem. Here, we add MD simulations in order to gain a deeper understanding of this system.

There are contradictory reports on the size distribution and morphology of the fibres, so this work began by using electron and optical microscopy in order to determine the size and shape of the fibres as well as to observe their growth. Electron microscopy allowed the high resolution morphological characterisation of the nanoscale fibres while optical microscopy revealed the larger structures *in situ* and enabled their growth to be observed in real time.

This initial experimental section is followed by a set of atomistic molecular and metadynamics simulations of FF nuclei. Since previous work in the literature showed that current coarse-grained models were unsuccessful, here atomistic simulations were chosen in order to provide an accurate representation of the molecule. Firstly the size of the nuclei was varied in order to assess their relative stability and then adsorption events of single dipeptides were investigated using metadynimcs.

Finally, spectroscopy was used in order to monitor the kinetics of fibre assembly. In particular, LD was used extensively and developed in order to tailor it to the requirements of FF fibres. LD was chosen as it had not been used before on this type of fibre but had provided useful information on the kinetics of similar systems.[565, 66] Right angle light scattering (RALS) was also employed to analyse the later stages of the assembly, when the fibres grew too large for LD.

References

[1] Gentilucci, L., Tolomelli, A. & Squassabia, F. (2006). Peptides and Peptidomimetics in Medicine, Surgery and Biotechnology. *Curr. Med. Chem., 13,* 2449-2466.

[2] Cavalli S., Albercio, F. & Kros, A. (2010). Amphiphilic Peptides and their Cross-Disciplinary Role as Building Blocks for Nanoscience. *Chem. Soc. Rev., 39,* 241-263.

[3] Kol, N., Barlam, D., Shneck, R. Z., Gazit, E. & Rousso, I. (2005) Self-Assembled Peptide Nanotubes are Uniquely Rigid Bioinspired Supramolecular Structures. *Nano. Lett., 5,* 1343-1346.

[4] Kholkin, A., Amdursky, N., Bdikin, I., Gazit, E. & Rosenman, G. (2010). Strong Piezoelectricity in Bioinspired Peptide Nanotubes. *ACS Nano, 4,* 610-614.

[5] Reches, M. & Gazit, E. (2003). Casting Metal Nanowires Within Discrete Self-Assembled Peptide Nanotubes, *Science, 300*, 625-627.

[6] Cipriano, T. C., Takahashi, P. M., de Lima, D., Oliveira Jr., V. X., Souza, J. A., Martinho, H. & Alves, W. A. (2010). Spatial Organization of Peptide Nanotubes for Electrochimical Devices. *J. Mater. Sci., 45,* 5101-5108.

[7] Andersen, K. B., Castillo-Leó, J., Bakmand, T. & Svendsen, W. E. (2012). Alignment and Use of Self-Assembled Peptide Nanotubes as Dry-Etching Mask. *Japanese Journal of Applied Physics, 51,* 06FF13.

[8] Song, Y. *et al*. (2004). Synthesis of Peptide-Nanotube Platinum-Nanoparticle Composites. *Chem., Commun., 22,* 1044-1045.

[9] Guo, C., Luo, Y. & Wei, G. (2012). Probing the Self-Assembly Mechanism of Diphenylalanine-Based Peptide-Amphiphile Nanofibres. *Science, 294,* 1684-1688.

[10] Bartles, T., Choi, J. G. & Selkoe, D. J. (2011). α-Synuclein Occurs Physiologically as a Helically Folded Tetramer that Resists Aggregation. *Nature, 477,* 107-110.

[11] Polymeropoulos, M. H. *et al*. (1997). Mutation in the α-Synuclein Gene Identified in Families with Parkinson's Disease. *Science, 276,* 2045-7.

[12] Stefanis, L. (2012). α-Synuclein in Parkinson's Disease. *Cold Spring Harb. Perspect. Med., 4:a009399.*

[13] Khan, S. E., Andrikopoulos, S. & Verchere, C. B. (1999). Islet Amyloid: A Long Recognized But Underappreciated Pathological Feature of Type 2 Diabetes. *Diabetes, 48,* 241-253.

[14] Marzban, L., Park, K. & Verchere, C. B. (2003). Islet Amyloid Polypeptide and Type 2 Diabetes. *Experimental Gerontology, 38,* 347-352.

[15] Langkilde, A. E., Morris, K. L., Serpell, L. C., Svergun, D. I. & Vestergaard, B. The Architecture of Amyloid-like Peptide Fibrils Revealed by X-ray Scattering, Diffraction and Electron Microscopy. (2015). *Biological Crystallography. 71,* 882-895.

[16] Factsheet: What is Alzheimer's Disease? (5/8/2015). *Alzheimer's society. Alzheimers.org.uk.*

[17] Buccianti, M. *et al.* (2002). Inherent Toxicity of Aggregate Implies a Common Mechanism for protein Misfolding Diseases. *Nature, 416,* 507-511.

[18] Azriel, R. & Gazit, E. (2001) Analysis of the Structural and Functional Elements of the Minimal Active Fragment of Islet Amyloid Polypeptide (IAPP): an Experimental Support for the Key Role for the Phenylalanine Residue in Amyloid Formation. *J. Biol. Chem., 276,* 34156-34161.

[19] Gazit, E. (2002). A Possible Role for π-Stacking in the Self-Assembly of Amyloid Fibrils. *FASEB J., 16,* 77-83.

[20] Westermark, P., Engström, U., Johnson, K. H., Westermark, G. T. & Betsholtz, C. (1990). Islet Amyloid Polypeptide: Pinpointing Amino Acid Residues Linked to Amyloid Fibril Formation. *PNAS, 87(13),* 5036-5040.

[21] Balbach, J.J, Ishii, Y., Antzukin, O. N., Lepaman, R. D, Rizzo, N. W., Dyda, F., Reed, J. & Tycko, R. (2000). Amyloid fibril formation by Aβ 16–22, a seven-residue fragment of the Alzheimer's beta-amyloid peptide, and structural characterization by solid state NMR. *Biochemistry, 39,* 13748–13759.

[22] Tjernberg, L. O., Na¨slund, J., Lindqvist, F., Iohansson, J., Karlstro¨m, A. R., Thyberg, J., Terenius, L., and Nordstedt, C. (1996). Arrest of beta-amyloid fibril formation by a pentapeptide ligand. *J. Biol. Chem. 271***,** 8545–8548.

[23] Findeis, M. A., Musso, G. M., Arico-Muendel, C. C., Benjamin, H. W., Hundal, A. M., Lee, J. J., Chin, J., Kelley, M., Wakefield, J., Hayward, N. J., and Molineaux, S. M. (1999). Modified- peptide inhibitors of amyloid-beta-peptide polymerization. *Biochemistry, 38*, 6791–6800.

[24] Serpell, L. C. & Rambaran, R. N. (2008). Amyloid Fibrils. *Prion, 2,* 112-117.

[25] Maack, T., Camargo, M. J. F., Kleinert, H. D., Laragh, J. H. & Atlas, S. A. (1985). Atrial Natriuretic Factor: Structure and Functional Properties. *Kidney International, 27,* 607-615.

[26] Westermark, G. T., Engstro¨rm, U., and Westermark, P. (1992). The N-terminal segment of protein AA determines its fibrillo- genic property. *Biochem. Biophys. Res. Commun.* **182,** 27–33.

[27] Benvenga, S., Trimarchi, F., and Facchiano, A. (1994). Homology of calcitonin with the amyloid-related proteins. *J. Endocrinol. Invest. 17,* 119–122 .

[28] Ariga, K., Hill, J. P., Lee, M. V., Vinu, A., Charvet, R. & Acharya, S. (2008). Challenges and Breakthroughs in Recent Research on Self-Assembly. *Sci. Technol. Adv. Mater., 9,* 014109.

[29] Feynman, R. (1960). There's Plenty of Room at The Bottom. *Engineering and Science, 23,* 22-36.

[30] Ghadiri, M. R., Granja, J. R., Milligan, R. A., McRee, D. E. & Khazanovich, N. (1993). Self-Assembling Organic Nanotubes Based on a Cyclic Peptide Architecture. *Nature, 366,* 324-327.

[31] Vauthey, S., Santoso, S., Gong, H., Watson, N. & Zhang, S. (2002). Molecular Self-Assembly of Surfactant-Like Peptides to Form Nanotubes and Nanovesicles. *PNAS, 99(8),* 5355-5360.

[32] Holmes, T. C, de Lacalle, S., Xing, S., Guosong, L., Rich, A. & Zhang, S. (2000). Extensive Neurite Outgrowth and Active Synapse Formation on Self-Assembling Peptide Scaffolds. *PNAS, 97(12),* 6728-6733.

[33] Hartgerink, J. D., Beniash, E. & Stupp, S. I. (2001). Self-Assembly and Minerilization of Peptide-Amphiphile Nanofibres. *Science. 294,* 1685-1688.

[34] Hwang, W., Marini, D. M.,Kamm, R. D. & Zhang, S. (2003). Supramolecular Structure of Helical Ribbons Self-Assembled from a β-sheet Peptide. *J. Chem. Phys., 118,* 389-397.

[35] Trent, A., Marullo, R., Lin, B., Black, M & Tirrell, M. (2011). Structural Properties of Soluble Peptide Amphiphile Micells. *Soft Matter, 20,* 9572-9582.

[36] Gudler, S., Sukthankar, P., Gao, J., Avila, L. A., Hiromasa, Y., Chen, J., Iwamoto, T. & Tomich, J. M. (2012). Peptide Nanovesicles Formed by the Self-Assembly of Branched Amphiphilic Peptides. *Plos ONE, 7,* e45374.

[37] Meegan, J. E., Aggeli, A., Boden, N., Brydson, R., Brown, A. P., Carrick, L., Brough, A. R., Hussain, A., & Ansell, R. J. (2004). Designed Self-Assembled β-sheet Peptide Fibrils as Templates for Silica Nanotubes. *Adv. Funct. Mater., 14,* 31-37.

[38] Yang, X., Tang, H., Cao, K., Song, H., Sheng, W. & Wu, Q. (2011). Template-Assisted One-Dimensional Silica Nanotubes: Synthesis and Applications. *J. Mater. Chem., 21,* 6122-6135.

[39] Mazza, M., Patel, A., Pons, R., Bussy, C. & Kostarelos, K. (2013). Peptide Nanofibres as Molecular Transporters: From Self-Assembly to *in vivo* Degradation. *Faraday Discussions, 166,* 181-194.

[40] Liu, J., Liu, J., Xu, H., Zhang, Y., Chu, L., Liu, Q., Song, N. & Yang, C. (2013). Novel Tumor-Targeting, Self-Assembling peptide Nanofiber as a Carrier for Effective Curcumin Delivery. *International Journal of Nanomedicine, 9,* 197-207.

[41]Wang, F., Li, Y., Shen, Y., Wang, A., Wang, S. & Xie, T. (2013). The Functions of RGD in Tumor Therapy and Tissue Engineering. *The International Journal of Molecular Sciences, 14(7),* 13447-13462.

[42] Uzunalli, G., Soran, Z., Erkal, T. S., Dagdas, Y. S., Dinc, E., Hondur, A. M., Bilghan, K., Aydin, B., Guler, M. O. & Tekinay, A. B. (2014). Bioactive Self-Assembled Peptide Nanofibers for Corneal Stroma Regeneration. *Acta biomaterialia, 10,* 1156-1166.

[43] Xue, W-F., Homans, S. W., Radford, S. E. (2008). Systematic Analysis of Nucleation-Dependent Polymerization Reveals New Insights into the Mechanism of Amyloid Self-Assembly. *PNAS. 105(26).* 8926-8931.

[44] Cohen, S. I. *et al.* (2012). Proliferation of Amyloid-β Aggregates Occurs Through a Secondary Nucleation Mechanism. *PNAS. 110(24).* 9758-9763.

[45] Parkinson, J., Kadler, K. E., & Brass, A. (1995). Simple Model of Collagen Fibrillogenesis. *J. Mol. Biol. 247,* 823-831.

[46] Tomski, S. J. & Murphy, R. M. (1992). Kinetics of Aggregation of Synthetic β-Amyloid Peptide. *Archives of Biochemistry and Biophysics. 294(1).* 630-638.

[47] Luhrs, T., Ritter, C., Adrian, M., Riek-Loher, D., Bohrmann, B., Dobeli, H., Schubert, D. & Riek, R. (2005). 3D Structure of Alzheimer's Amyloid-β (1-42) fibrils. *Proc. Natl. Acad. Sci. USA, 102,* 17342-17347.

[48] Görbitz, C. H. (2006). The Structure of Nanotubes Formed by Diphenylalanine, the Core Recognition Motif of Alzheimer's Amyloid Polypeptide. *Chem. Commun., 22,* 2332-2334.

[49] Reches, M. & Gazit, E. (2006). Controlled Patterning of Aligned Self-Assembled Peptide Nanotubes. *Nature Nanotechnology, 1,* 195-200.

[50] Sedman, V. L., Adler-Abramovich, L., Allen, S., Gazit, E. & Tendler, S. J. B. (2006). Direct Observation of the Release of Phenylalanine from Diphenylalanine Nanotubes. *J. Am. Chem. Soc., 128,* 6903-6908.

[51] Hill, R. J. A *et al.* (2007). Alignment of Aromatic Peptide tubes in Strong Magnetic Fields. *Adv. Mater., 19,* 4474-4479.

[52] Gruverman, A., Rodriguez, B. J. & Kalinin, S. V. (2006). Electromechanical Behaviour in Biological Systems at the Nanoscale. *Scanning Probe Microscopy: Electrical and Electromechanical Phenomena at the Nanoscale. Springer, 1,* 615-633.

[53] Reches, M. & Gazit, E. (2004). Formation of Closed-Cage Nanostructures by Self-Assembly of Aromatic Dipeptides. *Nanoletters. 4,* 581-585.

[54] Jeon, J., Mills, C. E. & Shell, M. S. (2013). Molecular Insights in Diphenylalanine Assembly: All-Atom Simulations of Oligomerization. *J. Phys. Chem. B., 117,* 3935-3943.

[55] Tamamis, P. *et al.* (2009). Self-Assembly of Phenylalanine Oligopeptides: Insights from Experiments and Simulations. *Biophysical Journal. 96.* 5020-5029

[56] Rissanou, A. N, Georgilis, E., Kasotakis, E., Mitraki, A. & Harmandaris, V. (2013). Effect of Solvent on the Self-Assembly of Dialanine and Diphenylalanine Peptides. *J. Phys. Chem. B., 117(5),* 3962-3975.

[57] Adler-Abramovich, L., Vaks, Lilach, V., Carny, O., Trudler, D., Magno, A., Caflisch, A., Frenkel, D. & Gazit, E. (2012). Phenylalanine Assembly into Toxic

Fibrils Suggests Amyloid Etiology in Phenylketonuria. *Nature Chemical Biology, 10,* 1038-1043.

[58] Hamley, I. W., Dehsorki, A. & Castelleto, V. (2013). Self-Assembled Arginine-Coated Peptide Nanosheets in Water. *Chem. Commun., 49,* 1850-1852.

[59] Krysmann, M. J., Castelletto, V., Kelarakis, A., Hamley, I. W., Hule, R. A. & Pochan, D. J. (2008). Self-Assembly and Hydrogelation of an Amyloid Peptide Framgent. *Biochemistry, 47(16),* 4597-4605.

[60] Zhou, M. Smith, A. M., Das, A. K., Hodson, N. W., Collins, R. F., Ulijn, R. V. & Gough, J. E. (2009). Self-Assembled Peptide-Based Hydrogels as Scaffolds for Anchorage-Dependent Cells. *Biomaterials, 30,* 2532-2530.

[61] Cochran, W., Crick, F. H. C. & Vand, V. (1952). The Structure of Synthetic Polypeptides. I. The Transforms of Atoms on a Helix. *Acta. Cryst., 5,* 581-586.

[62] Serpell, L. C., Berriman, J., Jakes, R., Goedert, M. & Crowther, R. A. (2000). Fiber Diffraction of Synthetic α-synuclein Filaments Shows Amyloid-Like Cross-β Conformation. *PNAS, 97(9),* 4897-4902.

[63] Jahn, T. R., Makin, S. M., Morris, K. L., Marshall, K. E., Tian, P., Sikorski, P. & Serpell, L. C. (2009). The Common Architecture of Cross-β Amyloid. *J. Mol. Biol., 395,* 717-727.

[64] Dafforn T. R., Rajendra, J., Halsall, D. J., Serpell, L. C. & Rodger, A. (2004). Protein Fiber Linear Dichroism for Structure Determination Kinetics in a Low Volume, Low-Wavelength Couette Flow Cell. *Biophysical Journal, 86,* 404-410.

[65] Marrington, R., Small, E., Dafforn, T. R. & Addinall, S. (2004). FtsZ Fibre Bundling is Triggered by a Calcium-Induced Conformational Change in Bound GTP. *J. Biol. Chem., 47,* 48821-48829.

[66] Hicks, M. R., Rodger, A., Lin, Y. P., Jones, N. C., Hoffman, S. V. & Dafforn, T. R. (2012). Rapid Injection Linear Dichroism for Studying the Kinetics of Biological Processes. *Anal. Chem., 84(15),* 6561-6566.

Chapter 2

Methods

2. Methods

In this chapter the methods used for this work are explained and it is divided into 3 sections: microscopy, simulations and spectroscopy. The principles behind each technique are explained as well as technical details required to repeat the experiments. This work is concerned with the characterization and assembly of FF fibres. These fibres are synthesised in all experiments by the same method. First a 2 mg/ml solution of FF obtained from Sigma-Aldrich was dissolved in deionised water by heating to 70 °C and stirring until the solution was clear. This was then transferred to the container needed for measurements in each technique and cooled, apart from in the thermal stability measurements where temperature was varied throughout the experiment. Upon cooling, the fibres assemble due to supersaturation. Our work found 40 °C to be the temperature which induced the fibres assembly, so all subsequent experiments were done at this temperature, including the right-angle light scattering, widefield deconvolution micrsocopy, and linear dichroism kinetics experiments. All of these experiments were performed in solution, with the exception of electron microscopy. It is important to examine the fibres *in situ* because we are interested in their dynamic properties. Even when investigating the fibres' structure, it is important to remember that drying can affect this.

2.1 Microscopy

The micro- and nano-sized details of a material can play a key role in determining its structural, electronic, optical, catalytic and biological properties on a macroscopic scale. Moreover, there are many interesting and functional systems which are composed of a large number of intrinsically small entities, for example, micron-sized cells or synthetic nanomaterials. The need to explore these small details and structures has lead to the development of the field of microscopy, which covers a vast range of techniques in which not only light is used as a probe, but also electrons and ions. These techniques span a range of resolutions from scanning probe microscopy (SPM) or TEM, which can create images with atomic resolution, to optical microscopy which enables the imaging of living biological complexes. This chapter focuses on electron and optical microscopy as the combination of these two techniques allowed the range of sizes of the FF fibres to be ascertained, and for the growth of individual fibres to be monitored in real time.

In contrast to other analytical techniques, microscopy does not measure the spatially averaged value of a parameter of the sample being probed, but instead reveals this information directly on a local scale. In the case of a system containing many particles, microscopy allows a direct observation of the size and shape of individuals whereas a bulk technique, such as spectroscopy, will only report an average value. Therefore, when using spectroscopic methods, it is important to ascertain the variation within a sample which leads to this averaged signal. In the case of FF fibres, many spectroscopic experiments have been performed (Chapter 5), which reveal important results about their assembly mechanism. However, it was first important for microscopy to be employed to assess the extent of their heterogeneity.

2.1.1 Optical Microscopy

Optical microscopy is a technique originating from the 17th century and is employed in a variety of research fields. A series of lenses is used to create a magnified image of an object with visible light (Figure 2.1). There are several advantages to optical microscopy over other microscopy techniques which include the fact that the sample can be kept in ambient conditions whilst being imaged, that it will usually not get damaged during the measurement and that the imagining can be done in real time. This is in stark contrast to electron microscopy which requires vacuum conditions and, very often, a sample preparation step to avoid electrical charging. In the case of FF fibres, optical microscopy can be performed on FF-containing water solutions kept at 40 °C, which are the standard conditions defined in the introduction to the methods chapter, and are identical to the spectroscopy experiments described in Chapter 5. Therefore optical microscopy can allow dynamic process to be witnessed on an individual fibre level, unlike most other forms of microscopy.

However, optical microscopy does not have the resolution required to detect the smaller fibres as typical optical microscopes cannot resolve structures smaller than around 200 nm. The resolution, R, is the smallest distance between two points that can still be distinguished as two separate entities and is mathematically described by Equation 2.1.

$$R = \frac{1.22\lambda}{2NA} \tag{2.1}$$

where NA is the numerical aperture of the microscope that can be found using the following equation

$$NA = n \sin \alpha, \tag{2.2}$$

where n is the refractive index of the medium and α is the collecting angle of the lens. The refractive index of the immersion oil which typically contains the objective lens is 1.4 and a standard collecting angle of the ocular lens is 90°.

When these values are used in Equation 2.2, a numerical aperture of 1.4 is obtained. The shortest wavelength of visible light is 400 nm and these values in Equation 1 produce a resolution of 170 nm. This is the maximum possible resolution attainable with standard optical techniques, and is known as the diffraction limit.[1, 2, 3]

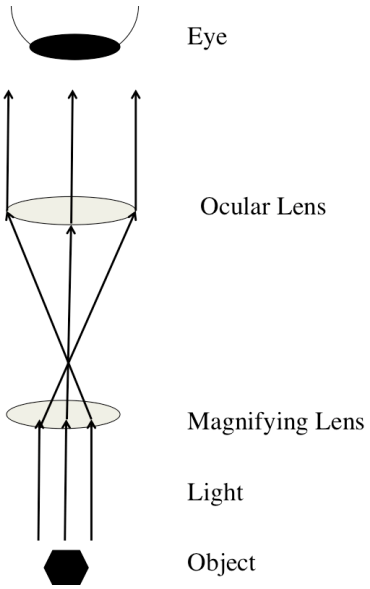

Figure 2.1 *A diagram of a basic optical microscope. Light illuminates the object and travels through the magnifying lens. Then the light goes through the ocular lens, which projects it to infinity and the eye, or a detector, finally creates the image.*

This work used a Zeiss Axioimager microscope with 50 – 1000 times magnification. Although the sample was kept in solution whilst being imaged, the microscope did not have the facilities to control the temperature of the specimen, so for kinetics measurements under the standard conditions (40 °C, in water) a different microscope had to be used. We chose a Deltavision 1 widefield microscope which is typically used for investigating live cells. In order to keep the cells alive it is contained within a weather control system, which can maintain the whole microscope and its surroundings at a chosen temperature. This was ideal for monitoring the fibres assembly as they could be kept in water at 40 °C. The fact that it was a widefield microscope allowed longer fibres to be imaged with respect to what would have been possible in standard microscopes.

This is achieved by the use of several detectors to simultaneously image a large field of view.

The experiments with the widefield microscope were performed in the standard conditions stated in the introduction to the methods section; this is identical to the spectroscopy experiments. The sample was pipetted into a dish which held 1.5 mL of solution, and the moment the sample was pipetted was time zero. The dish was preheated to 40 °C to ensure that the sample did not go below this temperature and a lid was placed on top to stop evaporation. Images were then taken of the fibres whilst they were growing. This is in contrast to a standard optical microscope where around 10 μL of solution is at room temperature and held between two glass slides.

2.1.2 Scanning Electron Microscopy

In order to measure the diameters of the smaller fibres, it was necessary to use a technique which allowed objects that were less than 200 nm to be viewed so scanning electron microscopy (SEM) was chosen. SEM uses electrons as a probe to image the top layer of a sample, with a depth that depends on the material of the sample and on the energy of the electrons, and can range from 1 nm to 1 μm. As opposed to other types of electron microscopies, such as TEM, SEM can rapidly image large areas of sample and is relatively easy to operate. It also uses a relatively low energy of electrons and therefore does typically not cause as much damage to a soft biomaterial as TEM. A Zeiss SUPRA 55-VP FEGSEM (field emission gun scanning electron microscope) is used for the following work.

In order to create a micrograph with SEM, a beam of primary electrons is directed towards the sample. These electrons interact with the specimen and cause other electrons to be emitted; these latter, so-called secondary electrons, are detected at a low angle (close to the surface) and used for creating an image of the sample. Secondary electrons are ejected from the valence band of the sample and carry information about the surface topography as their low energy does not allow them to escape from the sample if they have been generated more

than around 50 nm below the surface.[4] It is also possible to use backscattered electrons which are higher in energy and detected at a higher angle (close to the electron source). They carry information about the topography and atomic number of the sample, and probe it to a larger depth.[5]

The beam of electrons is scanned over the sample in a raster fashion to cover all points in a selected area. The secondary electron detector records an intensity at each point in the raster scan. This intensity is input to a cathode-ray tube (CRT) whilst the scan is taking place which produces a digital image of the sample in real time.[6]

The fact that SEM uses electrons instead of visible light means that it has a resolution of about 10 nm. This is because the energy of electrons typically used in SEM corresponds to a wavelength which is much smaller than the wavelength of visible light. Equation 2.1 shows that wavelength is directly proportional to the resolution, so that shorter wavelength electrons allow smaller objects to be observed.

SEM is typically an ionising technique and it is thus necessary to coat non-conductive samples with a conductive layer and then to ground them before placing them in an SEM. This prevents sample charging which would distort the electrons trajectories and thus the resulting image. Graphite was used here to coat the FF fibres. This results in a 250 Å layer of amorphous conductive carbon layer deposited on the sample.

A 10 μL solution of FF fibres in water was deposited onto a silicon substrate with a pipette and this was left in a fume hood overnight so that all of the water evaporated. This dried sample was coated in amorphous carbon and placed into the SEM (initial attempts to image uncoated samples resulted in highly distorted images). For this work the samples were imaged using a primary electron beam energy of 2 keV. In general, higher electron energies produce better quality images, however 5 keV was found to damage the fibres and 2 keV was therefore used as the best compromise between image quality and sample preservation.

The main drawback of SEM is that the sample must be dried, carbon coated, and then placed in a vacuum in order to be imaged. These conditions are far from the

standard conditions in which the fibres grow. This makes it impossible to look at any dynamic properties of the fibres with this technique.

2.1.2.1 Drying Effects

A further drawback of the necessity to work with dry samples is that the very act of drying a sample of fibres in solution can significantly alter its size distribution. In fact, as long as peptides are present in solution, removal of the solvent can cause a rapid and spatially inhomogeneous increase of the local supersaturation which leads to their further assembly into fibres, both adding to already existing fibres or creating new ones. The resulting sample is thus generally quite different from the starting sample and not representative of the fibre size and shape distribution as would have been observed under the standard conditions defined at the beginning of this chapter.

Several attempts were made to minimise or avoid these drying effects in order to use SEM to characterise the fibres. These methods all involved taking aliquots of the sample at different times during the growth process, followed by different attempts to remove the solution without evaporation. These methods included filtering and rapid solution pouring and are described in detail in Chapter 3. Another method used to avoid drying effects was cryo-SEM as described in the next subsection.

2.1.2.2 Cryo-Scanning Electron Microscopy

The main drawback of SEM is that it is impossible to observe a sample in ambient conditions. Whilst cryo-SEM does not completely overcome this problem, it does go some way to addressing it. Instead of drying the sample, a drop of it is frozen quickly in its solvent, typically with liquid nitrogen, and this frozen sample is placed in the SEM. This requires a special attachment chamber to a standard SEM. In this work the Zeiss SUPRA 55-VP FEGSEM was used with the Gatan Alto 2500 cryo-transfer system. After the sample has been frozen it is placed in this cryo-chamber and a knife which is inside the chamber is used to slice the drop of frozen sample. This exposes some of the fibres embedded in the frozen solvent and standard SEM can be used to image the exposed surface. The sample stage within the SEM is cooled in order to prevent sublimation.

2.1.3 Transmission Electron Microscopy

TEM has some similarities to SEM; it uses an electron beam, which is shone at the sample, and the electrons that interact with it are detected and used to create an image. However, its setup and the path followed by electrons from the source to the detector have more similarities with an optical microscope used in transmission mode. TEM works by firing a beam of highly energetic electrons through an extremely thin sample and by using a series of lenses to magnify and project the emerging electrons onto a fluorescent screen which creates an image of the specimen. TEM is not a scanning technique, but instead images all of the sample field of view simultaneously.

Electrons used for TEM typically have a much higher energy than those in SEM, usually around 200 keV. This is because the detector is placed on the opposite side of the sample to the electron source, so the electrons must have enough energy to penetrate through the thickness of the whole sample in order to be detected. This also imposes strict requirements on the sample; it must be less than 200 nm thick in order to be electron transparent. It must also be deposited onto a TEM grid, typically a thin copper grid of around 500 μm. These high-energy electrons can damage biomaterials or even completely destroy them. Overall the whole sample preparation procedure and the actual operation of the microscope is significantly more complex than SEM and typically requires a high level of skill and training. The main advantage of TEM is that, due to the high-energy beam, it is possible to achieve a higher magnification and a better spatial resolution than SEM. Moreover, TEM probes the whole depth of the sample, as opposed to SEM which only interrogates the surface.[7] A JEOL 2100 TEM was used in this work.

2.2 Simulations

Simulations are an invaluable tool to scientists as they can investigate systems which are impossible, costly or impractical to study in the laboratory. They can offer a deeper understanding of the reasons that cause a system to behave in a certain way, which makes them particularly useful in materials science.

There are many types of computer simulations which have been developed to study atoms and molecules to gain a deeper understanding of the behaviour of a system. From quantum mechanical methods, which can investigate events on the femtosecond time scale and the Å length scale, to fluid dynamics, which looks at large systems on the micron and millisecond length and time scales.[8] In this work, molecular dynamics simulations (MD) are used; this is an intermediate method that allows for nanosecond timescales to be probed and nanometer lengths. It is the most suitable for simulating a collection of many identical FF molecules, as they are approximately 1 nm in size. The time scale in MD is not appropriate for witnessing self-assembly events of large numbers of FF molecules, however this does not mean that it is not a useful technique in understanding the assembly. In order to obtain timescales relevant to self-assembly, a more coarse-grained method would have to be used; however, as discussed in Chapter 1, this does not successfully reproduce the real dynamics of FF. Therefore, atomistic MD must be used. There are several ways of adapting MD to speed it up, allowing for rare processes to be seen. One of these is metadynamics, and this is discussed in Section 2.2.2.

2.2.1 Molecular Dynamics [8, 9, 10, 11, 12, 13]

The discussion in this section follows that given in Phillips *et al*. Classical MD simulations are based on solving Newton's second law of motion

$$F = ma \tag{2.3}$$

where F is the force acting upon on a particle, m is its mass and a, its acceleration. This is solved numerically, with the acceleration of each particle due to the forces caused by interactions with other particles calculated at every time step. The force is calculated from a potential energy function. NAMD is a simulation package designed to implement MD for biomolecules and is used for all simulations in this work. The potential energy function used in NAMD is made up of five terms. Three of these terms describe covalently bonded atoms: they are stretching, bending and torsional bonded terms, defined by the following three equations.

$$U_{bond} = \sum_{bond\ i} k_i^{bond} (r_i - r_{0i})^2 \tag{2.4}$$

$$U_{angle} = \sum_{angle\ i} k_i^{angle} (\theta_i - \theta_{0i})^2 \tag{2.5}$$

$$U_{dihedral} = \sum_{dihedral\ i} k_i^{dihedral} [1 + \cos(n_i \phi_i - \gamma_i)] \tag{2.6}$$

where U is the potential energy "bond" refers to the number of covalent bonds, "angle" refers to pairs of covalent bonds which share a single atom at the apex and "dihedral" is defined as the atoms which are separated by 3 consecutive covalent bonds. The final two terms describe interactions to atoms that are not bonded to each other, or to a common atom. The first is the Lennard-Jones potential, which approximates the interaction between two neutral particles.

$$U_{LJ} = \sum_i \sum_{j>i} 4\varepsilon_{ij} \left[\left(\frac{\sigma_{ij}}{r_{ij}} \right)^{12} - \left(\frac{\sigma_{ij}}{r_{ij}} \right)^{6} \right] \tag{2.7}$$

where U_{LJ} is the Lennard-Jones potential, r is the distance between the two particles, ε is the depth of the potential well and σ is the distance at which the

potential between the particles is zero. The first term describes the overlap repulsion and the second term specifies the attraction due to van der Waals forces. The final term in the potential describes the Coulombic interaction between two particles.

$$U_C = \sum_i \sum_{j>i} \frac{q_i q_j}{4\pi\varepsilon_0 r_{ij}} \tag{2.8}$$

where q is the charge on the particle. The parameters in Equations 2.4 – 2.8 are usually found by fitting to a combination of experimental and quantum mechanical modelling data. The Equations 2.4 – 2.8 and the set of associated parameters together constitute the "force field" or "potential energy". There is no known perfect force field, and so defining the force field is equivalent to formulating the model of the system. In this work we have used the CHARMM27 force-field, which has been developed over 40 years and now provides a good description of many biologically relevant molecules, including amino acids (see references [14] and [15]). The last two non-bonded interactions present a problem when performing MD simulations as all of the atoms partake in non-bonded interactions with all other atoms. Therefore the calculation time for each timestep is large. A cut off is usually introduced for the Lennard-Jones potential, which means the interaction between particles that are far apart (in this case, 12 Å) is set to zero. This is a good approximation, as the Lennard-Jones potential goes to zero as $O(r^{-6})$ as the distance tends to infinity. However, with the Coulombic interaction, there is no cut off as this goes to zero too slowly (as $O(r^{-1})$) and instead, the particle mesh Ewald method is used (PME).

The PME is only used in the case of periodic boundary conditions, which are a set of conditions which approximate an infinite system by creating images of the unit cell to surround it. These images create an infinite lattice, where all atoms in the simulation not only interact with others in the unit cell, but also with the atoms in the images surrounding the unit cell. The PME is used in this case as the number of Coulombic interactions between all atoms and their images is too

large to calculate. In this work the PME is used when periodic boundaries are used. The PME is a fast method for calculating the Ewald sum of the electrostatic interactions. The Ewald sum consists of two parts: short-range and long-range interactions. The sum of the short-ranged interactions quickly converges, but the sum of the long-ranged interactions does not. However, the sum of the Fourier transform of the long-ranged interactions does converge so this is used for the PME in NAMD. The fast Fourier transform is used which involves mapping the charge density field onto a discrete uniform lattice, hence the particle mesh Ewald name.

Once the potential is known, the force can be calculated using the following equation.

$$F = -\nabla U \tag{2.9}$$

This must be done for all particles in the system, so that the total force acting on each particle is found. Then Equation 2.3 is used to calculate the acceleration, and this acceleration can be used to calculate the new position of the particle after a given time interval. This is repeated for all particles in the system at each time step. In order to calculate the new position of the particle from the acceleration, numerical integration must take place. There are several different numerical integration methods which can be used for this. The NAMD simulation package is used for all simulations in this work, and it uses an extension of the Verlet method for numerical integration. The Verlet method produces a more accurate result than simpler methods, such as Euler's (Equation 2.10). It is derived from the Taylor expansion for $r_{t+\Delta t}$ (Equation 2.11).

$$r_{t+\Delta t} = r_t + v\,\Delta t \tag{2.10}$$

$$r_{t+\Delta t} = r_t + v_t \Delta t + \frac{1}{2} a_t (\Delta t)^2 + \frac{da}{dt}\frac{\Delta t^3}{6} + O(\Delta t^4) \tag{2.11}$$

where r is the position of the atom, v is its velocity and t is the time. In a similar way, $r_{t-\Delta t}$ can be found.

$$r_{t-\Delta t} = r_t - v_t \Delta t + \frac{1}{2} a_t (\Delta t)^2 - \frac{da}{dt} \frac{\Delta t^3}{6} + O(\Delta t^4) \tag{2.12}$$

Equations 2.11 and 2.12 are then summed to eliminate the second and fourth terms to produce the equation for finding the new position of a particle used in the Verlet method.

$$r_{t+\Delta t} = 2r_t - r_{t-\Delta t} + a_t (\Delta t)^2 \tag{2.13}$$

This method therefore eliminates the velocity entirely from the equation, but instead, requires the position of the particle at the previous timestep as well as the current one. However, an expression for the velocity can still be calculated by subtracting Equation 2.12 from 2.11.

The NAMD software uses Langevin dynamics for the Canonical ensemble (constant number, volume and temperature), which is a modification of Newton's second law.

$$F = ma + \gamma m v - R(t) \tag{2.14}$$

where γ is the friction coefficient, v is the velocity, and $R(t)$ is a Gaussian random process.

$$R(t) = \sqrt{2 k_B T \gamma m \delta (t - t')} \tag{2.15}$$

where k_B is Boltzmann's constant, T is the temperature of the heat bath, and $\delta(t-t')$ is the Dirac delta function. The last two terms in Equation 2.14 represent the coupling to a heat bath; this is used in order to keep the system at a constant temperature, T. The Canonical ensemble is used in this work unless otherwise stated. Equation 2.14 has more terms than Equation 2.3, so the numerical integration becomes slightly more complicated. The Brünger-Brooks-Karplus (BBK) method, which is an extension of the Verlet method for Langevin dynamics, can be used to integrate Equation 11. This is Equation 2.15, known as the BBK integrator.

$$r_{t+\Delta t} = 2r_t - r_{t-\Delta t} - \frac{\gamma \Delta t}{2}[r_{t+\Delta t} - r_{t-\Delta t}] + \frac{(\Delta t)^2}{m}[F + R(t)] \tag{2.16}$$

This equation is used to calculate the new position of the atoms in an MD simulation. The total of the new positions of atoms at each timestep results in a simulation trajectory that can then be analysed.

2.2.1.1 Parameters [16, 17]

The FF structure used in this work was obtained from the Cambridge structural database. Chimera was used to build structures with many FF molecules. Unless otherwise stated, the simulations were carried out at 300 K with a 2 femtosecond timestep. The structures were solvated with TIP3P water. The length of all bonds in a molecule involving hydrogen atoms were constrained to a fixed length, which also makes water atoms completely rigid.

2.2.1.2 Root Mean Squared Deviation

The root mean squared deviation (RMSD) is a parameter which is used in the following work to analyze the trajectory of the simulations. It is a measure of how much on average the atoms in the structure move away from a reference structure, which in this case is the crystal structure. Firstly the structure is rotated and translated at each timestep to be overlaid with the initial configuration (Figure 4.1 (a)) and then Equation 2.17 is applied to calculate the average distance of all of the atoms from their starting point.

$$RMSD = \sqrt{\frac{\sum_{i=1}^{N_{atoms}} \left(r_i(t) - r_i(t_0)\right)^2}{N_{atoms}}} \tag{2.17}$$

where r is the position of the atom, t is the current time and t_0 is the initial time. This provides information about the physical stability of the structure.

2.2.2 Metadynamics [18]

Many experiments require tens or even hundreds of thousands of atoms to be simulated. The computational cost of calculating the dynamics of this is high, particularly when multiplied by the number of timesteps needed to see certain events. One reason that events can take a long time to occur is because the system gets stuck in a local energy minimum and may stay there for many nanoseconds. This is illustrated in Figure 2.2 (a). In this case, other energy minima will not be found in the length of time of a simulation, which is many nanoseconds. One way to overcome this is to use metadynamics. Metadynamics is a way to encourage the system to move away from its current configuration. In order to explain metadynamics it is first important to define collective variables (CVs).

CVs describe the process of interest and are biased during the simulation. For example, one might use the centre of mass of a group of atoms as the collective variable. The system is pushed away from values of the CV that have been visited for long periods of time, so in this case the group of atoms would be pushed to move around rather than stay stationary as they might have done in an MD simulation. This increases the chances of rare events being observed.

The forcing of the system away from states that have already been sampled is done by adding a Gaussian term to the potential energy function for that point. A common analogy used is that of filling in wells with sand. This addition increases the energy of being at that point, which makes it more likely that the

simulation will move away from this region. In our example this would result in the centre of mass of the atoms moving around during the simulation, driven by the Gaussian terms that are added periodically. This is illustrated in Figures 2.2(b) and (c). More and more Gaussians are added over time and the system will eventually escape the free energy well and be able to explore another part of the landscape. As the number of Gaussians added is known, it is possible to work backwards to find the true free energy landscape. The centre of mass would be the x-axis of Figure 2.2, and a Gaussian would be added to the energy of the average position that it held since the last Gaussian was added, and so would bias the trajectory to move away from that region.

In this work we have used the centre-of-mass separation between two groups of atoms as the CV. One group is an FF molecule and the other is a collection of FF molecules assembled into a fibre fragment. This is so that the metadynamics simulation will ensure that a range of centre of mass separations is simulated within a reasonable timescale. This collective variable is described in detail Section 4.2. The PLUMED plugin was used with NAMD in order to perform Metadynamics simulations.[19]

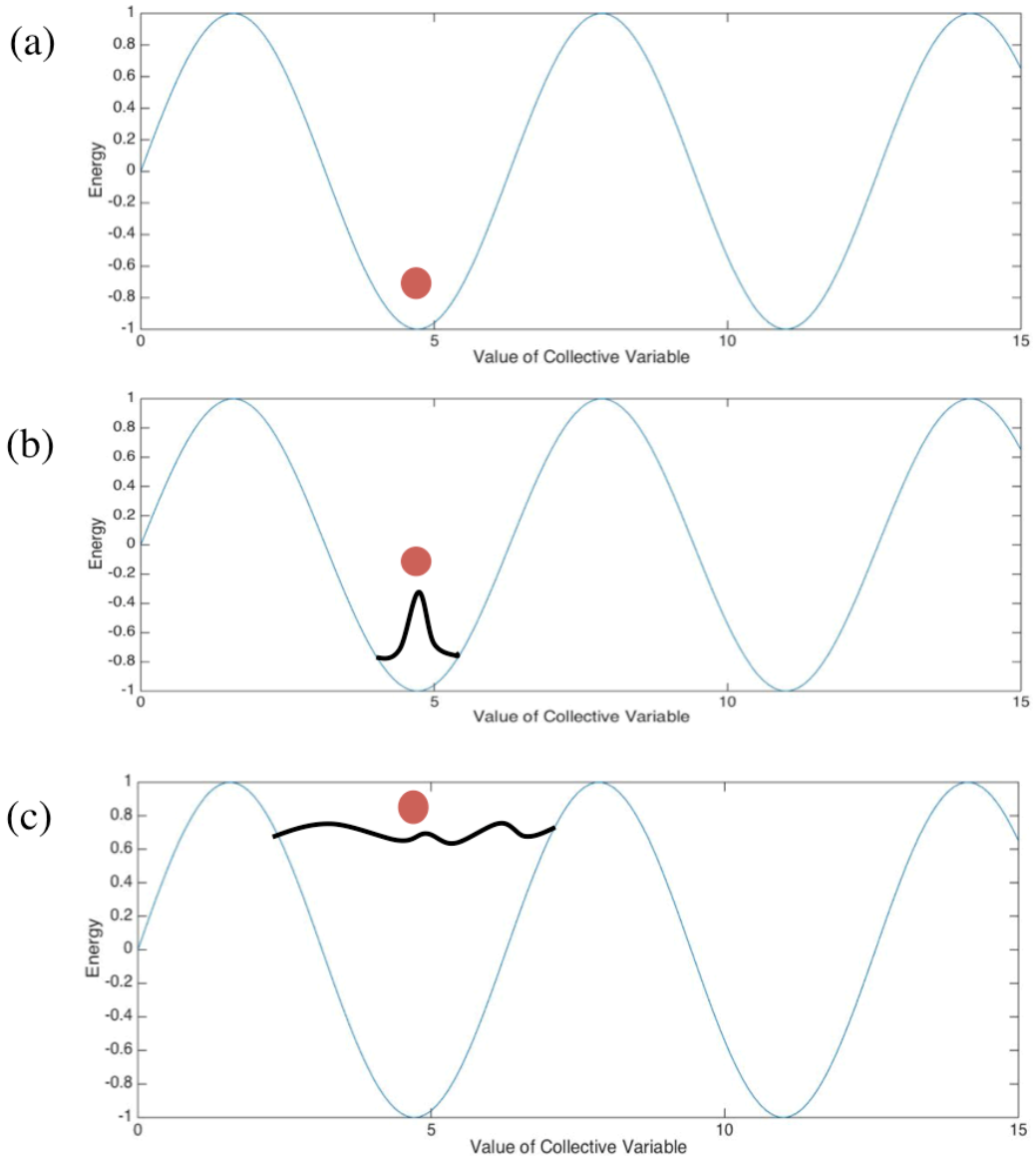

Figure 2.2 *(a) The free energy landscape of a system. The red dot represents the location of the system. (b) After the simulation has been running for a period of time, a Gaussian will be added to the average position in the landscape where the system is located. The black curve represents the Gaussian filling in the trough. (c) After more time, many Gaussians have been added causing the system to move away from the energy minima that it would have otherwise been stuck in.*

2.3 Spectroscopy

Spectroscopy forms a useful suite of techniques for looking at the behaviour and characterisation of a system of molecules, particularly if they are optically active. It allows for *in situ* measurements to be performed, as there is no requirement for drying. It is a quick, simple and non-invasive technique to carry out and so it can be used to look at fast, dynamic processes without any damage to the sample. There are a variety of spectroscopy techniques available, but in this work the majority of spectroscopy experiments performed were linear dichroism (LD). This was found to be the most useful for this system for several reasons which are discussed in Section 2.3.2. In order to understand LD, we first need to consider absorption spectroscopy.

2.3.1 Absorption Spectroscopy [20, 21]

Absorption spectroscopy makes use of the interaction between light and matter to probe the presence and amount of atoms or molecules present in a sample. Molecules can exist in many different electronic states, and this state can be modified upon interaction with electromagnetic (EM) radiation. The EM spectrum is shown in Figure 2.3. Different wavelengths of light can be used to probe different transitions in a molecule. The energy of a wave is related to its wavelength by the de Broglie equation (Equation 2.17).

$$E = \frac{hc}{\Lambda} \tag{2.17}$$

where E is the energy of the wave, Λ is its wavelength, h is Plank's constant and c is the speed of light in a vacuum. This relationship allows us to choose a specific wavelength of light in order to probe a transition of certain energy. In our absorption spectroscopy we choose the UV and visible wavelengths of light in order to probe electronic transitions.

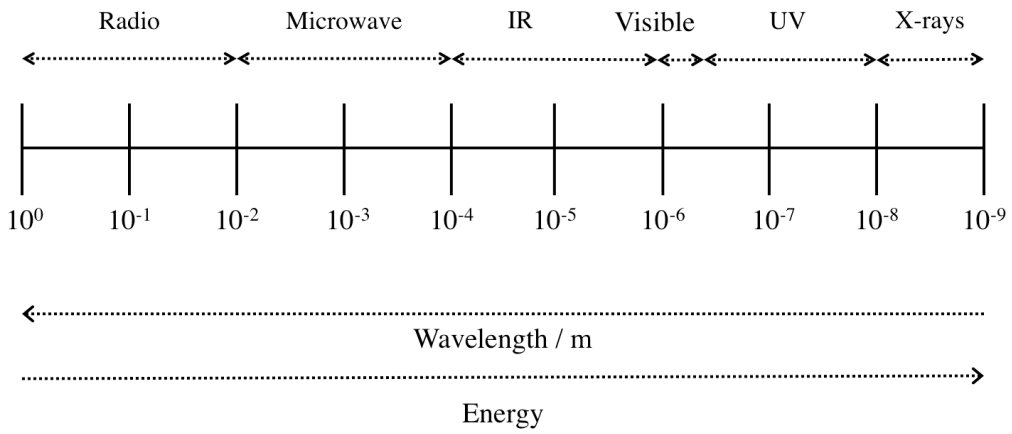

Figure 2.3 *The electromagnetic spectrum from long to short wavelengths.*

Electrons exist in discreet energy levels within a molecule and absorption spectroscopy allows us to excite electrons from their ground state, E_0, to an excited state, E_1, if we select the wavelength of light that has an energy equal to the difference between E_1 and E_0 (Figure 2.4). Once the electron has absorbed the photon, it will eventually lose the energy and return to the ground state. This loss can be through collisions with other molecules, converting the photon to heat, or emission of the photon. Absorption spectroscopy can be used to identify the molecules in a sample as different molecules have different absorption spectra.

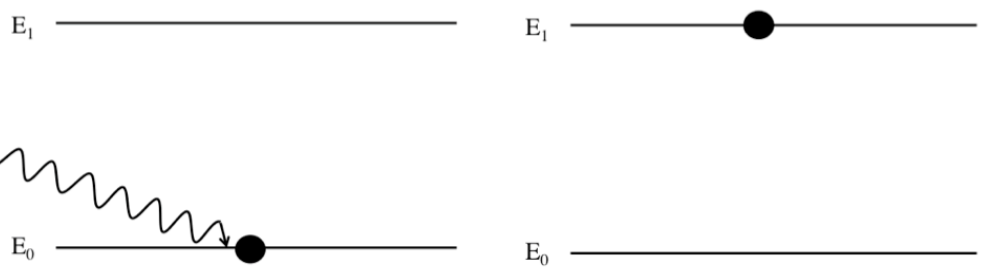

Figure 2.4 *Schematic illustration of a molecule absorbing a photon and being excited to a higher energy level. To a first approximation this can often be viewed as a single electron being excited from one orbital to another.*

All peptides have chromophores in their backbone which absorb UV light with wavelengths between 180 and 220 nm. Phenylalanine also has an aromatic

chromophore which can be excited from the ground state to its first excited state by shining light with wavelengths between 250 and 260 nm onto it.

A UV–visible absorption spectrophotometer consists of a light source which produces light with wavelengths typically between 187 and 900 nm. In the instruments used in this work, the light was spread by either a prism or a diffraction grating into a spectrum of light. The light is shone upon a slit, which only allows a small section of the light through, corresponding to the wavelength of light required. This slit can be moved, or the crystal/grating rotated, to select different wavelengths of light during an experiment, to produce an absorption spectrum which is a function of wavelength. This system is called a monochromater. The monochromatic light is then shone onto the sample. If the light is of the appropriate wavelength, the sample will absorb it. There is a photodetector placed on the other side of the sample to detect the amount of light which has passed through it (*i.e.* not been absorbed). When this is plotted as a function of wavelength a spectrum results. When the sample absorbs some light, the photodetector will detect a decrease in the amount of photons passing through the sample. The output from this experiment is the absorbance (A) which is defined in Equation 2.18 and is the ratio of the log of the intensity of incident light (I_0) and the light detected after it has passed through the sample (I).

$$A = log_{10}\left(\frac{I_0}{I}\right) \tag{2.18}$$

The absorbance increases as the intensity of light detected decreases, so we see a peak in the spectrum when the sample absorbs light. The intensity of this signal is (in the absence of intermolecular interactions or absorbance signals in excess of 3) proportional to the concentration of chromophores in the sample, so it is possible to calculate the concentration of a substance c using absorption spectroscopy with the Beer-Lambert law (Equation 2.19).

$$A = \varepsilon c l \tag{2.19}$$

This equation shows that the absorbance is directly proportional to the concentration of chromophores, the path length of the cuvette used to hold the sample, l, and the extinction coefficient, ε. In this work a Jasco V-660 spectrophotometer was used for all absorption measurements.

2.3.2 Linear Dichroism

Linear dichroism (LD) is a spectroscopic technique which has been shown to be a valuable tool for investigating the kinetics of fibre formation, as well as for structural characterization on small volumes of samples.[22] Dafforn *et al*. have shown that LD can be used to study fast kinetics of reactions of biological fibres such as the Aβ fibre assembly and the long-chain assemblies of α_1-antitrypsin polymers.[22] LD has also been used to observe biological processes such as DNAse digestion of DNA and GTP-induced polymerization of the bacterial cell division protein FtsZ.[23] Marshall *et al*. have used LD to investigate the structure of a small peptide derived from the yeast prion Sup35.[24] They were able to show the change in orientation of the tyrosine residue over time as the fibre geometry changed.

LD is an extension of absorption spectroscopy that can be used not only to identify molecules and their concentrations, but can also give information about the orientation of bonds within a sample. In this technique, instead of a single light beam, two perpendicular beams of linearly polarised light are shone onto the sample and the difference in absorbance of each of these polarisations is measured. In our instruments the two polarisations are incident alternately and a lock-in amplifier used to 'know' when each is passing through the sample. The particles in the sample must be oriented and one beam of light is parallel to this orientation direction and the other is perpendicular to it.

$$LD = A_{parallel} - A_{perpendicular} \tag{2.20}$$

Net alignment of molecules in the sample is thus essential for a non-zero LD signal because the electronic transition moments will only absorb light when they are aligned with the electric field of linearly polarised light. In the absence of an

oriented sample $A_{parallel}$ and $A_{perpendicular}$ are the same. The relationship between the LD signal and the orientation of the molecules is

$$LD = \frac{3}{2}SA_{isotropic}(3cos^2\alpha - 1) \quad (2.21)$$

where $A_{isotropic}$ is the absorbance of an unoriented sample, α is the angle between the transition moment and the alignment axis, and S is the orientation parameter, S =1 for an oriented sample and 0 for an isotropic one.

In this work, Couette flow has been used to orientate the fibres, in a cell consisting of a spinning capillary containing the sample, with a stationary rod in the middle (Figure 2.5). The molecules become aligned in the flow, and are potentially able to be detected by linear dichroism. The Couette cell is placed in a Peltier temperature controlled cell available from Dioptica Scientific Ltd Rugby UK. It has a 3 mm internal diameter capillary that spins at ~3000 rpm with a stationary 2.5 mm outer diameter rod suspended in the middle. A background spectrum is taken with no spinning (as we expect no signal from the isotropic sample) and subtracted from the spinning spectrum. When a series of measurements are taken the first non-spinning spectrum is used as a background for all of the subsequent measurements. A Jasco J-815 circular dichroism (CD) spectrometer adapted for LD spectroscopy was used in this work.

LD is particularly well suited for looking at the assembly of fibres. When a small molecule, such as a small peptide, is in solution it will not align in flow as it has a low aspect ratio. Once these small molecules have started to assemble into an elongated structure, they are able to align in flow, so they will produce an LD signal at their absorption frequencies. Couette flow is used as a means of aligning molecules in LD as the detector has the advantage of being able to observe elongated assemblies without detecting the corresponding monomers. This is because molecules that are not long enough to align in flow are invisible to LD. The fibre LD signal increases over time as the number of monomers in the fibres increases.

LD was used to investigate the kinetics of assembly of FF fibres. There were several challenges associated with using LD for this system because of the size of the fibres, the weakness of their chromophore, and their propensity for sticking to the narrow LD capillary which is difficult to clean. Small fibres are invisible to this technique because they are not long enough to be able to align in shear flow. There is also a maximum length that can be detected accurately for the fairly rigid fibres of this work dictated by the diameter of the capillary. The capillary has an inner diameter of 3 mm, and we eventually realized that when fibres grow longer than this they get stuck in the capillary and can no longer align properly in the flow (Figure 2.5). Therefore, the signal that we get from them after this point is no longer comparable to the signal from when they were shorter than 3 mm. However, when the fibres are short, LD can tell us all about the time frame of the kinetics.

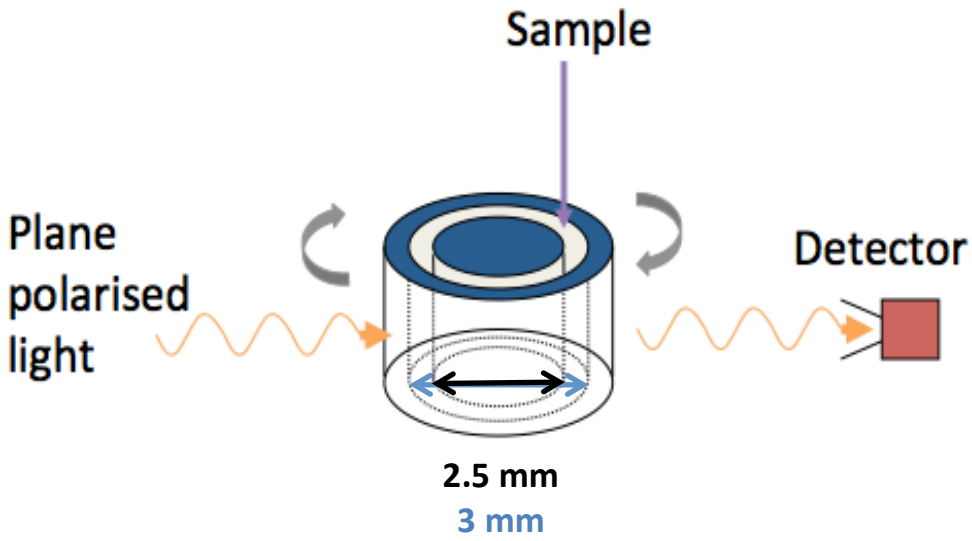

Figure 2.5 *The setup of the linear dichroism experiments of this work. Two perpendicular beams of linearly polarized light are shone at a sample which is in a spinning capillary with a stationary rod in the middle. The difference in absorbance of the two polarisations of light is measured by the detector.*

Phenylalanine's aromatic chromophore is a particularly weak one, and is usually not considered in the spectroscopy of proteins as tryptophan has a much stronger aromatic chromophore that absorbs light of the same wavelength. However, it

was essential to use this chromophore in this work as there is only phenylalanine present in FF. In order to increase the signal to noise ratio in the data, multiple accumulations of the same spectrum can be measured, and then averaged. However, it takes around 1.5 minutes to measure each spectrum, so in order to have good time-resolution data, the number of accumulations must be minimized. The optimal compromise between these two parameters was found to be 2 accumulations for each time point, 226 seconds apart, which is the time it takes to do 2 accumulations with the following parameters: a 1 nm bandwith, a 0.2 nm data pitch, a 0.5 second digital integration time, and a scanning speed of 100 nm/min. Therefore a kinetics measurement consisted of a background measurement at time zero with the spinning switched off, and then 2 spectra were measured and averaged to give one spectrum for each time point. This was repeated for 10848 seconds (~3 hours).

The fibres also stuck to the inside of the capillary, and the outside of the rod after each experiment, and did not come off after the standard method of cleaning. Old fibres seeded the formation of new ones so effective cleaning was essential. LD capillaries are difficult to clean as they are narrow, so usually they are rinsed several times with ethanol and water. In order to remove the fibres the capillary and rod had to be cleaned in a nitric acid bath. However, nitric acid degrades the plastic part of the rod, which is at the top, and the araldite of the capillary, which is used to seal up the bottom. Therefore new capillaries and rods were designed which have a Teflon stopper at the bottom and a Teflon cap at the top of the rod. A tool was designed to remove the Teflon stopper for cleaning. These were supplied by Crystal Precision Optics (Figure 2.6). This allowed for them to be soaked in a nitric acid bath overnight between experiments to eliminate any organic material left on them.

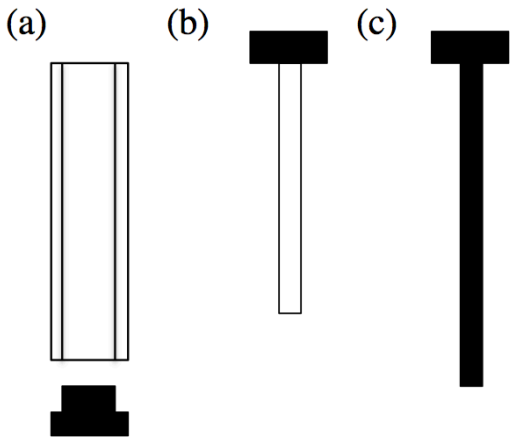

Figure 2.6 (a) *The new quartz capillary with a Teflon bottom that can be removed and cleaned in nitric acid. (b) The new quartz rod with a Teflon cap (black) at the top that can be cleaned in nitric acid. (c) Teflon tool for removing the bottom of the capillary in (a).*

Another problem encountered was the intense scattering signal produced by the fibres as they became large, which dominated the absorbance and LD spectra in later parts of kinetics runs. Light scattering is a function of wavelength and the size and shape of a particle. The fibres start to scatter light as they grow, and this scattering increases as they become larger. This is shown in the spectra in Chapter 5. The scattering part is the sloped curve going from 220 to 350 nm. It is diagonal because of the functional dependence on wavelength. In order to eliminate this scattering contribution a new background spectrum needs to be taken at each time point, instead of just at the start of the experiment. The spinning must be switched off for the background spectrum at each time point, which was not possible with the current hardware, so a new electronic LD sequencer was built.

The new sequencer is attached to the instrument that controls the spinning, the spectrophotometer and the computer (Figure 2.7). It enables the spinning to be programmed to switched on or off between measurements. This sequencer works by sending a trigger signal to the computer whilst switching the spinning on or off. This happens every 226 seconds, which is the time it takes to measure one time point.

The computer is programmed to wait for a trigger from the sequencer, which occurs at the moment when the spinning is switched on or off. Once the computer receives this trigger, it takes the next measurement. This always happens every 226 seconds, so that the sequencer changes state between spinning or not spinning every 226 seconds and the instrument measures the spectrum upon this change. This results in a series of spectra that alternately have the spinning switched off and the spinning switched on. The spectra with the spinning switched off can then be used as a background spectrum for the subsequent spectrum which has the spinning switched on. Ideally, this would eliminate any signal which is from light scattering rather than absorption. However, when this sequencer was used with FF fibers, it was found that the larger fibres stayed aligned when the sequencer switched the spinning off. This proved to be because the fibres length is comparable to the diameter of the capillary, so the fibres cannot move freely and they become stuck in the oriented fashion which they were in when spinning. Therefore the non-spinning spectra still had LD peaks in, rather than just the light scattering. This sequencer was not always used in this work unless stated. It is ideal for kinetics of other, smaller systems. It is possible to change the time period from 226 seconds to any desired time, and there is also a delay switch on the sequencer. This switch introduces a delay of 10 minutes into each iteration; this allows for the temperature to be changed and equilibrated if desired between measurements. The data from a typical series of experiments is shown in Chapter 5.

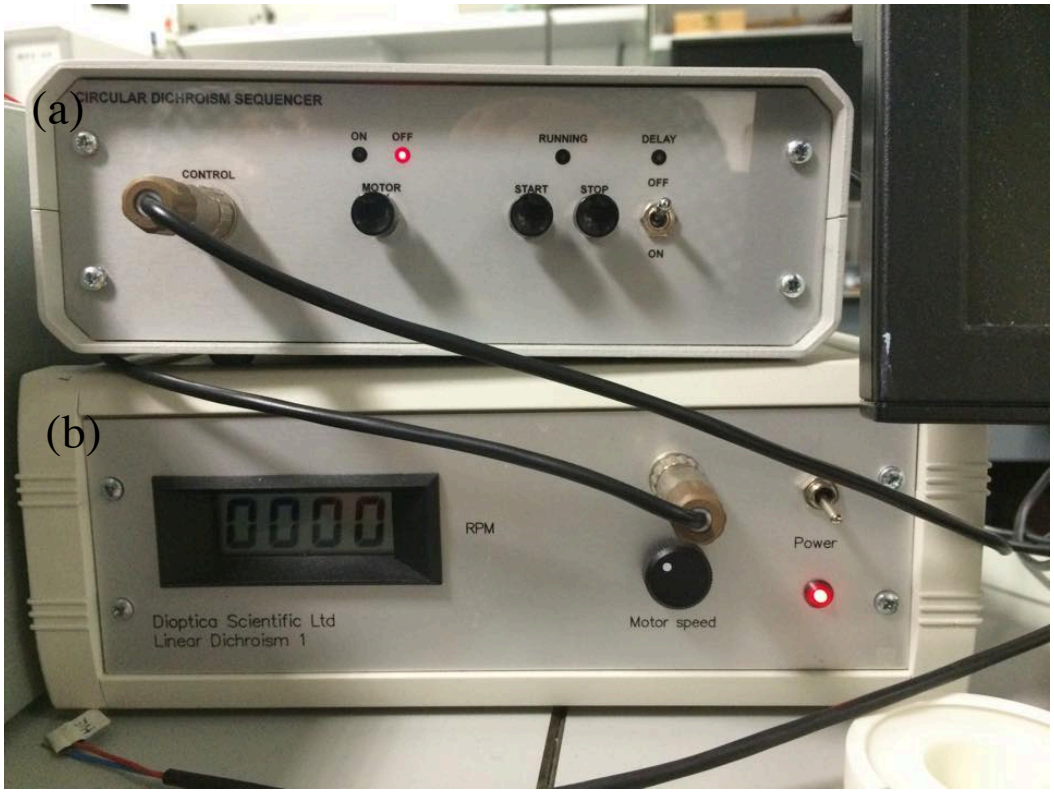

Figure 2.7 *(a) The new sequencer which allows for the spinning of the LD cell to be switched on and off automatically. (b) The control box for spinning the LD cell.*

In order to use the sequencer, a macro must be written in the Jasco J-815 CD spectrometer software. This was used for the kinetics measurements reported in Chapter 5. The variable temperature LD measurements were done using a macro. A background spectrum was taken with the spinning switched off at 70 °C and then the program was run. The macro was written so that it cooled the sample at 1 °C/min for 5 minutes and then took a measurement and repeated this until it reached 20 °C. In the case of cooling and heating measurements the macro then heated up from 20 °C in increments of 5 °C/min and took a measurement at each increment. The data for these experiments are shown in Chapter 5.

2.3.3 Right Angle Light Scattering

Right angle light scattering (RALS) is an easy technique to perform using a standard spectrofluorimeter. It is used in this way mainly in the life sciences to follow the kinetics of reactions. Marrington *et al*. have used this technique

coupled with LD to follow the assembly of the bacterial protein FtsZ into a polymer and the subsequent bundling.[25] They were able to measure the polymerization kinetics and the effects of Ca^{2+} and Mg^{2+} on this process by using RALS. It was also used by Mayer and Amann to monitor the polymerization of the bacterial actin MreB, and the effect of concentration on this process.[26] It is an attractive technique because it is very simple to carry out, and can be used on a variety of sizes and shapes of particles.

In this work a Jasco FP-600 spectrofluorometer was used for RALS measurements. It has a Peltier cell attachment, which was used for temperature control during experiments. The cuvette used for RALS in this work was 1 cm × 1 cm which is much bigger than the LD capillary. This means that there are no issues with the fibres becoming as large as the vessel holding them, and there is no problem with orientation as there is in LD, because RALS does not require particles to be oriented. Monochromatic light is shone onto the sample and the intensity of this light scattered at 90 ° is detected. This is very quick because only one wavelength is used per time point, rather than the whole spectrum as in LD. Therefore, the temporal resolution is much better than LD and a measurement was taken every second. As the size of the particles increases, the amount of light scattered also increases, so we can monitor the growing fibres. This is useful as a complementary technique to LD as, it allows us to probe the small fibres at the early stages which are invisible to LD, as well as probing large fibres that are so big that they get stuck in the narrow LD capillary.

An angle of 90 ° is ideal for light scattering measurements as this avoids the detection of light which passes straight through the sample, without interacting. Also by using a wavelength of light that is not absorbed by the sample, we avoid detecting emitted light, and instead, only detect light which has scattered. In this case 350 nm was used as FF does not absorb light at this wavelength.

The drawback of RALS is that although it is possible to detect that the size of the particles is increasing, the nature of the particle is unclear. It is necessary to use another technique, in this case LD or microscopy, to check that it is fibres that

are present, and not another large shape such as spheres or amorphous aggregates. It is possible to calculate the size of particles based on the light scattering intensity, if the shape of the particles is known and the sample is homogenous. However, the fibres were found to be heterogeneous so it was impossible to extract quantitative data about their size without using another technique, such as microscopy.

References

[1] Tkaczyk, T. C. (2010). Field Guide to Microscopy. *Spie*

[2] Shong, C. W., Haur, S. C., & Wee, A. T. S (2010). *Science at the Nanoscale*. *Pan Stanford Publishing*.

[3] Wöhler, C. (2013). 3D Computer Vision. Efficient Methods and Applications. *Second Edition*. *Springer*.

[4] Wittke, J. H. (2008). www4.nau.edu/microanalysis/microprobe-sem/signals.html. Accessed 16/03/2015

[5] Egerton, R. F. (2005). Physical Principles of Electron Microscopy. *Springer*

[6] Hunter, E. E. (1993). Practical Electron Microscopy: A Beginner's Illustrated Guide. *Cambridge University Press*

[7] Willaims, D. and Carter, B. (2009). Transmission Electron Microscopy: A Textbook for Materials Science. *Springer*

[8] Grotendorst, J., Marx, D., & Muramatsu, A. (2002). Quantum Simulations of Complex Many-Body Systems: From Theory to Algorithms. *NIC Directors*.

[9] Griebel, M., Knapek, S., & Zumbusch, G. (2000). Numerical Simulation in Molecular Dynamics. *Springer*.

[10] Schachinger, E., & Stickler, B. A. (2014). Basic Concepts in Computational Physics. *Springer*.

[11] Phillips, J.C. et al. (2005). Scalable Molecular Dynamics with NAMD. *J. Comput. Chem., 26(16),* 1781-1802.

[12] Frenkel, D., & Smit, B. (2002). Understanding Molecular Simulation. *Academic Press*.

[13] Brooks, B. R., Brooks III, C. L., Mackerell, A. D., Nilsson, L., Petrella, R., J., Roux, B., Won, Y., …Karplus, M. (2009). CHARMM: The biomolecular simulation program. *J. Comp. Chem., 30,* 1545-1615.

[14] Vymetal, J. & Vondrášek, J. (2010). Metadynamics As a Tool for Mapping the Conformational and Free-Energy Space of Peptides – The Alanine Dipeptide Case Study. *J. Phys. Chem. B, 114(16),* 5632-5642.

[15] König, G., Bruckner, S. and Boresch, S. (2013). Absolute Hydration Free Energies of Blocked Amino Acids: Implications for Protein Solvation and Stability. *Biophys. J., 104,* 453-462.

[16] Allen, F. H. (2002). The Cambridge Structural Database: a Quarter of a Million Crystal Structures and Rising. *Acta Cryst., B58,* 380-388.

[17] Pettersen, E. F., Goddard, T. D., Huang, C. C., Couch, G. S., Greenblatt, D. M., Meng, E. C., & Ferrin, T. E. (2004). UCSF Chimera—A Visualisation System for Exploratory Research and Analysis. *J. Comput. Chem., 26(16),* 1781-1802.

[18] Ferrario, M., Ciccotti, G., & Binder, K. (2006). Computer Simulations in Condensed Matter Systems: From Materials to Chemical Biology. *Springer.*

[19] Bonomi, M *et al.* (2009). PLUMED: a portable plugin for free-energy calculations with molecular dynamics. *Comp. Phys. Chem., 180,* 1961-1975.

[20] Platt, Y., & Stutz, J. (2008). Physics of Earth and Space Environments. *Springer.*

[21] Norden, B., Rodger, A., & Dafforn, T. (2010). Linear Dichroism and Circular Dichroism. *RSC Publishing.*

[22] Dafforn, T., Rajendra, J., Halsall, D. J., Serpell, L. C., & Rodger, A. (2004). Protein Fiber Linear Dichroism for Structure Determination and Kinetics in a Low-Volume, Low-Wavelength Couette Flow Cell. *Biophysical Journal, 8,* 404-410.

[23] Cheng, X., Joseph, M. B., Covington, J. A., Dafforn, T. R., Hicks, M. R., & Rodger, A. (2012). Continuous-Channel Flow Linear Dichroism. *Analytical Methods, 4,* 3169-3173.

[24] Marshall, K. E., Hicks, M. R., Williams, T. L., Hoffmann, S. V., Rodger, A., Dafforn, T. R., & Serpell, L. C. (2010). Characterizing the Assembly of the Sup35 Yeast Prion Fragment, GNNQQNY: Structural Changes Accompany a Fiber-to-Crystal Switch. *Biophysical Journal, 98,* 330-338.

[25] Marrington, R., Small, E., Rodger, A., Dafforn, T. R., & Adinall, S. G. (2004). FtsZ Fiber Bundling Is Triggered by a Conformational Change in Bound GTP. *The Journal of Biological Chemistry. 279 (47),* 48821-48829.

[26] Mayer, J. A., & Amann, K. J. (2009) Assembly Properties of the Bacillus subtilis Actin, MreB. *Cell Motiliy and the Cytoskeleton, 66,* 109-118.

Chapter 3

Microscopy Results

3. Microscopy Results

Microscopy has been key to the discovery and characterisation of FF fibres as discussed in the introduction. It is the only method to our knowledge which can reveal the fine details of their sizes and shapes and give direct information about the size distribution of these highly polydisperse systems as other techniques, such as spectroscopy, average over the entire fibre population. Previous microscopy work has shown that FF fibres are nano and micron-sized objects with an extremely high aspect ratio and a hexagonal cross section. This chapter starts with the results from SEM, which was employed to determine the size distribution of fibres after they had stopped growing. The speed of the fibres assembly was then varied and SEM was further used to observe the effect this change had on their size distribution. However, this did not allow for *in situ* measurements, as vacuum conditions are required for the operation of SEM. For the same reason it was also impossible to observe the size of fibres during the growth process, rather than at the end. TEM was used in an attempt to observe the fibres at different stages in their growth by cryo-preservation. Finally optical microscopy which, thanks to its compatibility with the aqueous solution fibre growth conditions, allowed the acquisition of real-time videos of the fibres assembly process to take place, but with lower spatial resolution then electron microscopy.

3.1 SEM

SEM was used to characterize the fibres' morphology, shape and size distribution. The fibres were synthesized and left in water overnight so that they had finished growing and the single peptides had been depleted (see Section 5.3). Then 10 μL of the solution was deposited onto silicon and left to evaporate in a fume hood overnight.

Figure 3.1 shows a typical sample of FF fibres synthesised by the method described in Chapter 2, with the modification that the solution was cooled to room temperature rather than left at 40 °C at the end of the process. The heterogeneity of the fibres is evident and larger than what has been reported in most previous literature:[1,2] the fibre diameters in Figure 3.1 range from hundreds of nanometres to tens of microns. Figure 3.2 shows that not all of the fibres are hollow as was previously thought.[1,2] For example Gazit states that 'the majority of structures are hollow tubes; however, in the self-assembly process, the ends of some tubes can become narrow'.[3] In Figure 3.2 (b) the fibres appear to be not only covered over at the end, but filled in for the whole length of the fibre. On the contrary, many are hollow such as the fibres in Figures 3.2 (a) and (c). Their hexagonal cross section, discussed in Chapter 1, is also visible in these images.

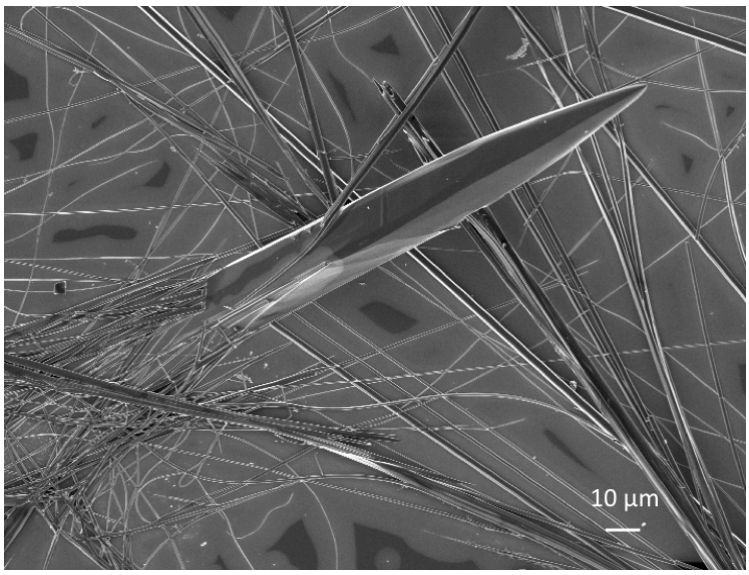

Figure 3.1 *A sample of FF fibres observed by SEM, showing their heterogeneous nature.*

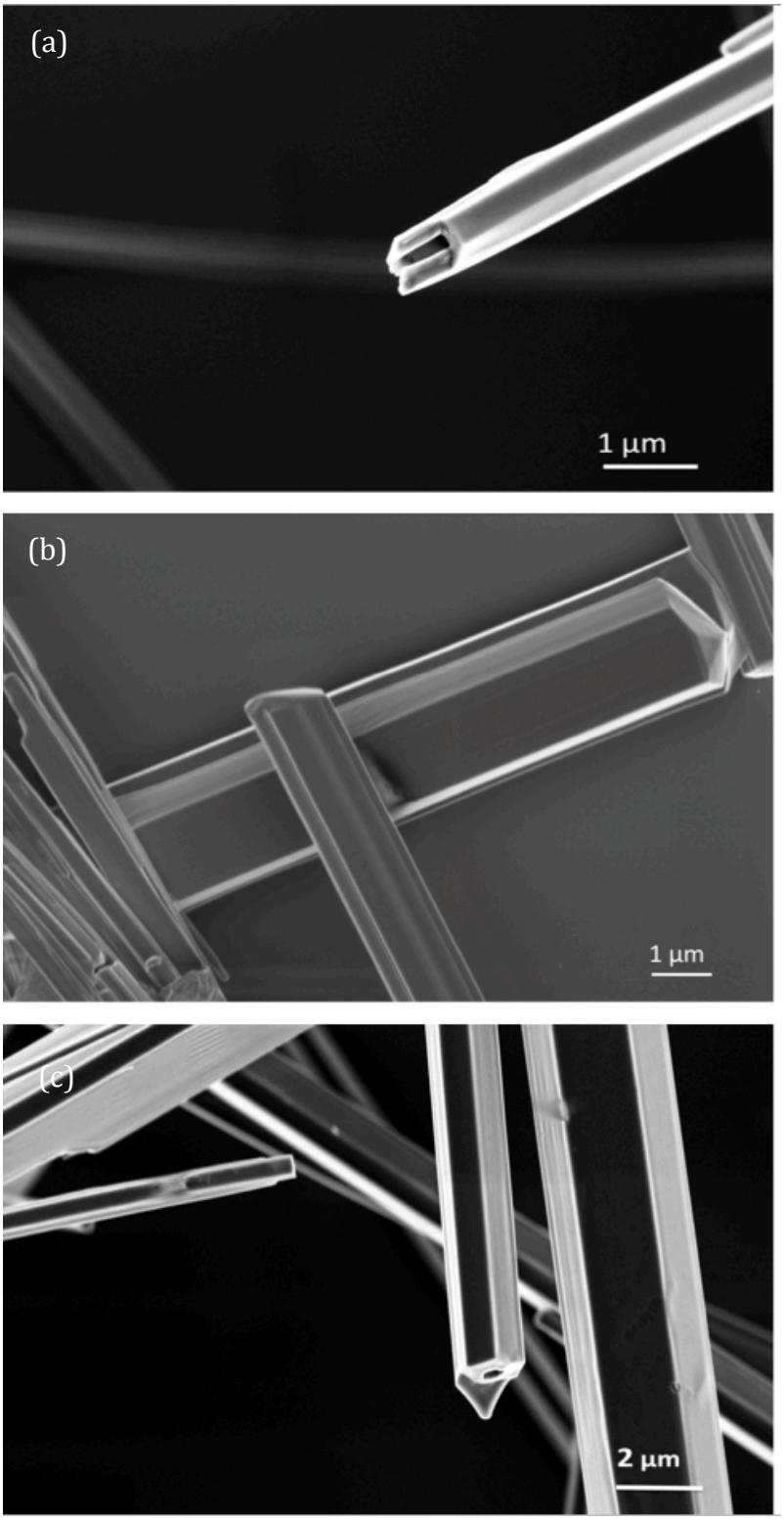

Figure 3.2 *Hexagonal FF fibres observed by SEM (a) A hollow fibre. (b) Fibres which appear to be filled in throughout their length. (c) Several hexagonal FF fibres.*

30 similar SEM images were captured for several samples of FF fibres in order to determine their size distribution. The widths of the fibres were measured using ImageJ software and plotted in Figure 3.3. It was first suggested that the fibre diameters only exist on the nanoscale,[1] however, in this work it was found that most fibres are much larger than this, and that there is a much wider range of sizes than has typically been shown before.[1] The average fibre diameter obtained from Figure 3.3 is 2.8 μm with a standard deviation of the mean of 78 %. It was very difficult to determine the diameter of the smaller fibres as they tend to be close together, as shown in Figure 3.1, so it is difficult to distinguish them. SEM also does not have a high enough resolution to see smaller, nano-sized fibres and as a consequence, the distribution in Figure 3.3 probably underestimates the contribution to the bin in the 0 – 1 μm. It was not possible to measure the lengths of fibres, as most of the time they extended over the field of view of the microscope. Moreover, fibres are often entangled (Figure 3.1) and this also hampers the possibility of properly evaluating their length.

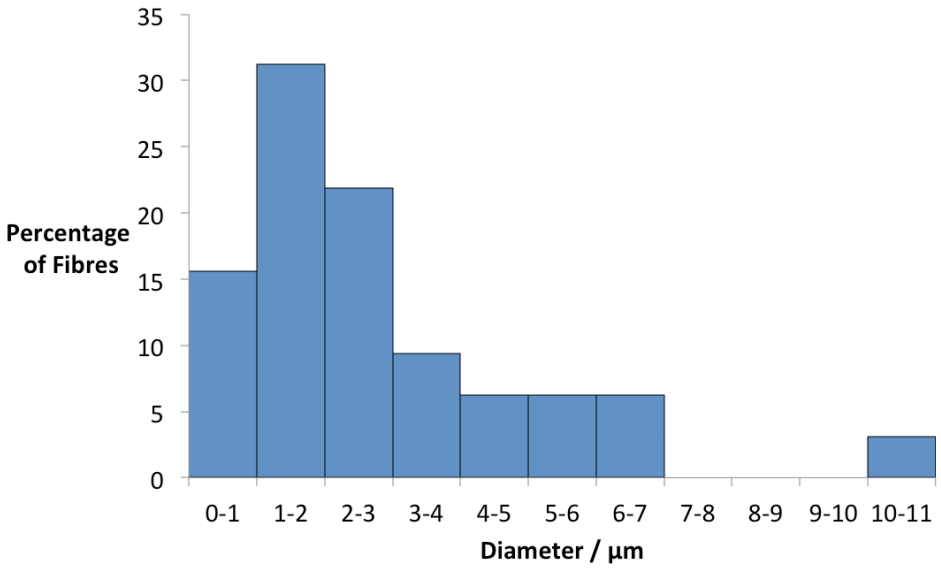

Figure 3.3 *Histogram of the distribution of the FF fibres widths evaluated from SEM images.*

Growth of the fibres is a process which depends upon the conditions that the fibres are in and as SEM is not an *in situ* technique it is important to ask oneself if the fibres in the images are really representative of the moment when the aliquot has been removed. This is probably not the case as when an aliquot is taken from a reaction mixture and deposited onto a substrate, the solvent starts to

evaporate and the concentration of single peptides increases. This change in conditions will cause the single peptides to self-assemble either by joining fibres or nucleating and growing new ones.

In order to control the fibre growth, many modifications have been made to the sample preparation procedure for SEM imaging with the aim of getting a better representation of the fibres shape and size distribution *in situ*. These methods included cryo-SEM – to freeze the fibres during the assembly process, various attempts of filtering the solution to separate the fibres from their growth solution without evaporation and rolling the solution off the substrate. These will be discussed in details in section 3.1.2 – 3.14 while section 3.1.1 shows the results that can be obtained from experiments using standard evaporation followed by SEM imaging.

3.1.1 Temperature-Controlled Fibre Synthesis

In the previous section the heterogeneity of a sample of FF fibres was demonstrated, however this quality is undesirable if the fibres are to be used for any type of application. Therefore, it is important to understand how the fibres grow in order to control their assembly so that they can be made more homogenous. These fibres form upon cooling, so one way to control their assembly might be to control the speed of cooling. Three different cooling rates were used and the size and homogeneity of the fibres produced by these methods were compared. In the previous section, the fibres were left to cool at room temperature overnight, however, in this section the fibres were cooled in a controlled way, using a Peltier fluorescence cuvette. This allowed for very precise control of the temperature of a sample. The three temperature gradients used were 2 °C/min, 1 °C/min and 0.5 °C/min. They were cooled in decrements of 10 °C at the specified cooling speed and then left to equilibrate for 10 minutes and this cycle was repeated until the sample reached 20 °C. A 10 µL drop of the fibre solution was then deposited onto a silicon surface, left to dry at room temperature for 24 hours, and analysed by SEM.

When the peptide solution was cooled from 70 °C to 20 °C at a speed of 2 °C/min, no visible fibres were observed, but instead the peptide precipitated.

This suggests that a cooling speed of 2 °C/min is too fast to initiate any proper fibre growth and instead the peptides, which have a low solubility in water at room temperature, simply precipitate. Cooling speeds of 1 °C/min and 0.5 °C/min were successful in producing fibres, but the different methods produced only slightly different size distributions.

Figure 3.4 shows an SEM image of FF fibres which were formed by cooling the rsolution at 1 °C/min. The average width of these fibres was found to be 0.7 μm, with a standard deviation of the mean of 45 %. Figure 3.5 shows an image of the fibres formed by cooling at 0.5 °C/min. These fibres had a mean diameter of 0.5 μm and standard deviation of the mean of 72 %. These values can be compared with the values from fibres that form when left to cool at room temperature, which is slower cooling than under these controlled conditions. We can estimate the rate of cooling using the heat transfer equation below.

$$Rate\ of\ cooling = \frac{kA(\Delta T)}{d} \qquad (1)$$

where k is the thermal conductivity, A is the surface area, ΔT is the temperature difference and d is the thickness. When the solution is at 70 °C it will cool quickly at a rate of around 5 °C/min but when the solution is at 25 °C it will have slowed down to a rate of 0.5 °C/min. The mean width in that situation was 2.8 μm with a standard deviation of the mean of 78 %. These results suggest that the fibres cooled at room temperature can grow to much larger widths than the fibres under controlled conditions, and therefore temperature can be used as a way to control fibre growth.

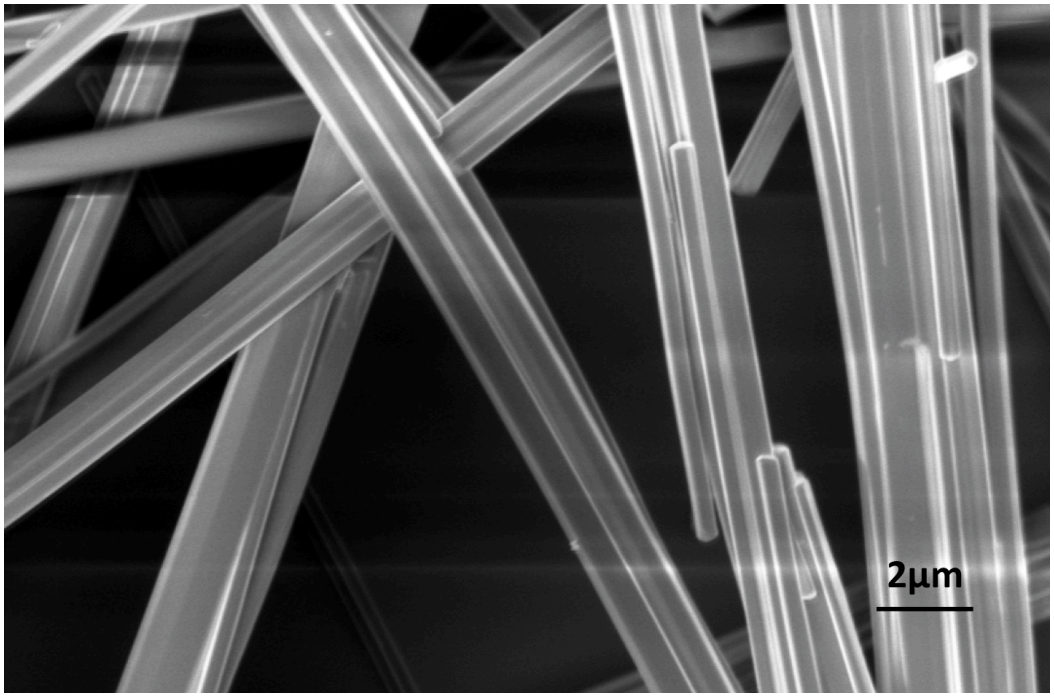

Figure 3.4 *FF fibres formed by cooling a solution of peptides at 1 °C/min, imaged by SEM.*

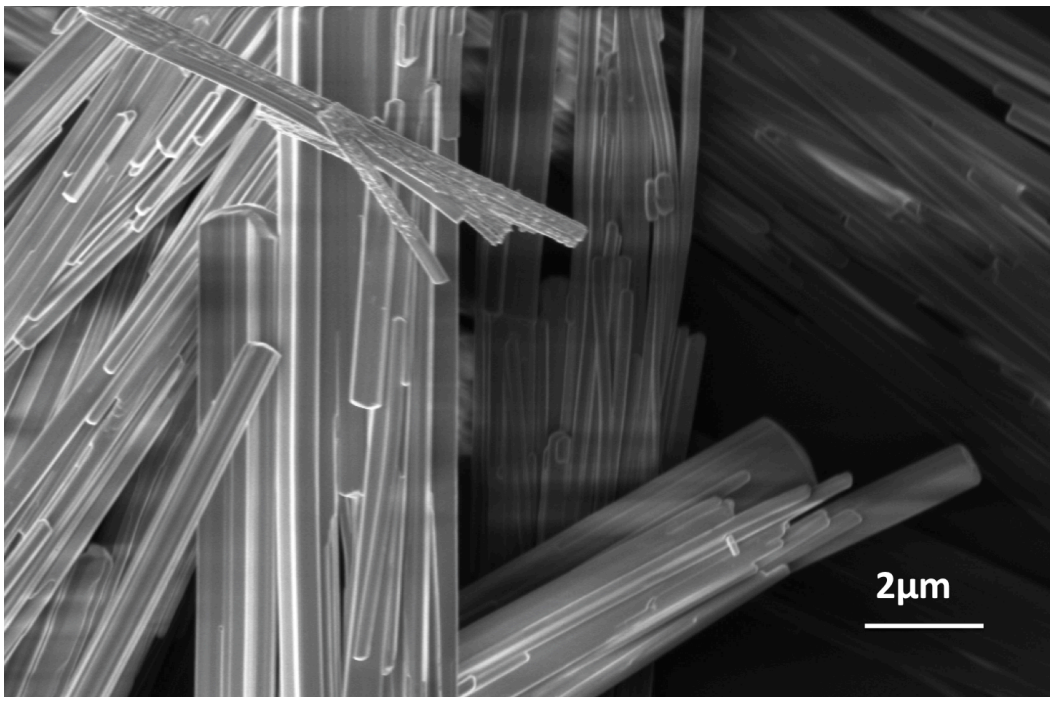

Figure 3.5 *FF fibres formed by cooling a solution of peptides at 0.5 °C/min, imaged by SEM.*

3.1.2 Cryo-SEM

With cryo-SEM it is possible to quickly freeze a sample and to image it without being limited by the issue of the vapour pressure of the solvent being incompatible with the vacuum conditions of the microscope. When applied to the FF fibres, the idea was to analyse samples at different time points during growth whilst they were still suspended in the solvent, with the aim of getting frozen snapshots of the fibres time evolution. The latter could then be correlated with the results of other kinetic techniques such as spectroscopy to help understand the fibre growth process.

In order to test the suitability of the technique, a sample of fibres was used that had finished growing, *i.e.* a sample that had been left overnight in solution. A drop of this solution was immersed in liquid nitrogen and the resulting frozen sample was placed into the SEM. Prior to the actual measurements, the top of the frozen drop was sliced off with a knife, leaving a flat surface that is exposed to the primary electrons of the SEM. Despite the cutting, not all fibres will be cut in two and some fibres are left sticking out of the ice and can be imaged.

Figure 3.6 shows the results of this experiment. Very few fibres could be observed that were shrivelled up and clearly not representative of the structures in solution. The small number of fibres meant that it was impossible to ascertain the fibre size distribution and therefore this technique was not pursued any further.

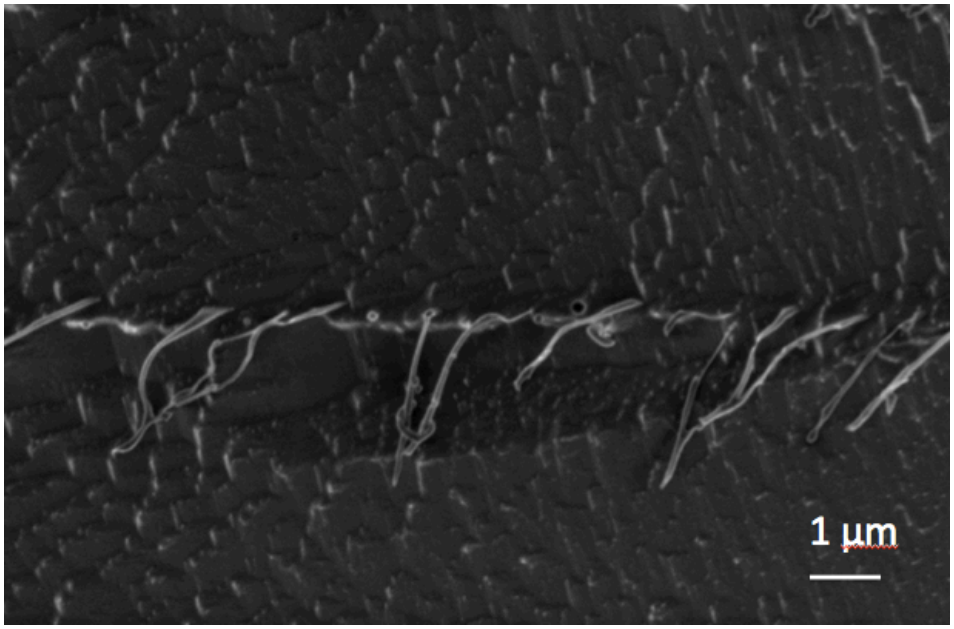

Figure 3.6 *A cryo-SEM image of FF fibres. The black background is ice and the fibres are sticking upwards out of it.*

3.1.3 Filtered Samples

Another method tested to avoid drying effects in SEM was to use a filter in order to remove most of the solution from the fibres before they were imaged. The solution was pushed through a 10 μm filter using a syringe, with the aim of retaining all larger fibres while removing the smaller ones and water which contained single peptides. The surface of the filter was then coated in carbon and imaged in the SEM. The original idea was to repeat this procedure at different moments during growth in order to obtain information on the changes in the fibres size distribution versus time.

Figure 3.7 shows the resulting SEM image of the filter which appears very bright. This is because the substrate is made of a non-conductive material, which results in a negative charging because of electron build-up upon irradiation. The incoming electron beam gets thus significantly deflected, and this causes the charged surface to show up as a bright area.

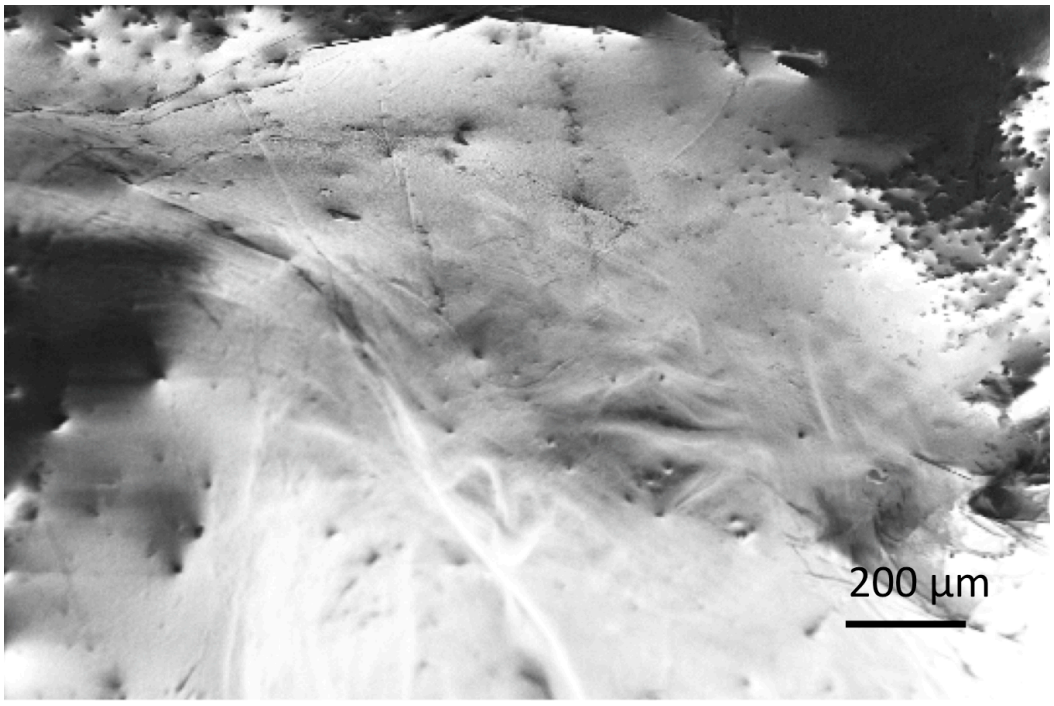

Figure 3.7 *An SEM image of a filter with fibres deposited onto it.*

Although the filtration method appears to successfully remove water from the fibres, it does not allow for successful imaging of the fibres. This is because a

filter is not a suitable substrate for use in an SEM. Therefore, this technique was not pursued further to study the fibres growth.

3.1.4 Water Tipped Off

Another method attempted in order to remove water whilst avoiding drying effects was to simply tilt the silicon substrate so that the water rolled off after the sample had been deposited, leaving the fibres behind. In order to test the effectiveness of this technique, fibres were synthesised using the standard method described in Chapter 2. The cooling of the solution was done in an LD capillary whilst LD measurements were being taken at intervals. The corresponding LD results are shown in Chapter 5. Aliquots were taken from this capillary at the start of the experiment and then at 80, 160 and 240 minutes.

The first aliquot (0 minutes) was deposited onto the silicon substrate and the water was rolled off as described above. The sample was then analysed in the SEM and the resulting images are shown in Figure 3.8. As this was the start of the experiment, the expectation was that no fibres would be present. However, Figure 3.8 (a) clearly shows a number of fibres. It is also clear from Figure 3.8 (b) that remnants of the 10 μL of water must have been still present on the sample after the tip-off and that the remaining solution has dried while shrinking. This will have caused a successive increase of the monomer concentration until they have started to assemble into the fibres that can be seen in Figure 3.8 (a). We can therefore conclude that this method also does not remove enough water to stop fibres from assembling and that the SEM images of the different aliquots cannot be assumed to faithfully represent the fibre population at the time the aliquot was removed from the growth solution.

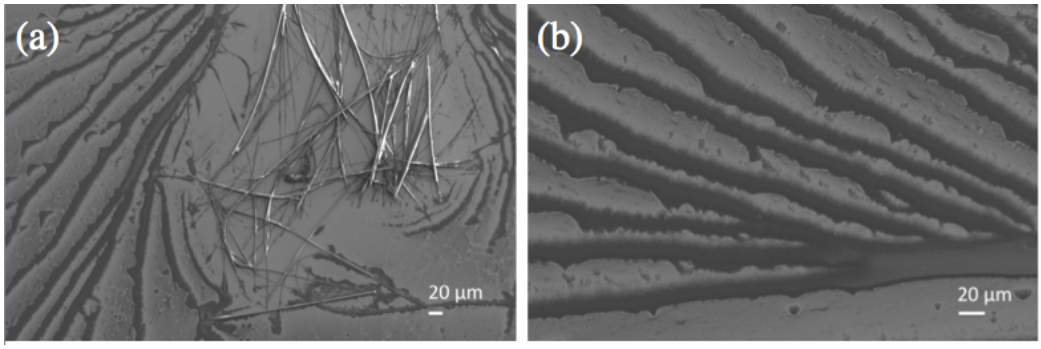

Figure 3.8 *SEM images from the aliquot taken at the start of an experiment monitoring the kinetics of FF dissolved in water at 2 mg/ml. (a) shows fibres and (b) shows water marks.*

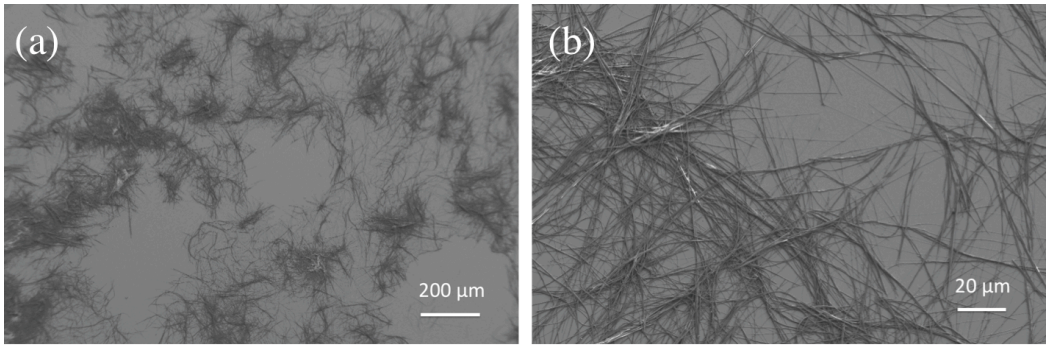

Figure 3.9 *SEM images from the second aliquot, taken 80 minutes into an experiment monitoring the kinetics of FF dissolved in water at 2 mg/ml.*

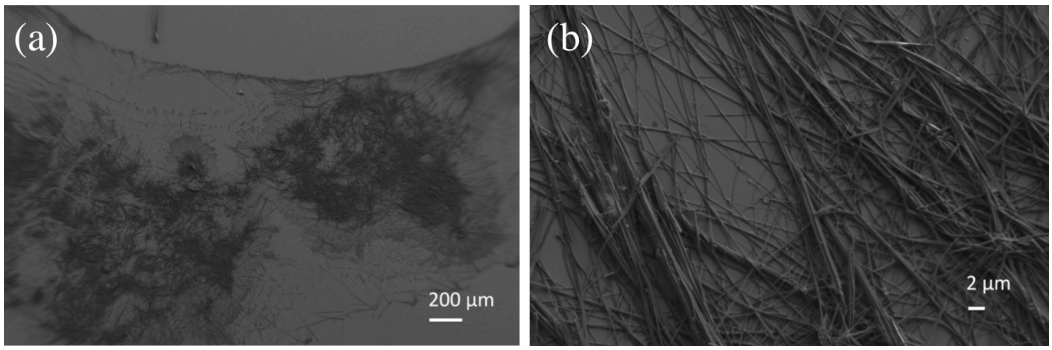

Figure 3.10 *SEM images from the third aliquot, taken 160 minutes into an experiment monitoring the kinetics of FF dissolved in water at 2 mg/ml.*

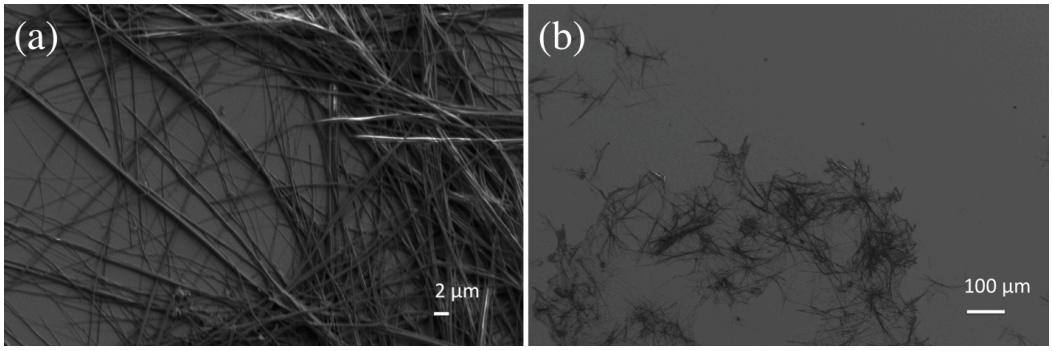

Figure 3.11 *SEM images from the fourth aliquot, taken 240 minutes into an experiment monitoring the kinetics of FF dissolved in water at 2 mg/ml.*

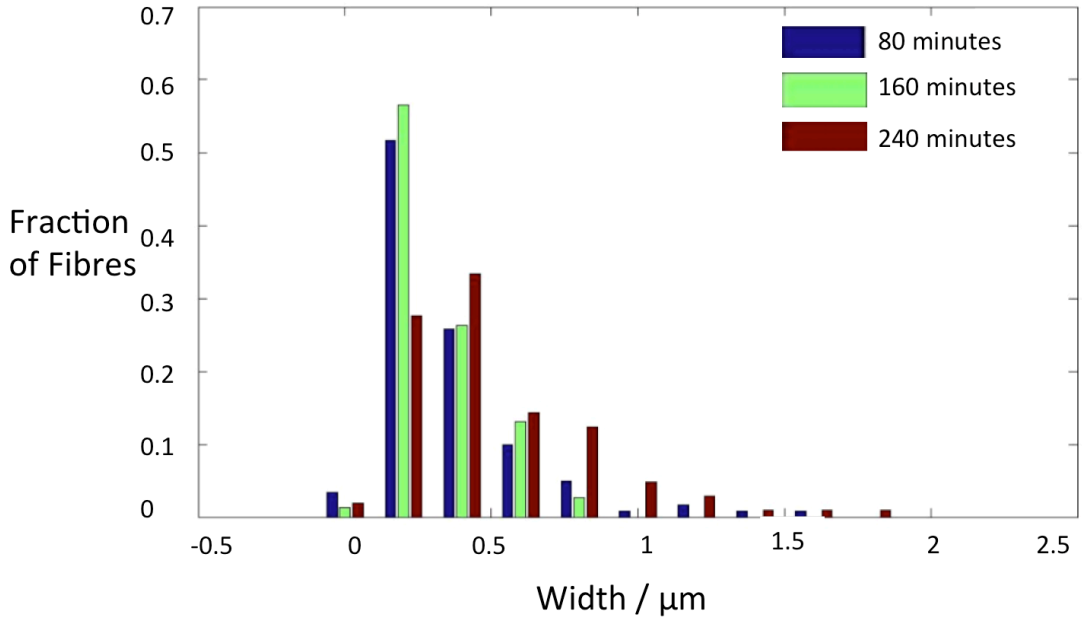

Figure 3.12 *Histogram of the widths of the FF fibres at 80, 160 and 240 minutes during their growth in water.*

Nevertheless, when comparing the SEM images of the three different aliquots (Figures 3.8 – 3.11), a clear trend can be observed in the evolution of the measured fibre size distribution. As illustrated in the histogram in Figure 3.12, the diameters of the fibres shift to larger sizes, as expected (the 0 minute time point was not used as there was an insufficient number of fibres for significant statistics). However, because of the previous observation about the formation of fibres upon evaporation of the solvent, histograms as that of Figure 3.12 cannot be used for a further quantitative analysis of the fibre population during growth.

3.2 TEM

Cryo-TEM is a popular microscopy technique which has been used to view different stages in the assembly of biomolecules into supramolecular structures leading to the discovery of their assembly mechanism.[4,5,6] Therefore, TEM was attempted on the FF fibres with a view to using cryo-TEM to image intermediate stages in the growth process.

TEM requires the electrons to permeate through the depth of the sample in order to be detected on the other side. Therefore a sample must be thin and the thicker a sample is, the higher the energy of electrons needs to be to penetrate the sample. Gazit and co-workers analysed small autoclaved FF fibres which were under 200 nm in diameter using TEM.[7] However, the fibres used in this work have a much larger size range, reaching widths of up to tens of microns, so high electron energies must be used. Initially a beam energy of 200 keV was used. However, this immediately damaged and destroyed the sample. Next, a lower energy of 80 keV was used, but this still destroyed the fibres. This is considered to be a low energy for TEM as it is typically not enough to penetrate through a thin sample. Therefore, a lower energy would certainly not penetrate through the fibres so TEM could not be used to image them. Sampling can also be an issue with imaging fibres on a grid with TEM, as the fibres may fall through the grid spacing when deposited so alternative methods had to be found.

3.3 Optical Microscopy

In order to image the fibres *in situ*., as opposed to the dry conditions required by electron microscopes, optical microscopy was used. Optical microscopes allow the size and shape of the fibres to be viewed whilst they are in solution. These microscopes also have a much wider field of view than electron microscopes which allows the whole length of a fibre to be measured. Finally, it is possible to use a specially adapted microscope, described in Section 2.1, to follow the fibre growth in real time.

3.3.1 Confocal Microscopy

First, a confocal optical microscope with 50 – 1000 times zoom was used as a further means to characterise the fibres. The fibres were grown in the same manner as in previous sections, by being heated to 70 °C at 2 mg/ml in water and then cooled to 20 °C. The fibres were then deposited onto the glass microscope slide and another slide was placed on top, so that the fibres were still in solution. The fibres were imaged at room temperature and two of these images with different magnifications are shown in Figure 3.13. These images show that it is possible to measure the width of some of the fibres using this technique. However, the resolution of the confocal microscope is much lower than that of SEM so it is hard to distinguish the fibres' hexagonal faceting and difficult to measure their widths. The large field of view of this microscope does capture the whole length of some fibres, however it is also difficult to measure lengths precisely in these images as the fibres are entangled and overlaid with each other.

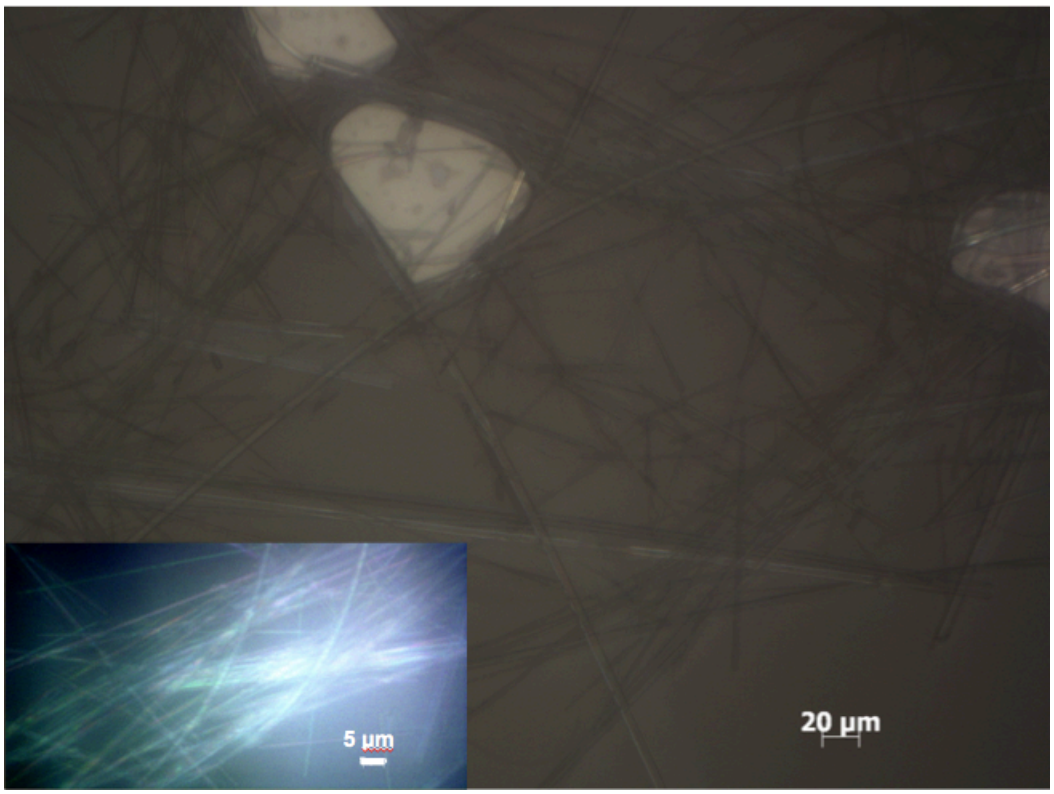

Figure 3.13 *Optical microscope images of FF fibres viewed with a confocal microscope.*

Confocal microscopy was subsequently used in an attempt to observe the fibres assembling in real time. The peptide was dissolved in water at 70 °C and a concentration of 2 mg/ml. A drop of this solution was deposited in between two microscope slides which is a good approximation to the solution used in spectroscopy experiments (Chapter 5). The microscope slides had been heated in an oven to 40 °C, which meant that the solution was quickly cooled to the temperature of the slides. The slides were then placed under the microscope and an image was acquired every 5 minutes during the experiment at the same location. However, at the end of this experiment no fibres were observed. Instead a precipitate was formed, which could be amorphous FF. This happens when a solution of FF is cooled quickly to room temperature, as observed in Section 3.1.1. This seems to indicate that the cooling rate of the solution is too fast for the formation of the fibres even with the glass slides pre-heated to 40 °C (they probably cool down to room temperature very quickly once put into the microscope sample holder), resulting in the precipitation of FF, which is not soluble at 2 mg/ml at room temperature. Therefore this technique could not be used to observe FF assembling into fibres, and a microscopy technique with temperature-control had to be used.

3.3.2 Widefield Temperature-Controlled Optical Microscopy

Widefield optical microscopy with weather control is commonly used in the life sciences to view living organisms. So-called "weather control" allows the temperature and atmosphere of the sample to be maintained at desired levels in order to keep an organism alive. As demonstrated by the experiments presented in the previous section, such an experimental setup is also essential for observing the assembly of FF fibres as the reaction mixture needs to be kept at a high temperature in order for successful fibre synthesis to take place. As a consequence, in these experiments, the microscope and its surroundings were maintained at 40 °C.

A 2 mg/ml solution of FF in water was heated to 70 °C. A pipette was then used to deposit 1.5 mL of this solution into a microscope petri dish with a lid. The time at which the pipetting occurred was used to define the start of the

experiment. The dish was placed into the microscope, which was at 40 °C, and then a series of images were taken. Under these conditions it was possible to view the fibres growing in real time, obtaining images such as those in Figure 3.14. The white circle highlights a possible nucleation point with fibres growing radially outwards from it.

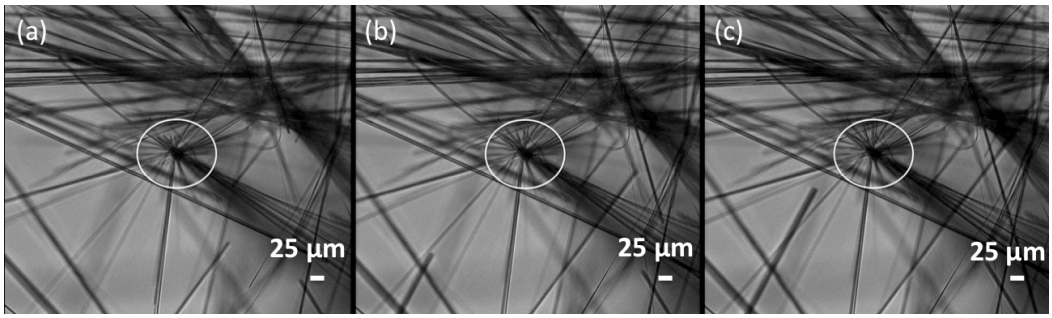

Figure 3.14 *Fibres growing over a period of half an hour imaged by temperature-controlled optical microscopy. (a) Is taken 70 minutes after the start of the experiment and (b) and (c) are taken at 15 minute intervals. The white circle shows a possible nucleation point with fibres growing outwards from it.*

Figure 3.15 shows the example of an individual fibre followed in its growth over time. This specific fibre was found just 360 seconds after the start of the experiment and its growth was observed continuing for around 100 seconds until it went out of the field of view. Similar experiments were repeated several times and many individual growing fibres were observed. For each of these experiments the length that the fibres grew in a set period of time was used to calculate their longitudinal growth speed by simply dividing it by the time period. An average growth speed was found by using averaging data from multiple experiments. This was done at different times from the growth start, averaged over all the experiments, and the resulting data is shown in Figure 3.16. The speed of growth decreases rapidly and then levels off after 1 hour (see Chapter 5 Section 5.2.3.4 for further discussion).

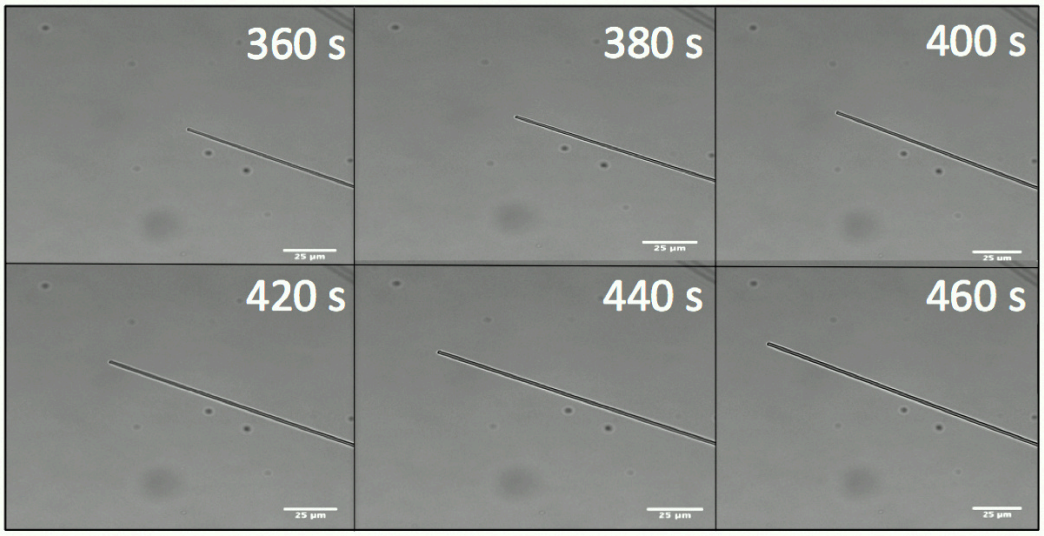

Figure 3.15 *Growth of an individual fibre observed by temperature-controlled optical microscopy. The first image was taken 360 seconds after the start of the experiment and then the subsequent images were taken at 20 second intervals.*

The data of Figure 3.15 were also used to estimate the average length of the fibres as a function of time. This was done under the assumption of zero length at $t = 0$ and of a constant growth speed in between the measured points reported in Figure 3.16. Based on this, an estimate of the fibres length can be obtained by multiplying each measured growth speed by the time at which it was determined and by adding up all the resulting length increments. Figure 3.17 explains this procedure in more details. It should be noted that the growth speeds were actually not measured at fixed intervals but were evaluated whenever a growing fibre was found within the view range of the microscope.

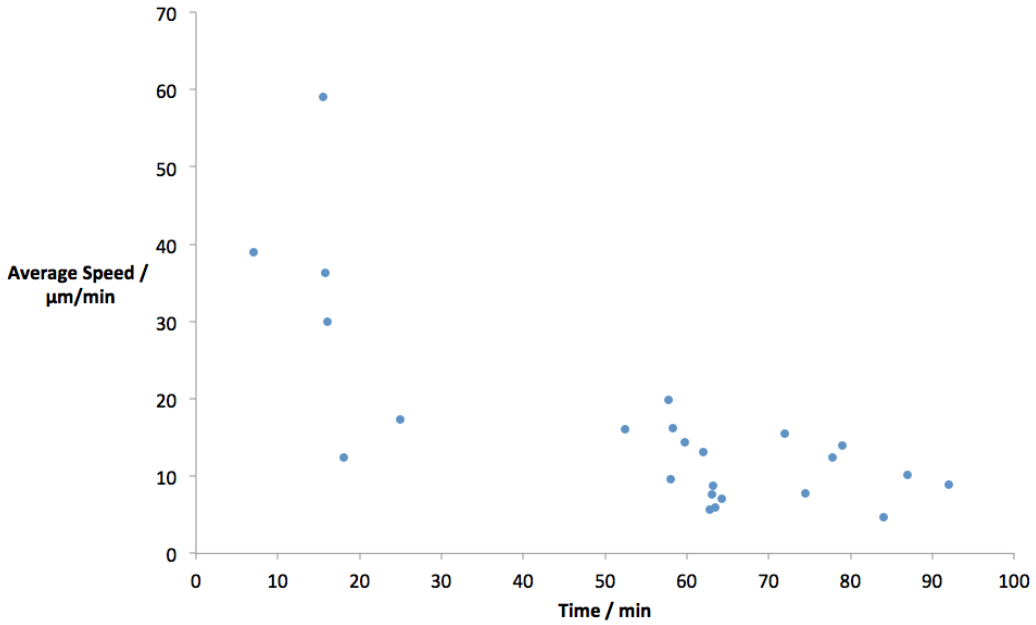

Figure 3.16 *Average speed of growth of the fibres' length over time, measured by temperature-controlled optical microscopy on samples of 2mg/ml FF in water at 40 °C.*

The resulting estimates of the average fibre length are shown in Figure 3.18. This information can be compared to spectroscopy data for a similar experiment, where the fibres are synthesised under the same conditions. This is further discussed in Chapter 5.

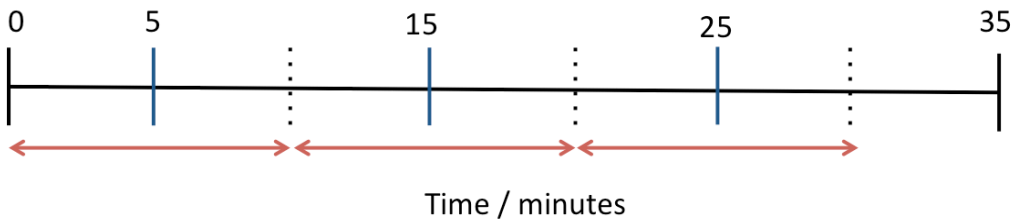

Figure 3.17 *Example of how the average fibres length vs. time was estimated. Blue lines represent the times at which the average fibres' growth speeds were measured and the red arrows indicate the time intervals over which these were assumed to be constant.*

It was possible to conclude from the widefield microscopy measurements that the fibres were growing laterally as well as elongating throughout the experiment which eliminates the possibility that fibres stay at a given width, and only extend

in length during assembly. The growth speed of the fibre widths was measured only in a limited number of instances as their evaluation turned out to be particularly challenging. In fact, the measured increases in the fibres' width were very small, often corresponding only to a couple of pixels in the microscopy image within the time that the length of the fibre had grown out of the field of view. These data are represented in Figure 3.19 and show an overall decrease of the growth speed of the widths over time. Due to the challenges in determining these values, the data will be plagued by a large uncertainty and should thus be taken with some caution, however the overall trend can be believed.

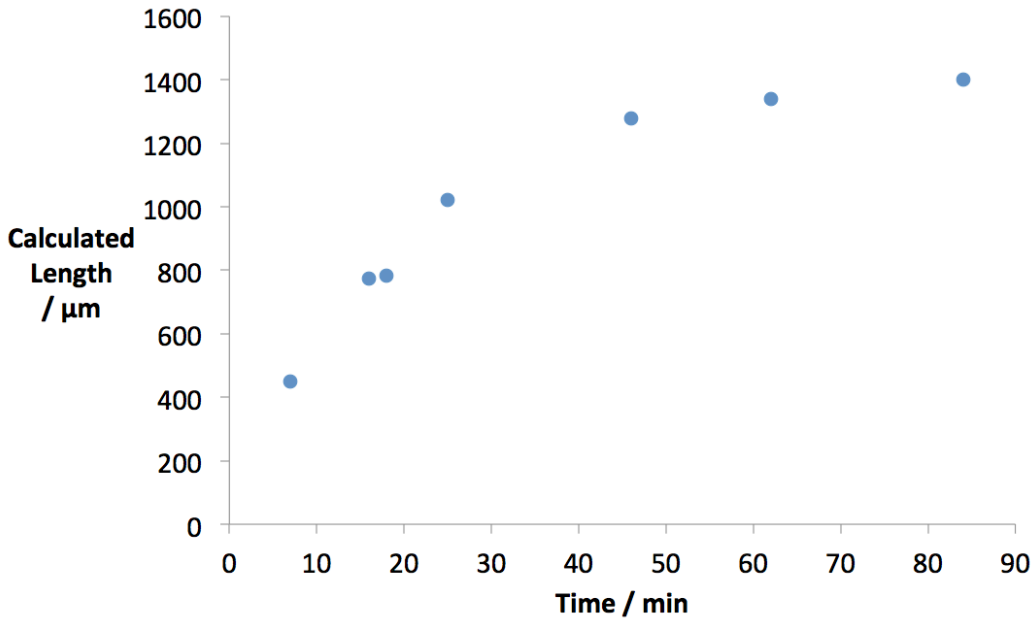

Figure 3.18 *Estimate of the average length of fibres during their growth calculated from temperature-controlled optical microscopy data.*

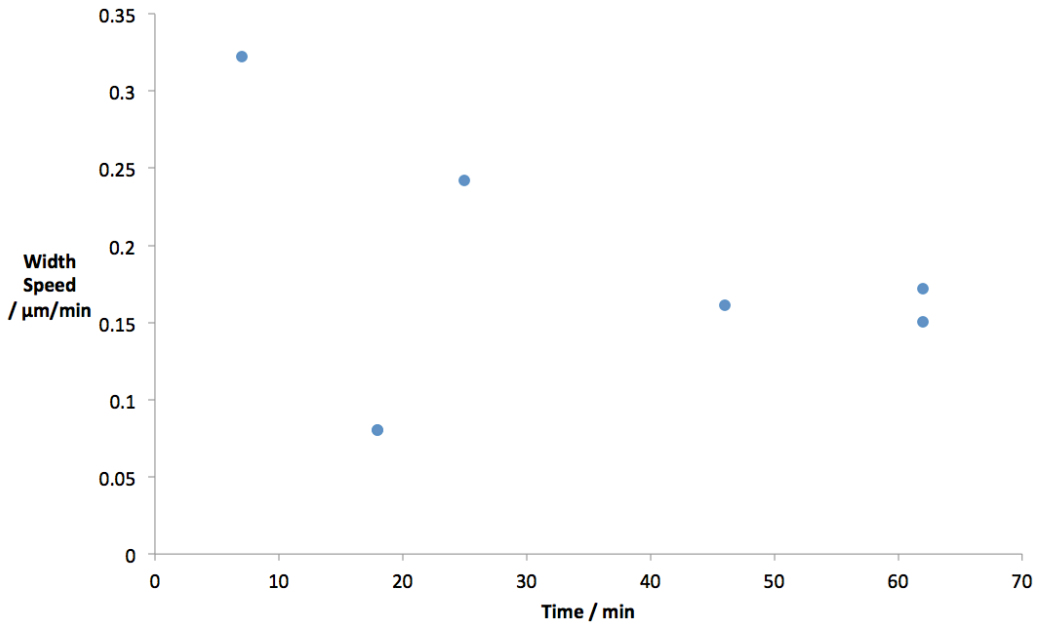

Figure 3.19 *Growth speed of the width of fibres as a function of time.*

3.4 Conclusion

The use of SEM has shown that, contrary to suggestions in the literature, there are FF fibres which appear to be completely filled in as opposed to hollow. We have also been able to quantify the distribution of widths of the fibres and found them to have a larger range than previous work. By controlling the speed of cooling during the synthesis of fibres, we were able to decrease this size distribution.

We were able to successfully use widefield optical microscopy with weather control to observe the fibres growing in real time. The decrease in speed of growth of the lengths and widths of the fibres was then obtained from a series of images of the fibres growing. They showed that the fibres do in fact grow wider throughout the first four hours of the growth, but it is very small when compared to the length growth. We also found evidence of nucleation sites, suggesting that the fibres grow by nucleation-driven assembly.

3.5 Future Work

A variety of microscopy techniques were used to elicit new information about the topology and assembly of FF fibres. However, the attempts at TEM were

unsuccessful. The reason for this is not known for certain, but could be due to sampling problems or stability of the fibres under the electron beam. It is possible to remedy these issues by growing the fibres on the substrate so they are attached to it, and by using cryo-SEM to increase the stability of the biomaterial. Under these conditions, TEM may be possible and could show images of a much higher resolution than have been shown in this work.

References

[1] Reches, M. & Gazit, E. (2003). Casting Metal Nanowires Within Discrete Self-Assembled Peptide Nanotubes, *Science, 300*, 625-627.

[2] Görbitz, C. H. (2006). The Structure of Nanotubes Formed by Diphenylalanine, the Core Recognition Motif of Alzheimer's Amyloid Polypeptide. *Chem. Commun., 22,* 2332-2334.

[3] Adler Abramovich, L. Aronon, D. Beker, P. Yevnin, M. Stempler, S.,Buzhansky, L. Rosenman, G. & Gazit, G. (2009). Self-Assembled Arrays of Peptide Nanotubes by Vapour Deposition, *Nature Nanotechnology, 4,* 849-854.

[4] Young, A., Stoilova-McPhie, S., Rothnie, A., Vallis, Y., Harvey-Smith, P., Ronson, N., Kent, H., Brodsky, M. F., Pearse, B. M. F., Roseman, A. & Smith, C. J. (2013). Hsc70-induced Changes in Clathrin-Auxilin Cage Structure Suggest a Role for Clathrin Light Chains in Cage Disassembly. *Traffic, 14,* 987-996.

[5] Barry, N. P. E., Pitto-Barry, A., Sanchez, A. M., Dove, A. P., Procter, R. J., Soldevila-Barreda, J. J., Kirby, N., Hands-Portman, I., Smith, C. J., O'Reilly, R. K., Beanland, R. & Sadler, P. J. (2014). Fabrication of Crystals from Single Metal Atoms. *Nature Communications, 5,* 1-8.

[6] Barry, N. P. E, Pitto-Barry, A., Romero-Canelón, A., Tran, J., Soldevila-Barreda, J. J., Hands-Portman, I., Smith, C. J., Kirby, N., Dove, A. P., O'Reilly, R. K. & Sadler, P. J. (2014). Precious metal carborane polymer nanoparticles: characterisation of micellar formulations and anticancer activity. *Faraday Discussions online*.

[7] Adler-Abramovich, L., Reches, M., Sedman, V. L., Allen, S., Tendler, S. J. B., & Gazit, E. (2006). Thermal and Chemical Stability of Diphenylalanine Peptide Nanotubes: Implications for Nanotechnological Applications. *Langmuir, 22,* 1313-1320.

Chapter 4

Simulation Results

4. Simulation Results

Molecular simulations offer a unique insight into structures and their dynamics which cannot be accessed through traditional laboratory methods. Past MD simulations have been unable to successfully reproduce the dynamics of FF systems as discussed in the introduction. The start of this chapter shows the investigation of small FF assemblies, as it is not possible to simulate these large fibres atomistically for a sufficiently long time period to see fibre formation, and currently, there has not been a successful coarse-grained model of FF which can reproduce the structure of the fibres. These assemblies varied in size and ranged from 54 to 750 FF molecules, initially arranged in the crystal structure. The variation of structures simulated allows for an insight into the reasons why fibres form with a high aspect ratio. The second part of this chapter is concerned with molecule-surface interactions. A single FF molecule was placed near the surface of a partial fibre and its adsorption was simulated using metadynamics methods.

4.1 Test of the Suitability of the CHARMM27 Force Field

The CHARMM27 force field is designed for simulating proteins and peptides, and contains within it parameters for the naturally occurring amino acids.[1] In this work it was used for the simulation of FF molecules using the NAMD simulation package.[2] To test that it provided an accurate description of the FF system an infinite crystal was first simulated. This consisted of FF molecules arranged into their crystal structure as determined by X-ray diffraction and obtained from the Cambridge Structural Database as determined by Görbitz.[3] The simulation cell had periodic boundary conditions in three dimensions in a parallelepiped shape and the simulation was run for 0.4 nanoseconds with a 0.5 fs time step. An NPT (constant number, pressure and temperature) ensemble was used with a Nosé-Hoover Langevin piston method to control the pressure with an oscillation period of 100 fs and an oscillation decay time of 50 fs. A Langevin thermostat was used to control the temperature with a damping coefficient of 1 ps^{-1}. The particle mesh Ewald method was used for calculating electrostatics with a grid spacing of 1.0. There were 750 FF molecules in the simulation. The initial size of the cell was defined by 3 cell basis vectors which are as follows, (121, 0, 0) (-61, 105, 0) (0, 0, 28).

The first and last frames of the simulation are shown in Figure 4.1. These frames show that there is very little change in the positions of the molecules during the simulation. This is confirmed by the RMSD, which is calculated with comparison to the crystal structure and is an average parameter of the RMSD of every atom in the simulation.

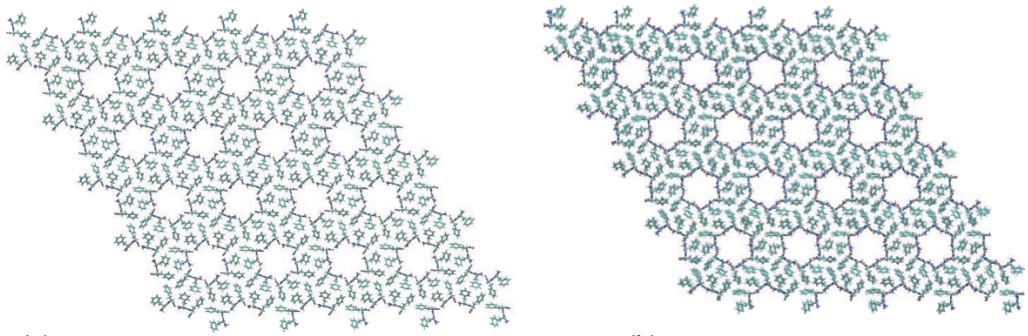

Figure 4.1 *The initial (a) and final (b) configurations of FF molecules in a simulation designed to test the suitability of the CHARMM27 force field.*

The RMSD as a function of time is shown in Figure 4.2.

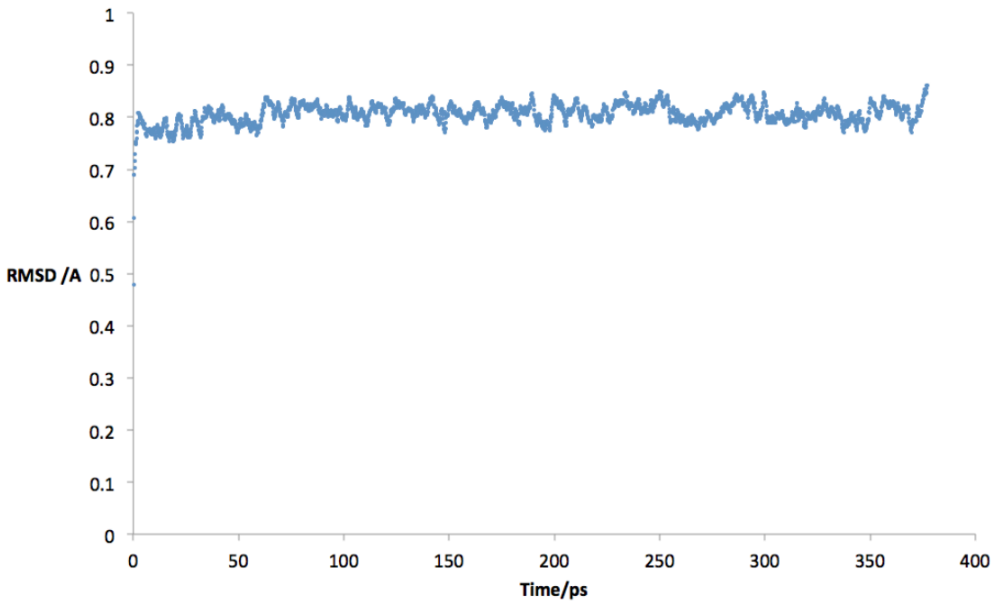

Figure 4.2 *The RMSD of the FF infinite crystal MD simulation.*

The RMSD equilibrates by about 50 ps, and thereafter gives an average value of 0.81 ± 0.02 Å; this is very small when compared to the size of the simulation cell which has a maximum dimension of 121 Å. This is what we expect for an accurate force field, as the crystal structure is clearly a stable one in reality. Another measure of physical stability is the dihedral angle of the peptide, which is defined by the nitrogen in the N-terminus of the peptide, the following two carbon atoms in the peptide backbone and the second nitrogen. The average

dihedral angle for this simulation is shown in Figure 4.3. This parameter has an average value of 150° ± 2° during the course of the simulation with no distinct change in structure from the original crystal, which has a dihedral angle of 147 °. Therefore we can conclude that CHARMM27 provides a reliable set of parameters for the atomistic simulation of FF.

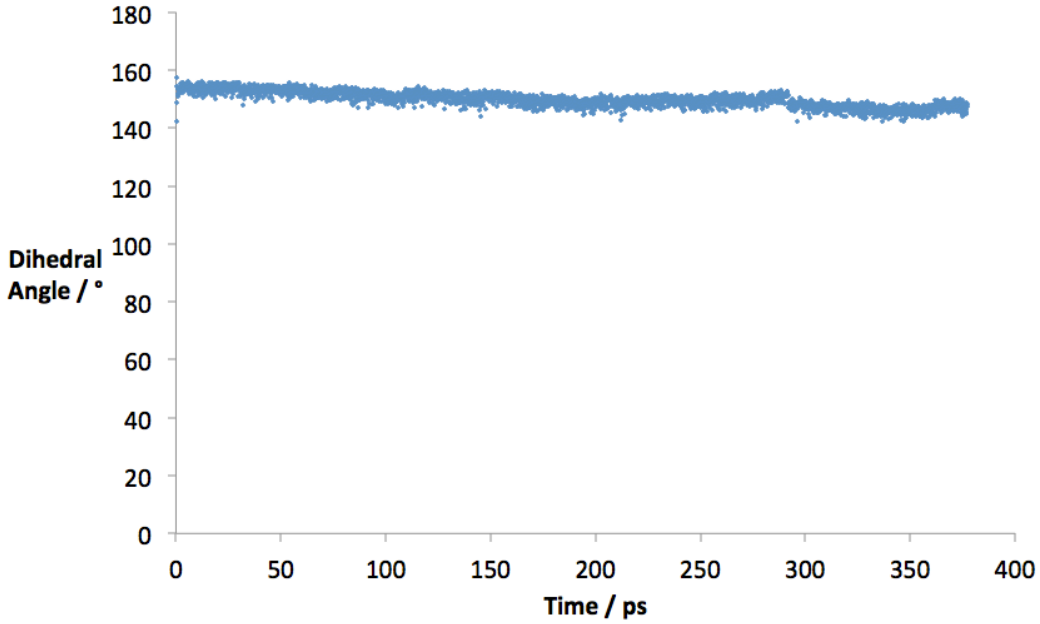

Figure 4.3 *The dihedral angle of the FF infinite crystal simulation.*

4.2 Stability of Small Assemblies of Diphenylalanine

In order to examine the nucleation and early growth of FF fibres, small assemblies of FF molecules were simulated. This makes it possible to investigate the size of the critical cluster, and whether the cluster stabilizes more easily with more layers or lateral extension. The shape of our fibres (Figures 3.1 – 3.4) is entirely consistent with the FF crystal structure wherein 6 FFs are arranged in hexagonal units. We therefore performed MD simulations of small fragments of FF crystals. In order to probe independently lateral and axial growth we then chose two sets of assemblies: the first set had 4-hexagonal cylinder assemblies (structure C in Figure 4.4 b) of varying depths (where depth is defined as the dimension varied in Figure 4.4 a), and the second set had 3-layer assemblies of differing widths (Figure 4.4 b). This allowed us to compare the stability of different sized FF nanocrystals.

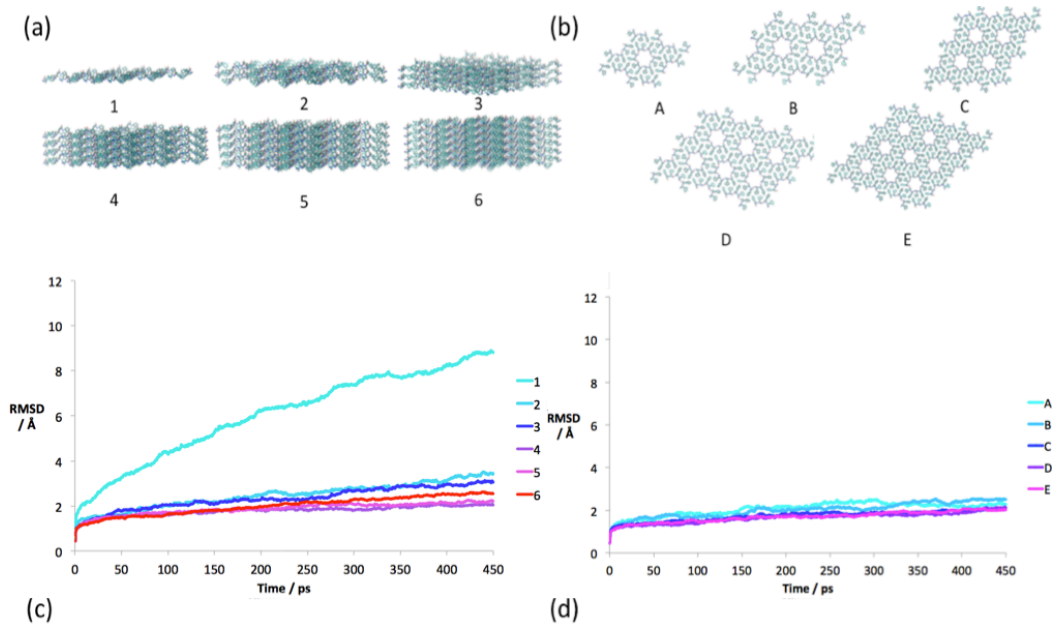

Figure 4.4 *Diphenylalanine structures used in the MD simulations and their RMSDs in solvated atomistic molecular dynamics simulations. (a) Structures with increasing number of FF layers from 1 to 6 (waters omitted for clarity). (b) Structures increase lateral extension from A to E. (c) The RMSDs of the structures in (a). (d) The RMSDs of the structures shown in (b).*

The first set of structures varied from 1 to 6 layers (Figure 4.4 (a)) and all other dimensions were kept constant. Explicit liquid water surrounded the peptide molecules and the simulations were run for half a nanosecond. The rearrangement of the cluster in these simulations was quantified using the RMSD of the peptide atoms along the simulation trajectory (Figure 4.4 (c)). Small RMSD values indicate that the structure is stable. The RMSD of the atoms in structure 1 (Figure 4.4 (a) and (c)) correspond to the molecules completely abandoning their original layout so that the structure no longer resembles the crystal and dissolves (Figure 4.4). These atoms had an average RMSD of 11 ± 3 Å. However, for structures 2-6, the molecules are more similar to their original assembly, with average RMSDs between 2 and 4 Å and standard deviations lower than 1.2 Å. This is shown in the final frames of the simulations in Figure 4.5, where the 1st structure has completely abandonded its original arrangement whereas the other structures look similar to their starting configuration (Figure 4.4 (a)). The small differences between the RMSDs for structures 2 – 6 indicates an increase in stability as more layers are added.

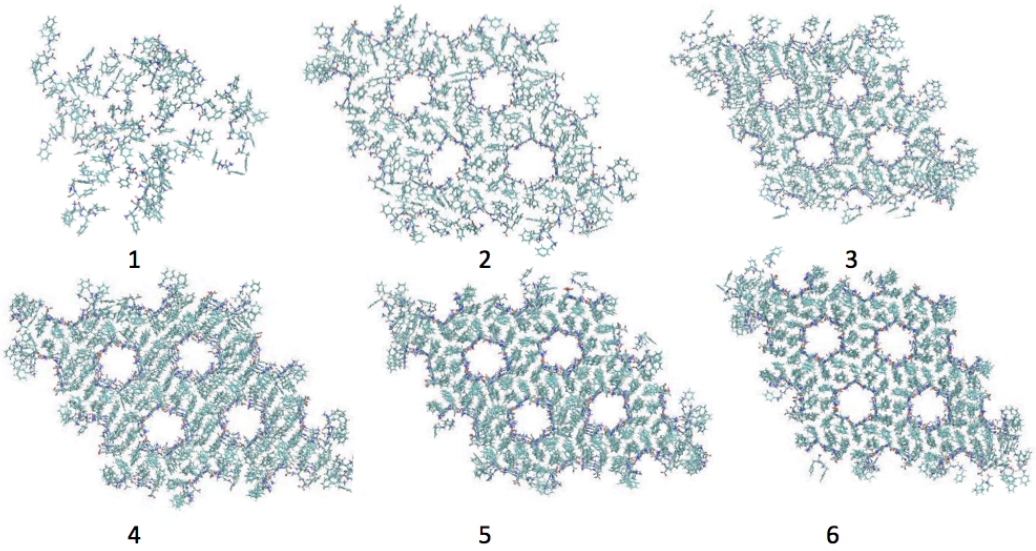

Figure 4.5 *The final frames of the 1-6 layered simulations of FF molecules which started off in the crystal structure. By the end of the 1-layered simulation the FF has become amorphous, however all of the others retain the same overall arrangement.*

Next, the lateral extension of an assembly of FF molecules was varied and the number of layers kept constant at three layers (Figure 4.4 (b) and (d)). Three layers were chosen because the final frame of the 3 – 6 layered simulations had similar RMSDs (Figure 4.4 (c)), which suggests that using a higher number of layers would not be beneficial. A visual inspection of the lateral extension simulations indicated that all of the structures had a similar level of stability, when compared to the variation in the depth study. This is confirmed by the RMSDs which are similar for structures A to E (Figure 4.4 (d)). These RMSDs do have a slightly positive slope which indicates that they may still dissolve if the simulations were run for longer, and therefore we cannot conclude that these structures would be stable in solution. However, structure A (Figure 4.4 (b)) is long lived, which suggests that it is already above the critical cluster size. This investigation has also revealed the difference in relative stability between the depth analysis and the width variation.

The difference in increase in physical stability obtained in these two sets of simulations is consistent with the high aspect ratio of the fibres. The RMSD dramatically decreases when the small assembly increases in length, which is not

the case when the assembly is extended laterally. This means that these structures become much more stable upon elongation as opposed to lateral extension, which is consistent with the structure preferentially growing longer instead of wider.

4.3 Adsorption Events

4.3.1 Molecular Dynamics

Adsorption events of single FF molecules are key to the self-assembly process. Therefore, a simulation was set up in which a single FF molecule was placed near to the surface of a small nucleus of FF molecules in the arrangement of the crystal structure (Figure 4.6) with no constraints on their geometry.

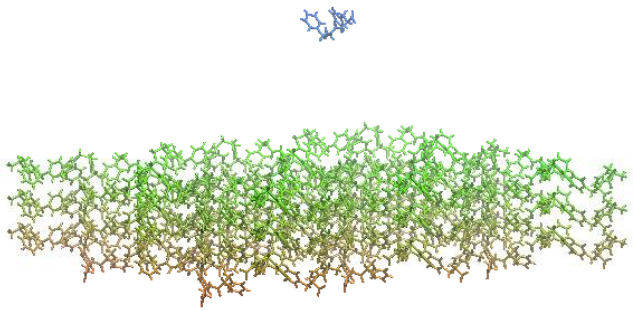

Figure 4.6 *A single FF molecule placed near the surface of a finite nucleus of FF molecules. The colours of molecules in this figure are varied so that the individual molecule can be easily distinguished. The peptides were surrounded by 8275 TIP3P water molecules.*

These 109 peptides were solvated in 8275 TIP3P water molecules and the simulation was run for 0.38 ns. However, no adsorption event was observed during this time; the FF molecule and the assembly stayed separate. The FF molecule had a diffusion coefficient of 3.7 $Å^2$ ns^{-1} and did not move close enough to the nucleus to attempt an adsorption event. This is illustrated in Figure 4.7 which shows the distance between the single FF molecule and the closest FF molecule within the nucleus. The single peptide starts at 22 Å away and the closest it ever gets to the nucleus is 19 Å away. In order to speed up the

adsorption event the simulation was repeated with no water. However, the assembly of FF molecules was not stable under these conditions and became amorphous within half a nanosecond at 290 K. This is shown in Figure 4.8. Consequently, in order to monitor adsorption events, an alternative method was used.

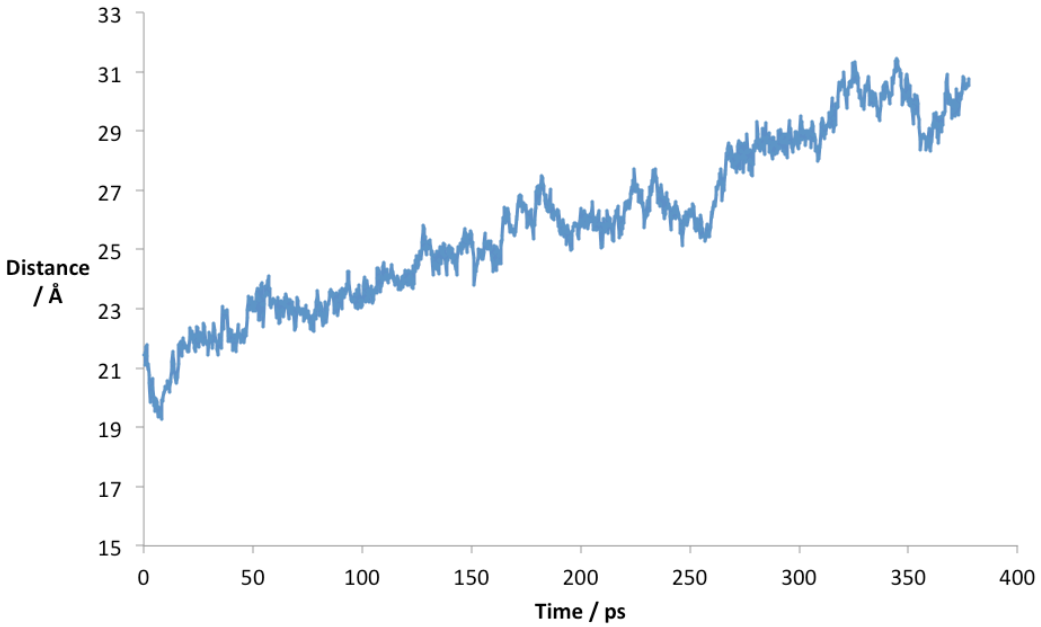

Figure 4.7 *The distance between the single FF molecule and the closest FF molecule in the nucleus over the course of a simulation to monitor FF adsorption.*

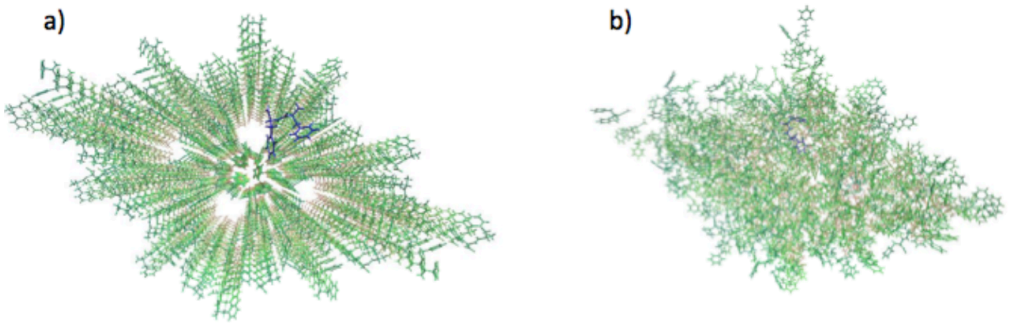

Figure 4.8 *(a) The top view of the first frame of a molecular dynamics simulation with no water and (b) the final frame. The structure has become amorphous without the presence of water.*

4.3.2 Metadynamics

Metadynamics is a simulation technique which allows for events to be witnessed that would be highly unlikely to occur in the timescale of a standard molecular dynamics simulation. This is because they take more than the time available with molecular dynamics. The details of how this works are described in Section 2.2. In this work a small nucleus of FF molecules in the arrangement of the crystal structure was used with a single FF molecule placed near its surface. This finite crystal and single molecule were surrounded with 10627 water molecules. The size of the simulation cell was 54 x 69 x 119 Å and the NVT (number, volume and temperature) ensemble was used. The Gaussians used had a height of 0.1 and a width of 0.35 kcal mol^{-1} with a deposition stride of 1000 time steps. In a metadynamics simulation it is necessary to describe a set of collective variables that describe the overall changes being studied. A time-dependent bias is then introduced into the potential energy function which induces these collective variables to change, and the system does not get stuck in one state. In this work, the chosen collective variable is the z projection of the distance between the centre of mass of the single molecule and the centre of mass of the assembly of molecules, as shown in Figure 4.9. This means that all values of distance will be sampled in a relatively short time, and the single FF molecule will get driven to the surface of the nucleus. The plot of the collective variable over the course of the simulation illustrates this (Figure 4.10). We see that it continuously changes throughout the simulation.

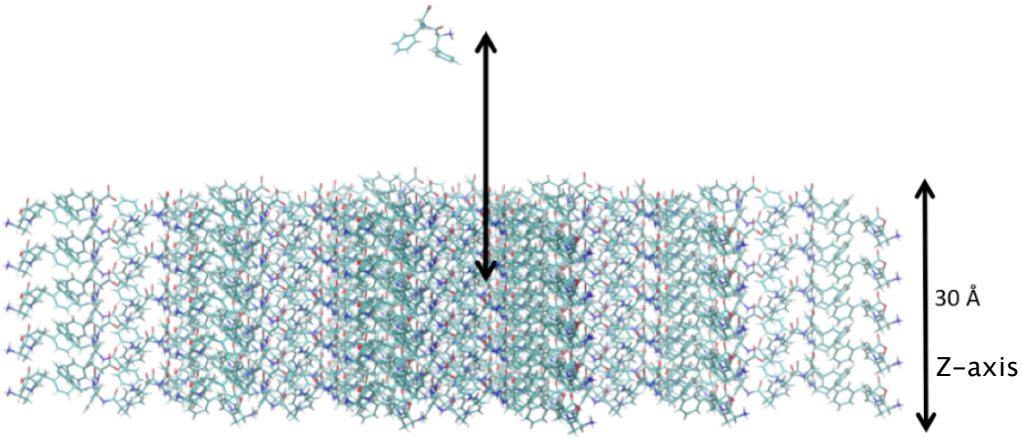

Figure 4.9 *The collective variable is the z projection of the distance between the centres of mass of the nucleus and the single FF molecule.*

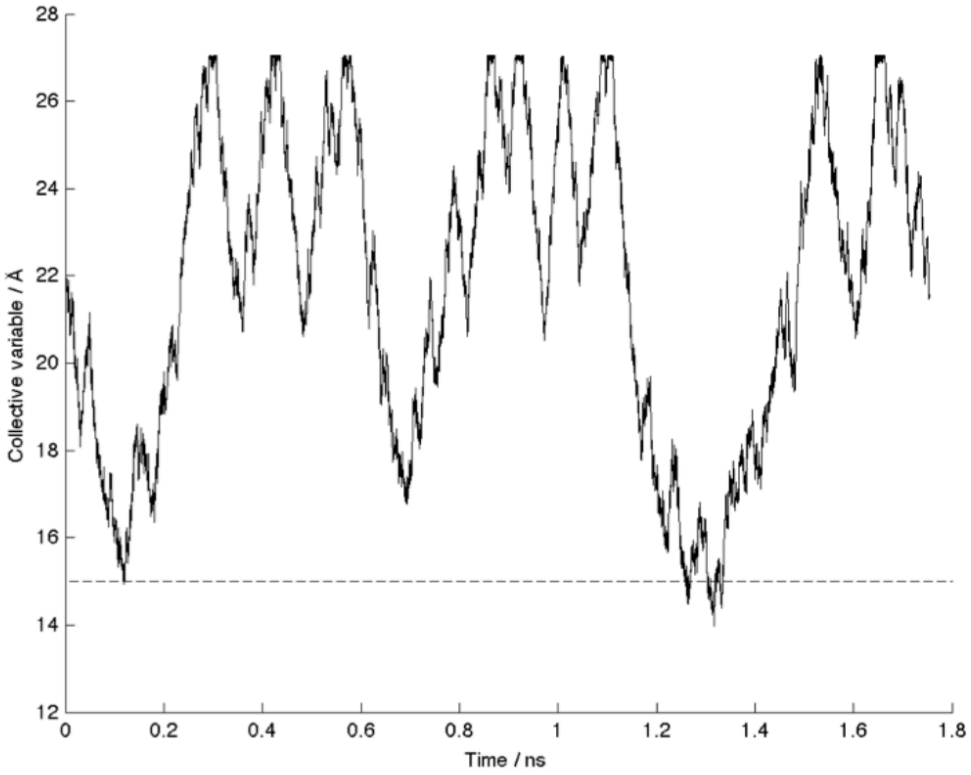

Figure 4.10 *The collective variable (the distance between the single molecule and the nucleus shown in Figure 4.9) plotted over the time of the simulation. The dotted line at 15 Å shows the point where the single molecule meets the surface of the nucleus. The top of the simulation cell was at the point where the collective variable was 27 Å which is why it does not go above this value.*

The thickness of the nucleus in Figure 4.9 is 30 Å, and the origin is at the centre of the nucleus, so when the collective variable reached around 15 Å, it was in contact with the surface. This simulation was periodic and therefore had images of the simulation cell surrounding it. Therefore, when the single molecule reached the top of the simulation cell (around 27 Å) it was adsorbing onto the bottom surface of the nucleus. We can see that there are three separate possible adsorption events on the top of the nucleus and nine possible events on the bottom of the nucleus from Figure 4.10 which are short lived.

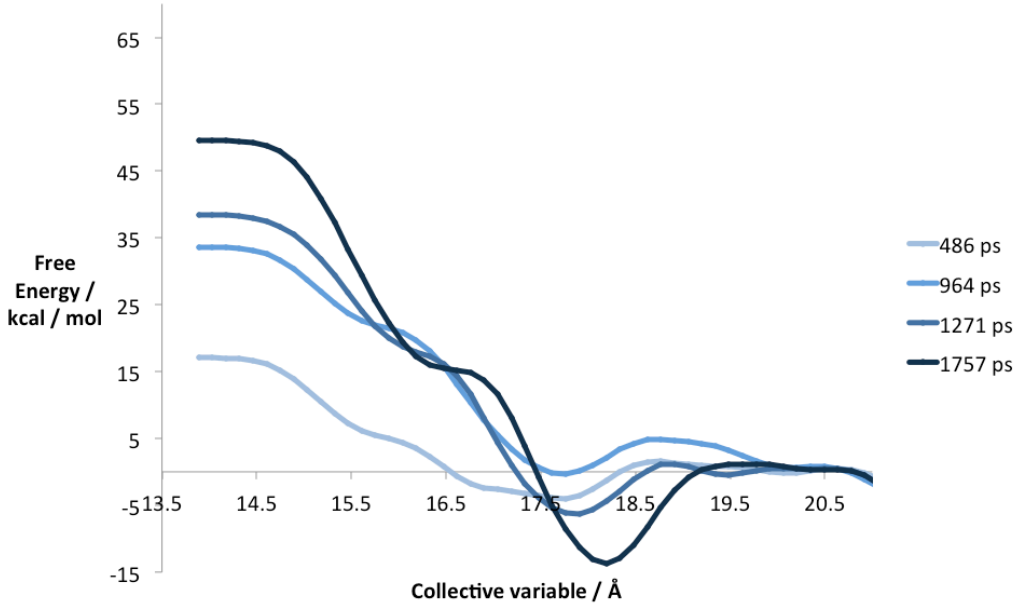

Figure 4.11 *The free energy profile of the structure shown in Figure 4.6 at four different times in the simulation. 1757 ps is the final frame.*

The free energy profile for the simulation is shown in Figure 4.11. This shows that the free energy has not converged over the course of the simulation. It also shows evidence for two adsorption states, with the lowest energy state between 17 Å and 18 Å and possibly another, higher energy adsorption state between 16 Å and 16.5 Å. There is a large energy difference between these states of 30 kcal mol^{-1} and the more favourable state is around 2 Å above the other state. It is possible to estimate the adsorption energy from this data using the following equation.

$$A = -kT \ln\left(\frac{1}{L}\int e^{-\frac{F(z)}{kT}}\, dz\right) \tag{4.1}$$

A is the adsorption energy of a FF molecule onto the surface of the FF nucleus. T is the temperature, k is Boltzmann's constant, L is the range of the collective variable, z, and $F(z)$ is the free energy. Application of this equation to the data with integration limits of 14 Å and 21 Å produced an adsorption energy of -11.7 kcal mol^{-1}. This corresponds to around 10 kT and therefore shows that the molecule is very stable once it has adsorbed and is unlikely to be released.

4.4 Conclusion

This work has used atomistic simulations to show that small FF nuclei display an increase in physical stability when they are increased in length as opposed to laterally, where length refers to the long dimension of the fibre, and lateral refers to the radial aspect. This is consistent with the high aspect ratio of the fibres observed by SEM (Chapter 3). Metadynamics simulations have revealed possible short-lived adsorption events of a single peptide onto the surface of a small nucleus. However, "short-lived" in terms of metadynamics does not correspond to the state being short-lived in real terms. This is because the nature of metadynamics simulations causes the state of the system to change, so any state will appear short-lived, when in reality it may not be. Several possible adsorption states were found, with the lowest energy state around 3 Å away from the surface of the nucleus. The adsorption energy of a FF peptide onto the surface of a nucleus was found to be around 10 kT which suggests that it is a very stable state. This indicates that the growth of FF fibres in not surface limited, but instead must be diffusion limited.

4.5 Future Work

Following on from the adsorption studies, it would be pertinent to look at the adsorption of a FF molecule onto the side of a small nucleus rather than on the top and bottom. This would allow for a comparison of the two adsorption energies and a further insight into the reasons for the shape of the fibres.

The next step would be to set up Monte Carlo (MC) MD simulations. Whereas normal MD simulations calculate trajectories of particles based on solving equations of motion, MC simulations move particles around based on weighted random numbers, which means that unlike MD they are not deterministic. An advantage of using the MC method is that it typically samples a large number of configurations when compared to MD. However, MC does not allow for the trajectories of atoms to be observed, which is why MD and MC are combined to create MCMD simulations. This combined technique extends the effective timescale when compared to MD alone whilst generating a single trajectory.[4] There are several ways to combine MC and MD methods. One example of this is

the mixed MCMD algorithm which moves some atoms by the MD method and others by the MC method.[5]

References

[1] Brooks, B. R. *et al*. (2009). CHARMM: The Biomolecular Simulation Program. *J*. *Comp*. *Chem*., *30*, 1545-1615.

[2] Phillips, J.C. *et al*. (2005). Scalable Molecular Dynamics with NAMD. *J*. *Comput*. *Chem*., *26(16),* 1781-1802.

[3] Song, Y. *et al*. (2004). Synthesis of Peptide-Nanotube Platinum-Nanoparticle Composites. *Chem*., *Commun*., *22,* 1044-1045.

[4] Neyts, E. C. & Bogearts, A. (2012). Combining Molecular Dynamics with Monte Carlo Simulations: Implementations and Applications. *Theor*. *Chem*. *Acc*., 132:1320.

[5] Laberge, L. & Tully, J. (2000). A Rigorous Procedure for Combining Molecular Dynamics and Monte Carlo Simulation Algorithms. *Chem*. *Phys*., *260,* 183-191.

Chapter 5

Spectroscopy Results

5. Spectroscopy Results

The techniques reported so far in this work have been focused on investigating small systems, either fractional fibres with MD in Chapter 4 or a small number of fibres with microscopy in Chapter 3. This is essential for a complete characterisation and understanding of the fibres and their assembly mechanism. However, it is important to check that these individual events are representative of the system as a whole, as it has been established that the fibres are heterogeneous. Spectroscopy is ideal for this check as it is a bulk technique which allows for an average property to be measured.

First the absorbance spectrum of FF was measured as a reference for subsequent experiments, and the same technique was used to find the extinction coefficient of FF. Then LD was used to follow the assembly of FF into fibres as a function of temperature and of time. Many factors in this experiment were varied to optimize the experimental setup and the results are shown in Section 5.2.3. Right angle light scattering was then used to monitor the entire assembly process and finally absorbance spectroscopy was used again to deliver a further insight into this process.

5.1 Absorbance

5.1.1 Absorbance Spectrum

UV/Vis absorbance spectroscopy was performed on FF in methanol. Although water was used for all other measurements, it is not ideal for the reference absorption spectrum of the FF peptide as FF has a low solubility in water at room temperature. Methanol is a good substitute as it does not absorb light in the same region as FF and FF is soluble in methanol to 0.005 M at room temperature in this solvent. The absorbance spectrum for FF is shown in Figure 5.1. The peaks correspond to the phenyl chromophores, which typically occur in the 250 – 280 nm region.

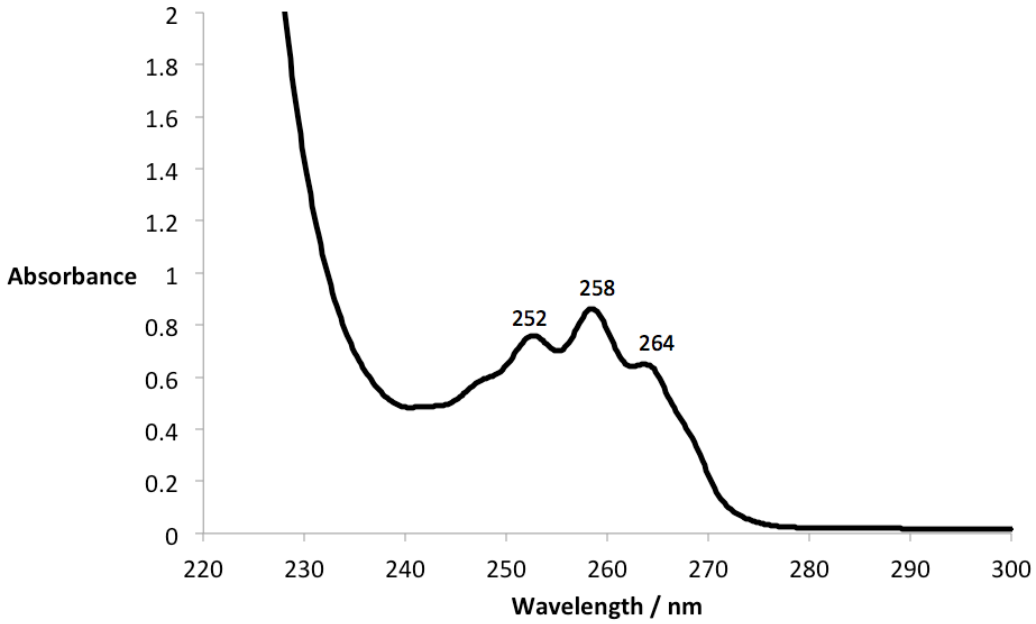

Figure 5.1 *The absorbance spectrum of FF (5 mM). The peaks are labelled with the relevant wavelength in nanometers. The cuvette had a 1 cm x 1 cm cross-sectional area and 2 ml of solution was used. This measurement was taken at room temperature.*

5.1.2 Extinction Coefficient

A useful parameter in spectroscopy is the extinction coefficient, which is defined in Section 2.3.1. This parameter can be used to find the concentration of a solution if the absorbance intensity is measured using the Beer-Lambert law

(Equation 2.3). Conversely, the extinction coefficient can be calculated from the absorbance intensity of a solution of known concentration. Here, a series of concentrations of FF solution were made and the absorbance spectrum of each one was measured. In order to be able to use water as a solvent, a Peltier-controlled sample holder was used which kept the cuvette and its contents at 70 °C. At this temperature, FF dissolves at 2 mg/ml in water, which is high enough for good signal to noise ratio absorbance measurements to be taken. Five concentrations between and including 1 and 2 mg/ml were used and these absorbance spectra are shown in Figure 5.2.

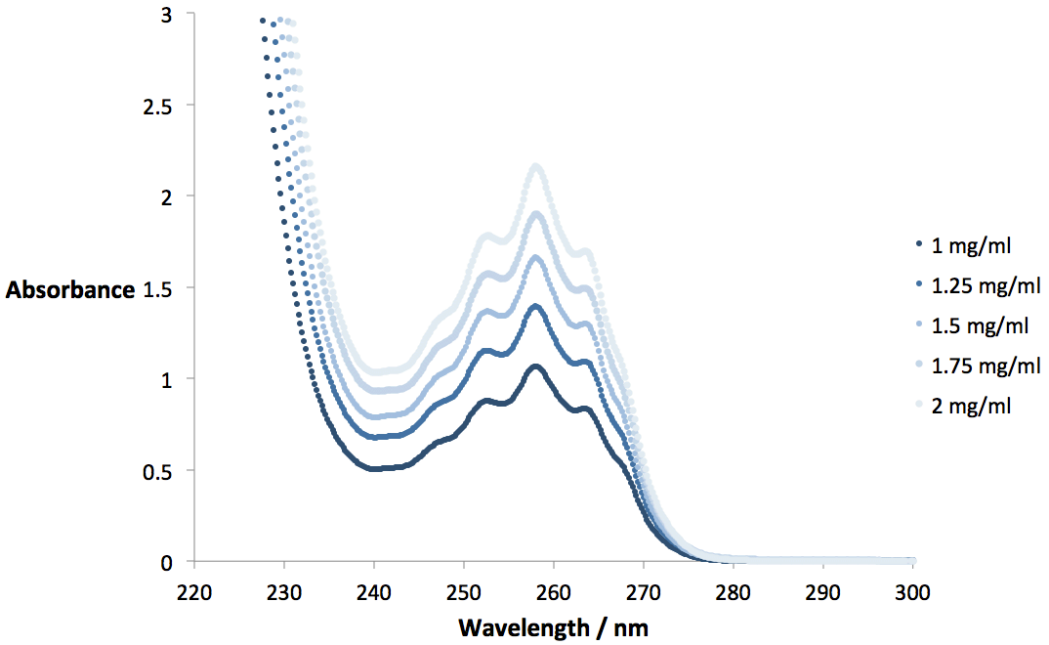

Figure 5.2 *The absorbance spectrum of FF in water at five different concentrations ranging from 1 to 2 mg/ml. The molecular weight of FF is 312 g/mol. The cuvette had 1 cm x 1cm cross-sectional area and 2 ml of solution was used. This measurement was taken at 70 °C.*

The absorbance increases with concentration as expected, and this relationship can be seen in Figure 5.3. This is a plot of the absorbance at 258 nm as a function of concentration. The equation for the line of best fit is shown on the bottom right of the graph. The gradient of the line of best fit is equal to the absorbance divided by the concentration. Using the Beer-Lambert law, this quantity is

divided by the path length (1 cm) to obtain the extinction coefficient of FF at 258 nm, which is 1.1 ml mg^{-1} cm^{-1} (343 mol^{-1} dm^3 cm^{-1}).

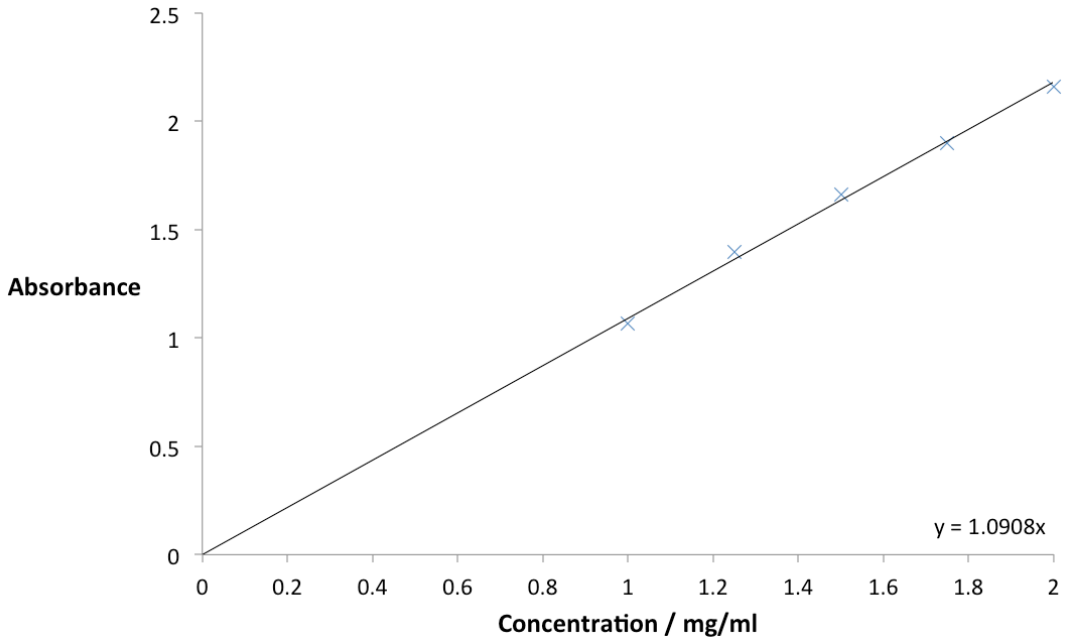

Figure 5.3 *The absorbance of FF at 258 nm as a function of concentration. The line of best fit is overlaid with the data and the equation of this line is displayed on the bottom right.*

5.2 Linear Dichroism

LD was used to monitor the kinetics of assembly of FF fibres under variable and constant temperature conditions, which provided new information about the fibres assembly mechanism. However, first it was important to find the optimum spinning speed of the capillary, which would produce the highest quality LD spectra. This is particularly important with FF as it has a low intensity spectroscopic signal.

5.2.1 Optimum Spinning Speed

In order to see a non-zero signal in LD, the molecules being probed must first be aligned. In this work we use Couette flow which is described in Section 2.3.2. Couette flow involves spinning the capillary that contains the sample, and in order to get the highest quality LD data the optimum spinning speed was found. This was done by spinning the fibres at different speeds and measuring the LD

spectrum, then comparing the intensities of the peaks. The higher the voltage applied to the Couette cell, the faster it spins. Here, 2, 3, 4, and 5 volts were used, and the results are shown in Figure 5.4. It is clear that the faster the cell spins, the larger the LD signal becomes. This is because the molecules alignment is higher when they are spinning faster. However, the increase was less significant after 3 V which suggests either the onset of non-laminar flow or saturation of orientation. This indicates that at this point Taylor vortex flow emerges which leads to turbulent behaviour. It is important to avoid turbulent flow with LD measurements, as its chaotic property can cause irreproducibility. Therefore 3 volts was used for all LD measurements as a compromise between high signal and avoiding turbulent flow. This equates to around 3000 revolutions per minute.

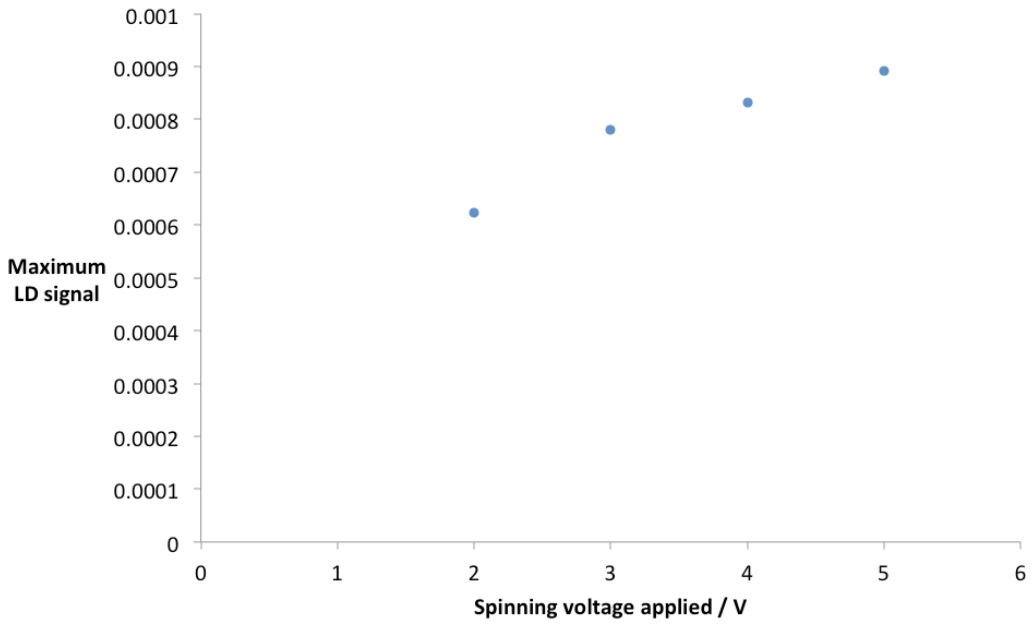

Figure 5.4 *The maximum LD signal from FF fibres at different spinning voltages (3 V ≈ 1000 rpm). A 60 µL solution with a concentration of 2 mg/ml was used at room temperature.*

5.2.2 Fibre Growth as a Function of Temperature

LD was performed on the FF peptide in water and this did not produce any signal, as expected, because the peptide has a low aspect ratio and so it does not align in Couette flow. Conversely the fibres should produce an LD signal as they

have a high aspect ratio. In order to confirm this, an experiment was performed which monitored fibre assembly from peptides with no signal, to long fibres that produce a signal of the same shape as observed in the previous absorbance experiments. The sample was dissolved in water at 70 °C as in other experiments and this was transferred into the LD capillary which was also at 70 °C. A background measurement was taken at this point, with the spinning switched off, which was to be subtracted from each subsequent spectrum. The spinning of the Couette cell was then switched on and the sample was cooled at 1 °C/min for 5 minutes. Upon reaching 65 °C, a spectrum was measured and this cycle was repeated every 5 °C until 20 °C was reached. Typical results for this experiment are shown in Figure 5.5. They show that the magnitude of the FF peaks increases as the temperature decreases, indicating that the fibres are lengthening over the course of the experiment. This is the first assessment of the FF fibres assembly and its dependence on temperature to our knowledge.

It is also apparent that the baseline of the data changes from a flat line to a diagonal one that goes from negative to positive intensity as the wavelength increases. This is due to the increase in light scattering that occurs as the size of the particles increase, which is a function of wavelength. In general, the intensity of light scattering decreases as the wavelength increases, as wavelength to the power of minus 4, if Rayleigh scattering is occuring. However, it is important to note that the LD signal is a difference between two absorbance intensities, as shown in Equation 2.19. This means that the scattering signal is also a difference between two light intensities (Equation 5.1).

$$Scattering_{LD} = Scattering_{parallel} - Scattering_{perpendicular} \qquad (5.1)$$

where $Scattering_{LD}$ is the total scattering of light as observed in the LD spectra, $Scattering_{parallel}$ is the scattering of light which is polarised parallel to axis of orientation and $Scattering_{perpendicular}$ is the scattering of light which is polarised perpendicular to this. The light polarised parallel to the axis of orientation is usually scattered more than the light polarised perpendicular to this in the case of fibres, as they will be in alignment with the parallel light.[1] In this

case we would observe a decrease in the scattering intensity with increasing wavelength, because the positive term in Equation (5.1) is the dominant one. However, it was shown in Chapter 3 that the fibres grow long (to a size comparable to the width of the wavelength of the light) within the first few minutes of the experiment. This means that the length of the fibres are no longer governed by the Rayleigh scattering regime, which requires the scatterer to be much smaller than the wavelength of light used. Therefore the amount of parallel polarised light scattered will not increase anymore, as the fibres are too long. Instead, the scattering of light caused by the increase in the width of the fibres dominates the $Scattering_{LD}$ signal. The $Scattering_{perpendicular}$ term will increase much more than the $Scattering_{parallel}$ term upon increasing width of the fibres. Therefore the negative term in Equation 5.1 becomes dominant, which results in the inverse of the typical scattering signal, where the intensity of scattered light is negative at low wavelengths, and this is indeed what we observe.

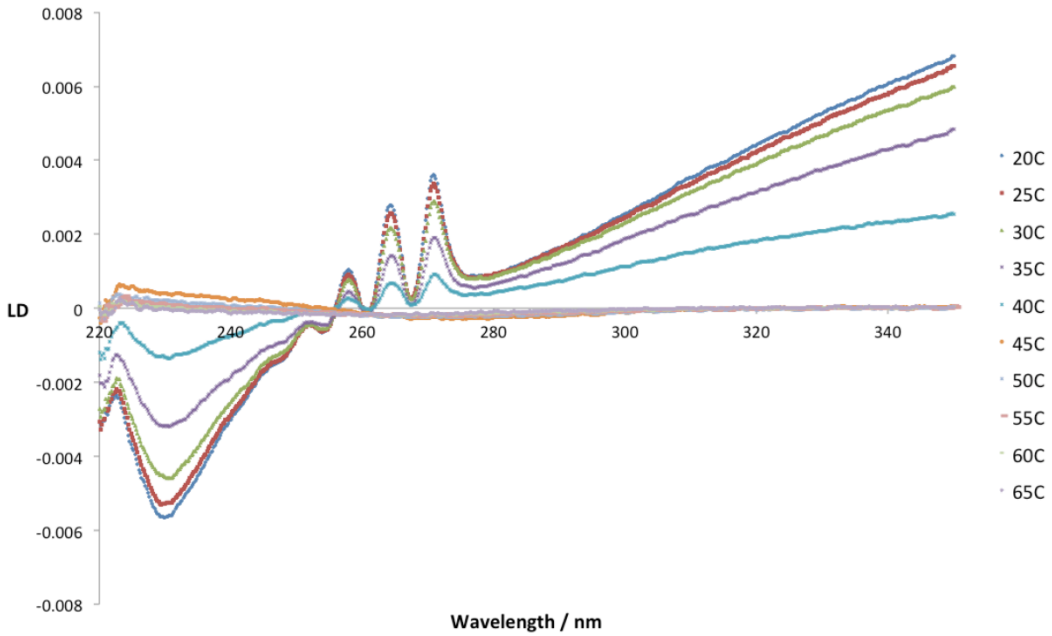

Figure 5.5 *The LD signal of FF fibres whilst they grow as the reaction mixture is cooled. Initially there is no signal, but as the fibres start to assemble the peaks appear. The 60 μL solution had a 2 mg/ml concentration of FF and was cooled from 70 °C to 20 °C during the experiment.*

The first peaks appear at 40 °C, which indicates that there must be fibres present at this temperature, so they must have started to assemble before 40 °C. We can, therefore, conclude that LD is an effective way for monitoring the formation of FF fibres, and that fibres start to assemble between 70 °C and 40 °C.

This experiment was repeated several times, but with a heating cycle included after the cooling to investigate the hysteresis of the reaction. An example of the data from such an experiment is shown in Figure 5.6. Again, we see the peaks due to the presence of fibres start to occur at around 40 °C in the cooling part of the cycle which is consistent with the previous experiment.

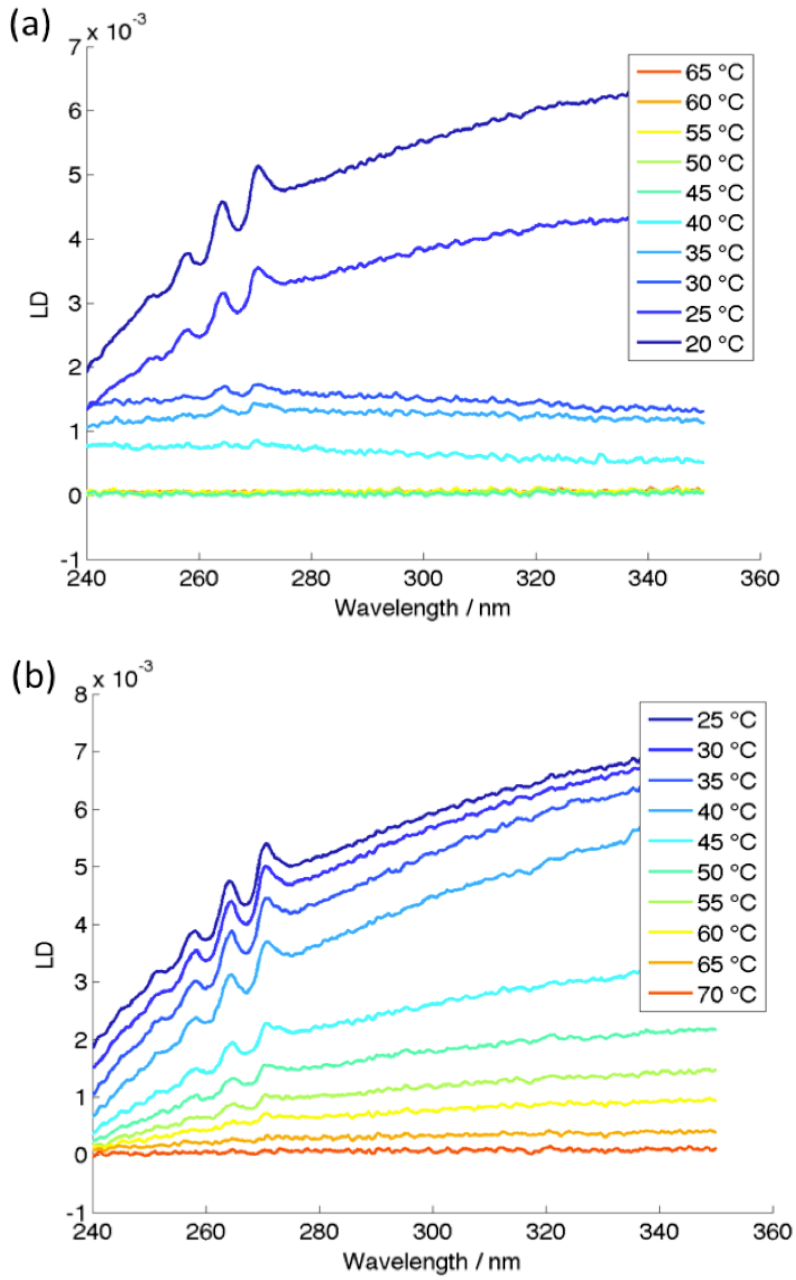

Figure 5.6 *LD signal of FF fibres (a) forming from a 2 mg/ml FF solution as the sample is cooled from 70 °C at 1 °C/min and then (b) dissolved as the solution is heated at the same rate.*

When the solution was heated back up, the signal decreased, which shows that the fibres disassemble upon heating. By the time the temperature reached 70 °C the signal was absent. In order to appreciate the temperature dependence in a more quantitative way, Figure 5.7 shows a plot of the integrated intensity of the

250 – 270 nm peaks versus temperature. This area was evaluated after subtracting the baseline for each spectrum. The baseline was found by performing a fit to the data from Figure 5.6 using the 'polyfit' function in Matlab, and an example of this fit with one of the spectra is shown in Figure 5.8.

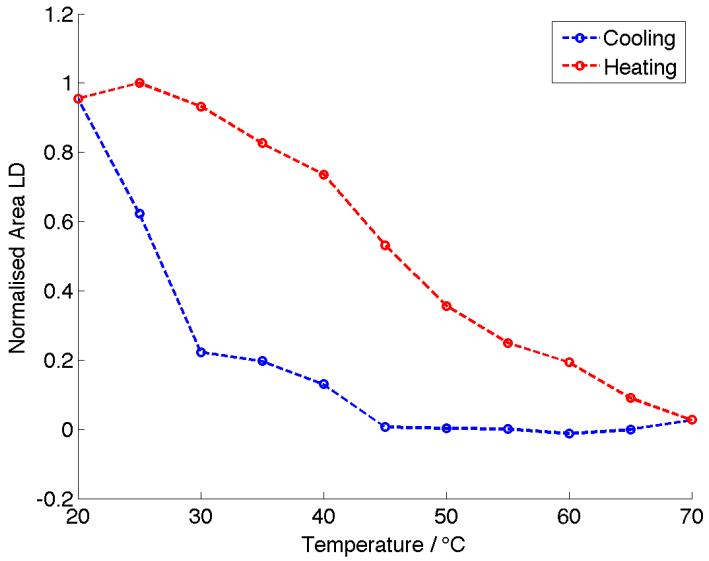

Figure 5.7 *Formation and dissolution of fibres at a concentration of 2 mg/ml as a function of temperature, shown here by plotting the areas under the LD curves of Figures 5.6 (a) (blue) and (b) (red) scaled to a maximum value of 1. The sample was cooled from 70 °C at 1 °C/min and then heated up at the same rate.*

The data in Figure 5.7 show that there is a clear difference between the formation and dissolution processes for these fibres. The fibres do not assemble at high temperatures but once they reach a temperature where they can start to assemble they form quickly. Conversely the dissolution is a steadier process.

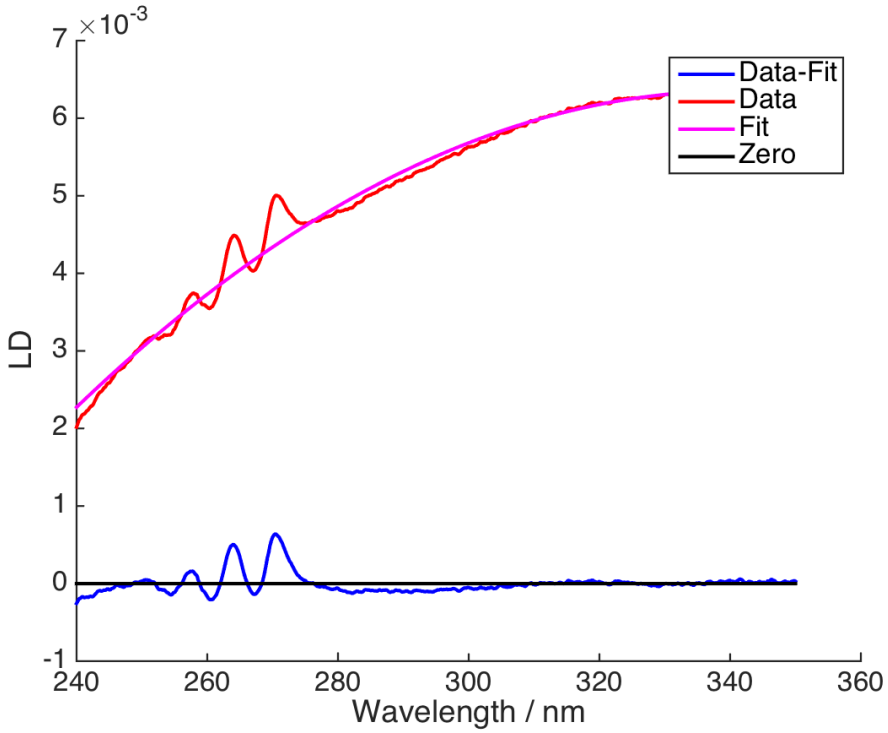

Figure 5.8 *An example of a fit to LD data of FF fibres at 2 mg/ml at 20 °C from the thermal stability measurements using a spinning voltage of 3V. The fit is described in Section 5.2.3.2.*

5.2.3 Fibre Growth as a Function of Time

To investigate the kinetics of fibre formation, an experiment was performed which measured an LD spectrum every 5 minutes of a solution of FF which was assembling into fibres. It was induced to do so by first being heated to 70 °C and then rapidly cooled to 40 °C inside the spectrometer. Before being cooled, a background spectrum was measured with the spinning switched off. Once the sample had reached 40 °C the spinning was switched on and the first spectrum was measured. Every experiment in this section was performed under these conditions. The data from this experiment are shown in Figure 5.9.

Figure 5.9 shows that the fibres do indeed assemble when cooled to 40 °C as we observe the phenyl chromophore peaks. The area under the peaks is plotted in Figure 5.10, and this highlights additional information about the assembly process. For example, it is apparent that the fibres continue to grow for the whole 4-hour period of the experiment. They also start to assemble around 40 minutes

after the solution was cooled at the start of the procedure. This experiment was repeated several times and the results varied each time the experiment was run. For example, Figure 5.11 shows one replicate which had different characteristics. Figure 5.12 illustrates the earlier onset of the fibres formation when compared to the previous identical experiment. It was around 20 minutes in this case which is significantly quicker than the 40 minutes in the first experiment. The growth in this experiment stops after 2.5 hours, which is in contrast with the other experiment where the growth did not stop within 4 hours. There are many reasons that could cause the data to be irreproducible, and they are considered in the sections below.

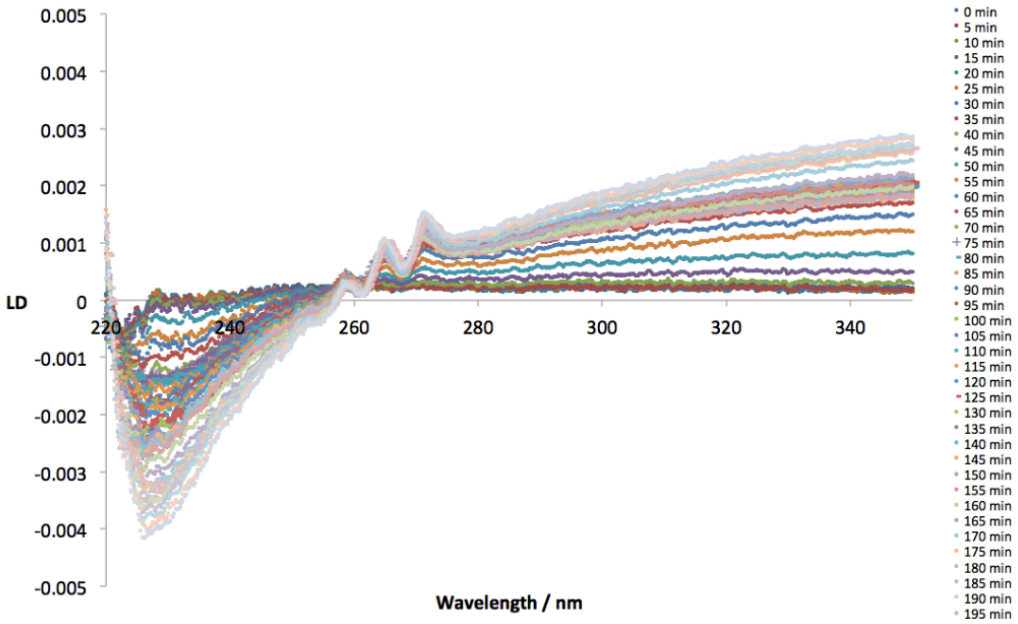

Figure 5.9 *The LD signal of FF fibres at 2mg/ml assembling at 40 °C for 4 hours.*

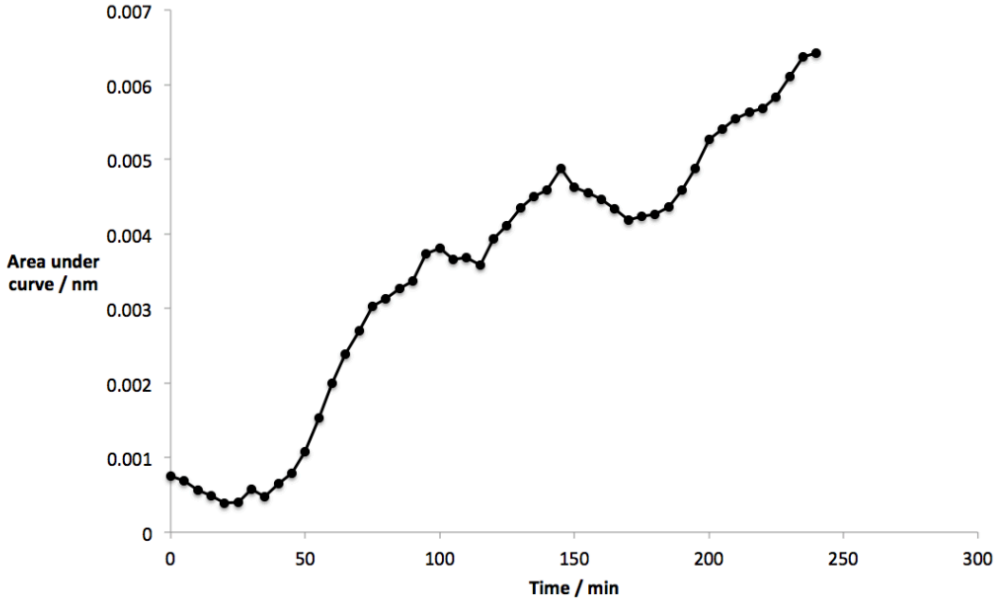

Figure 5.10 *The area under the peaks of the LD data in Figure 5.9. The experiment used LD to monitor the fibres formation at 40 °C for 4 hours at a concentration of 2 mg/ml.*

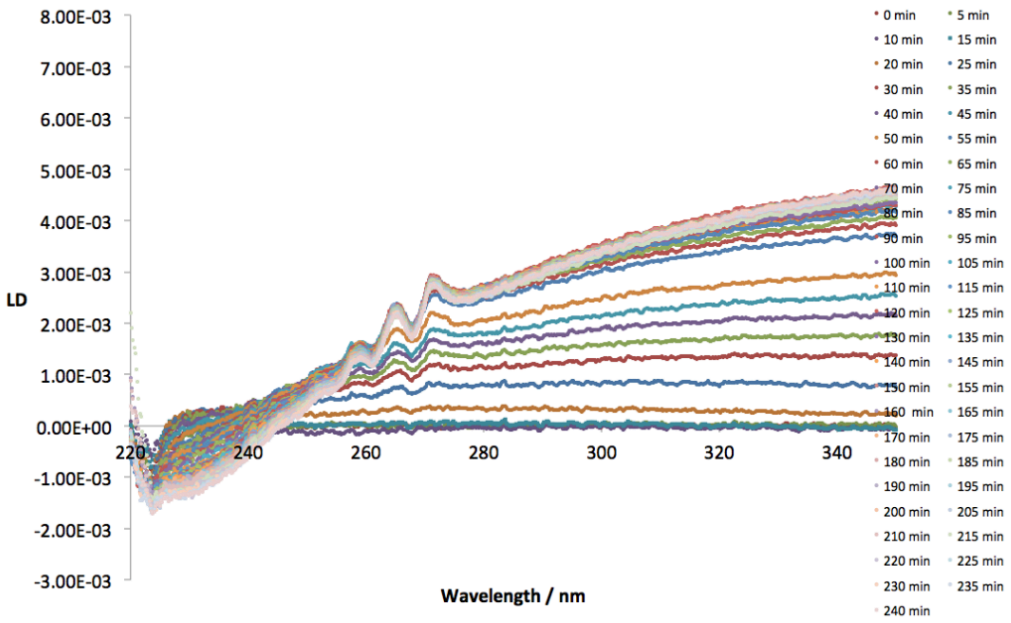

Figure 5.11 *The assembly of FF fibres at 40 °C monitored by LD. The fibres are at a concentration of 2 mg/ml and are monitored for 4 hours.*

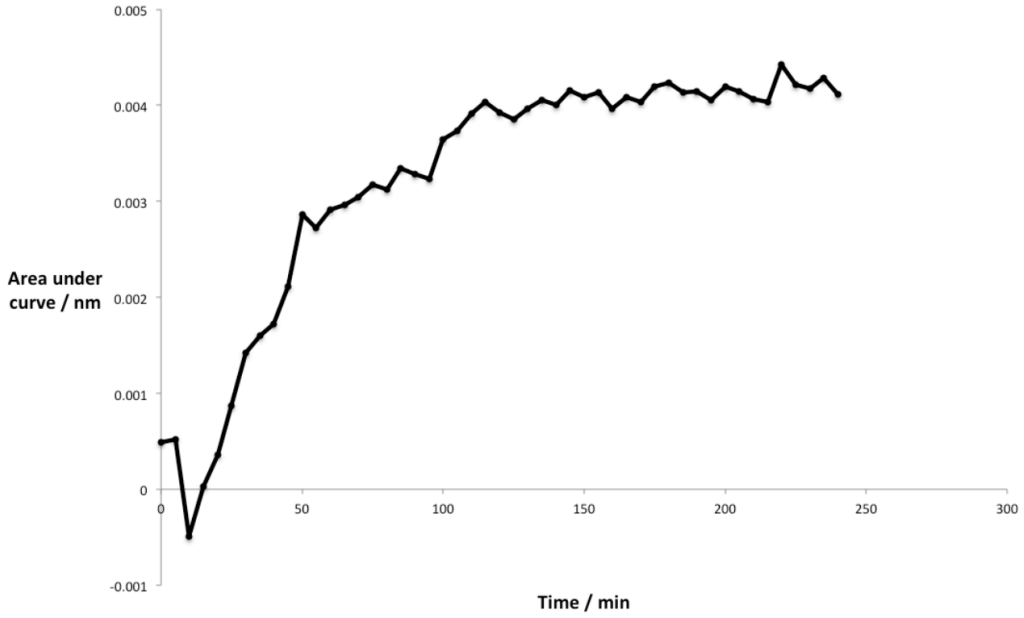

Figure 5.12 *The area under the peaks of the LD data in Figure 5.11. This is an experiment following the assembly of FF fibres at 40 °C monitored by LD. The fibres are at a concentration of 2 mg/ml and are monitored for 4 hours.*

5.2.3.1 Capillaries

One reason for irreproducible results could be related to the LD capillary used to hold the sample during the experiments. The LD capillary is only 3 mm wide, which makes it difficult to clean thoroughly (Figure 2.5). The standard method is to rinse it with water three times and then with ethanol three times. In this case, as visible fibres were often left after this cleaning process, a small damp Kimwipe was rolled up and inserted into the capillary in order to wipe away the fibres. The capillary was then rinsed again before use. However, it is likely that there would still be remnants of fibres left at this point, which could affect subsequent experiments. For example, if there is a small part of a fibre present in the capillary at the start of an experiment, this fibre could seed one fibre to grow which could then break up in the Couette flow and seed several others, causing the signal to be observed much earlier than if the capillary was clean. If this were the case, the amount of fibres left in the capillary after cleaning would vary from one experiment to another, naturally leading to variations in the growth rate, and therefore irreproducible results in the experiments that measure it.

An acidic solvent that dissolves organic matter well, such as nitric acid, would normally be used to clean organic matter that will not dissolve in water. However, nitric acid dissolves parts of the LD capillary that are not quartz. Figure 5.13 shows that the base of the capillary is sealed with araldite and the top of the rod is made from plastic. Acid dissolves araldite and degrades the plastic at the top of the rod, and therefore cannot be used to clean them.

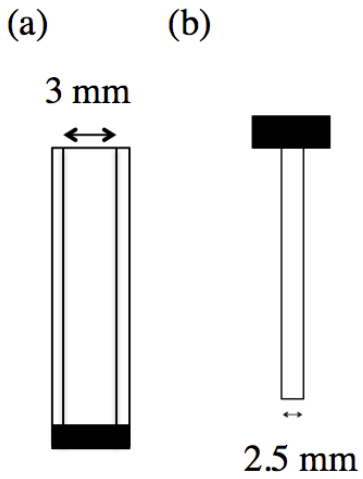

Figure 5.13 *(a) The LD capillary made from quartz with a 3 mm internal diameter, and sealed at the base with araldite. (b) The rod used in LD which is placed inside the capillary during measurements. It has a 2.5 mm diameter and a plastic top which rests on the top of the capillary.*

As there was no way to completely remove the fibres from the capillary, a new one was designed. It was made completely from standard glass instead of quartz, which meant that it had a lower melting temperature. Therefore, a glass blower was able to mold the bottom of it into a sealed end, eliminating the requirement for araldite (Figure 5.14). It was possible to leave this capillary to soak in nitric acid overnight, which dissolved all traces of the fibres.

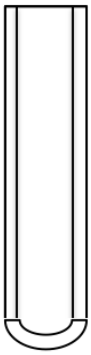

Figure 5.14 *A capillary made entirely from glass, it started as a cylinder and a glass blower created the seal at the bottom.*

Quartz is typically used in LD, and often in spectroscopy because it is pure, and therefore light does not interact with it and instead goes straight through to the sample. However, glass has impurities in it which may interact with light, absorbing or scattering it.[2] Phenylalanine has a particularly weak chromophore, and therefore a low spectroscopic signal. This weak signal combined with impurities in the glass meant that it was not possible to see any LD signal from the fibres using this capillary. Therefore another new capillary was designed and built.

The second new capillary was made from quartz, as glass did not work, and is shown in Figure 2.6. It consists of a quartz cylinder with a removable Teflon stopper at the base. A new quartz rod was made this time as well with a Teflon top. This is because previous attempts to clean the rod with nitric acid caused damage to the plastic top part. A Teflon tool was made for use with this capillary which could be inserted into it to push out the Teflon base. This meant that between LD experiments, the base was removed and cleaned with acid. The remaining part of the capillary then only had quartz in it which could be left in an acid bath overnight. The rod was left submerged in a vial of acid overnight as well, with the Teflon part left dry at the top. This top part never came into contact with the reaction mixture so did not need to be cleaned.

An experiment was set up to monitor the assembly of FF at 40 °C with the new Teflon-quartz capillary and the data from this are shown in Figures 5.15 and 5.16.

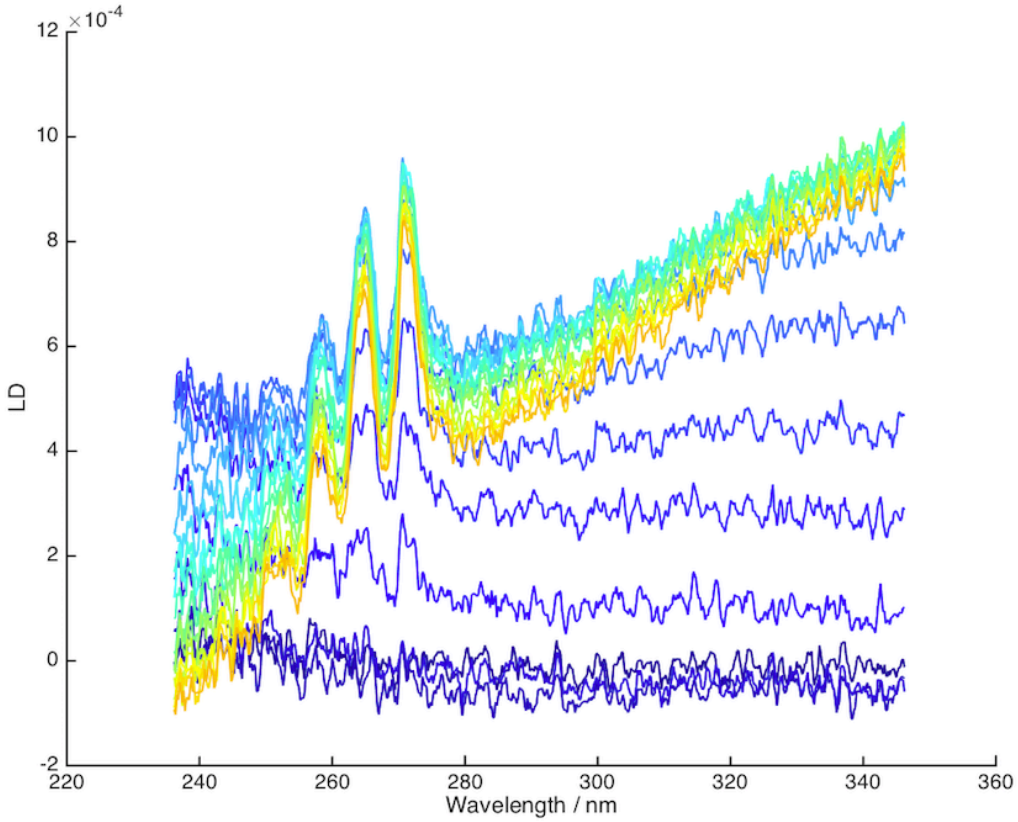

Figure 5.15 *The LD signal of FF fibres as they assemble at 40 °C. The dark blue spectra are the initial spectra and the colour of the spectra lightens as time progresses, with the final spectra appearing in yellow. This experiment was performed over the course of 4 hours on a 2 mg/ml solution of FF.*

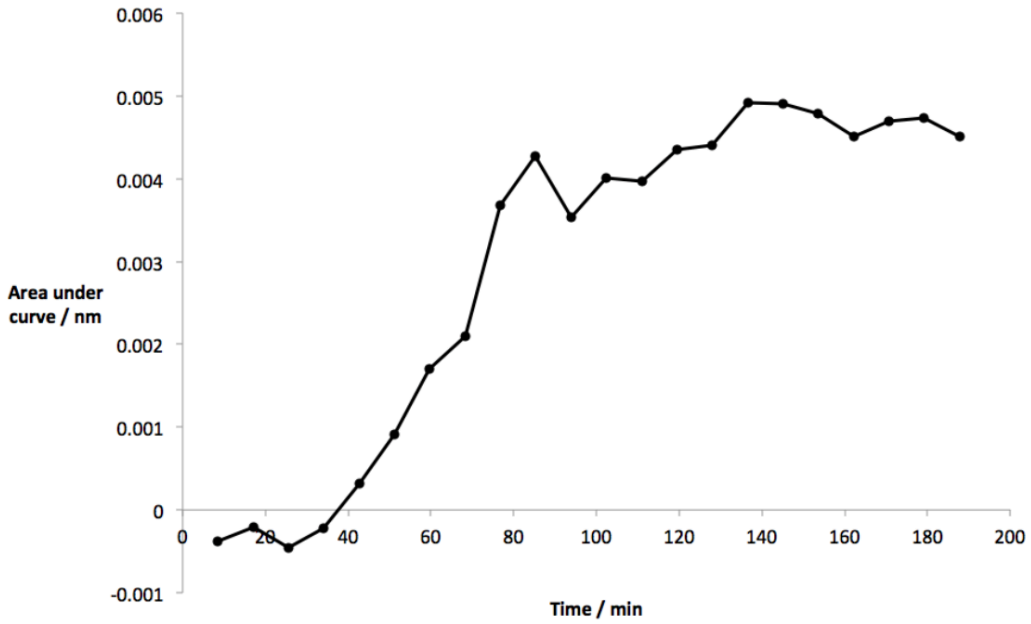

Figure 5.16 *The area under the peaks in the LD signal in the figure 5.15. This experiment monitors the assembly of a 2 mg/ml solution of FF fibres at 40 °C. The fibres are detected at around 40 minutes in this experiment which lasts for 4 hours.*

The spectra at the start of the experiment are shown in blue and the final spectra are shown in yellow in Figure 5.15. The data were particularly low in magnitude, which is why it looks noisy, and Figure 5.16 shows the area under the curve, which suggests that fibres are detected at around 40 minutes. This experiment was repeated to see if the variability in the results was still present. One replicate is shown in Figure 5.17; the scattering background in the spectra is noticeably different from the previous experiment. The area under the curve in Figure 5.18 shows that the fibres were not detected until 70 minutes into the experiment. This shows that the variability is indeed still present even when a new thoroughly cleaned capillary is used.

The signal also significantly increased in intensity in Figure 5.17 when compared to the previous experiment (Figure 5.15). This change in scattering pattern and signal intensity could indicate a problem with the fibres alignment. This is because the form of the light scattering depends on the orientation of the fibres, for example, if the fibres are oriented perpendicular to the direction of the Couette flow, the scattering would be high at low wavelengths, and low at high wavelengths. The signal intensity also depends on the orientation of the fibre: the lower the orientation, the lower the LD signal. Therefore, it appears that in the first experiment (Figure 5.15) the orientation was lower than in the second (Figure 5.17).

These experiments did not conclusively demonstrate whether the thorough cleaning of the capillaries is important or not in affecting the assembly of FF fibres. However, they have shown that this is certainly not the only source of irreproducibility, as it is still present when the capillary and rod are cleaned in acid. The fact that a second experiment with thorough cleaning took longer to initiate indicates seeding is the main problem and is not happening.

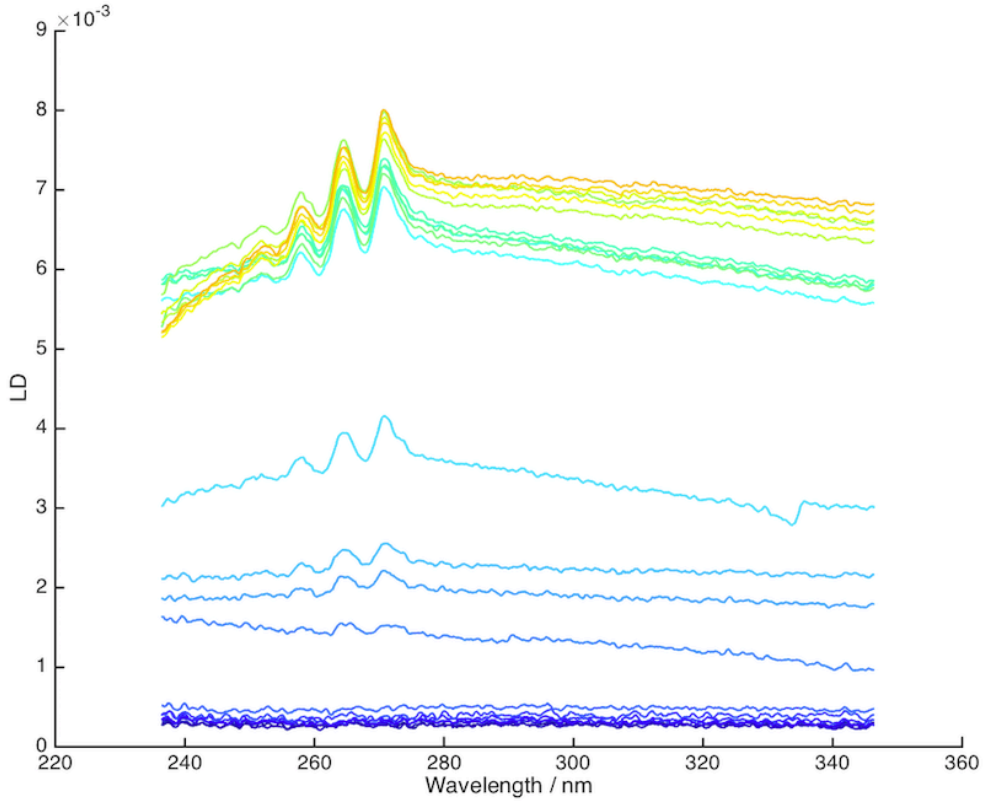

Figure 5.17 *The LD signal of a 2mg/ml solution of FF fibres as they assemble at 40 °C for 4 hours. The dark blue spectra are the initial spectra and the colour of the spectra lightens as time progresses.*

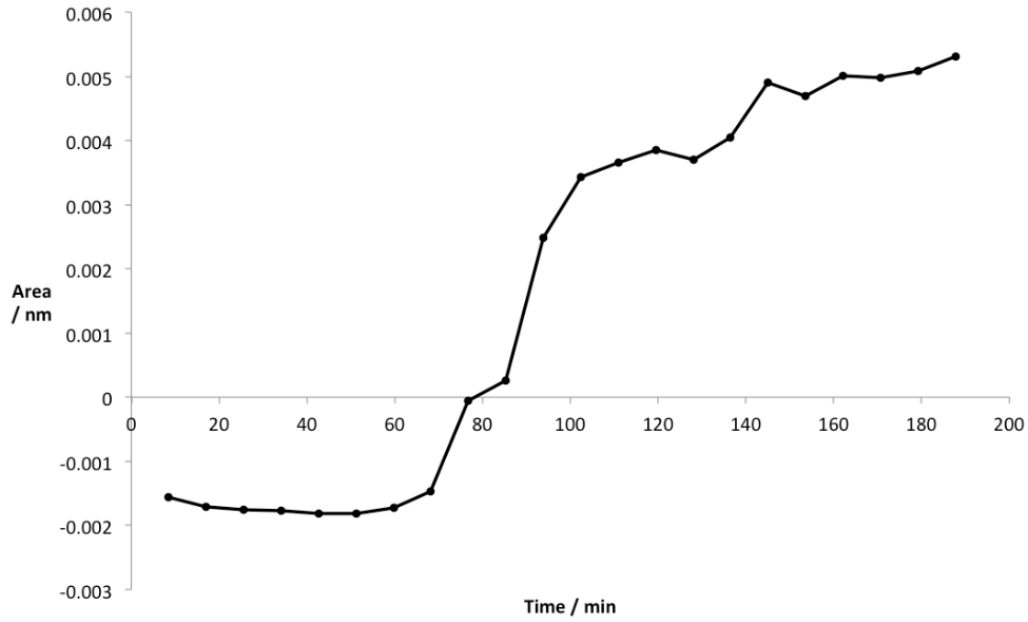

Figure 5.18 *The area under the peaks of the LD signal in the previous figure. The fibres are detected at around 70 minutes in this experiment, which monitors the assembly of a 2 mg/ml solution of FF fibres at 40 °C.*

5.2.3.2 Removal of Light Scattering from Data

In order to obtain the area under the curve in LD kinetics data, it is necessary to do a mathematical fit to the background of the data. The best fit was found using the 'polyfit' function in Matlab, which was a second order polynomial. The fit was checked visually for each spectrum and appeared to be a good fit to the scattering. An example of this is shown in Figure 5.8. However, the fit is worse when the signal is very small and the noise is large. The time when the fibres are first detected is of interest, and this is when the signal is at its lowest, so the fit is the worst. It is therefore possible that this is the source of variation in the time at which the fibres are first detected.

The best way to solve this problem is to avoid any fitting and instead take a new background (non spinning) spectrum for every time point in the measurement. This background will contain the entire scattering signal without the chromophore peaks and this can then be subtracted from the data to leave just the peaks which are of interest. This can be achieved by switching the spinning off for the background measurement and then switching it back on for the LD measurement. When the spinning in switched off the fibres should no longer be aligned so the LD signal will be zero. However, when the spinning is switched back on, the fibres will align in Couette flow and can be detected by LD.

In order to be able to switch the spinning on and off at the right point in time between background and non-background measurement, a sequencer was made which communicated with the spectrometer and computer. This automated the switching so that it was precise. This sequencer is shown in Figure 2.7, and was used in an experiment to monitor the kinetics of FF assembly. A detailed description of how it worked is given in Section 2.3. It allowed for the spinning to be switched on, a measurement to be taken, the spinning to be switched off and a measurement taken and then the cycle to be repeated many times. The measurement with the spinning switched off could then be used as a background spectrum and subtracted from the subsequent measurement.

The background spectra are shown in Figure 5.19 and the LD data in Figure 5.20. It is possible to see from Figure 5.19 that there is a signal from the chromophores in the background, which was unexpected. This means that even though the spinning was switched off, the fibres stayed aligned and were therefore capable of producing an LD signal. When the background spectra are compared to the data, they are very similar and it is clear that if one were subtracted from the other, the result would be close to zero. We concluded that the fibres stayed aligned because they were stuck, and unable to rotate. It has already been shown in Chapter 3 that the fibres grow to lengths which are in the millimetre size range. This is similar to the size of the internal diameter of the LD capillary, so it is likely that once there are fibres present that have grown to millimetres in length, they will get stuck and disrupt the orientation of the whole sample.

Thus, the new sequencer for switching the spinning off and on cannot be used to monitor the assembly of FF fibres as they stay aligned when the spinning is switched off. Therefore it was not used in any subsequent experiments. However it can be used for studying the kinetics of assembly of smaller structures with LD. This experiment has shown that there is certainly a problem with the alignment of fibres once they grow to a certain length, and this will affect the LD signal from that point onwards in any kinetics experiment. This could be a cause of irreproducible data at the end of an experiment, however, it should not affect the time at which fibres are detected.

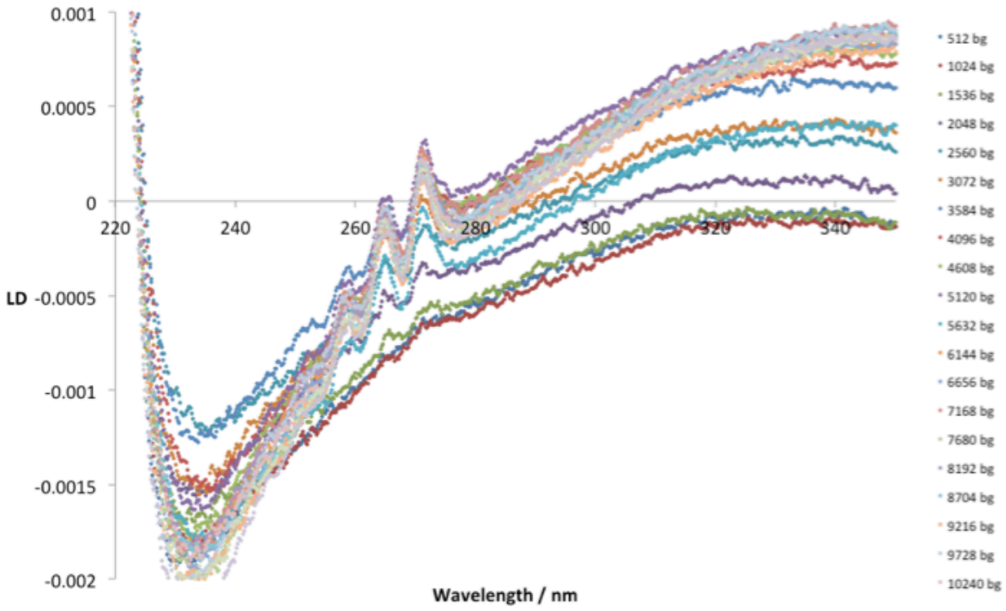

Figure 5.19 *The background measurements during an LD experiment which were taken when the spinning was switched off. This experiment followed the assembly of FF fibres at 40 °C for 4 hours at a 2 mg/ml concentration.*

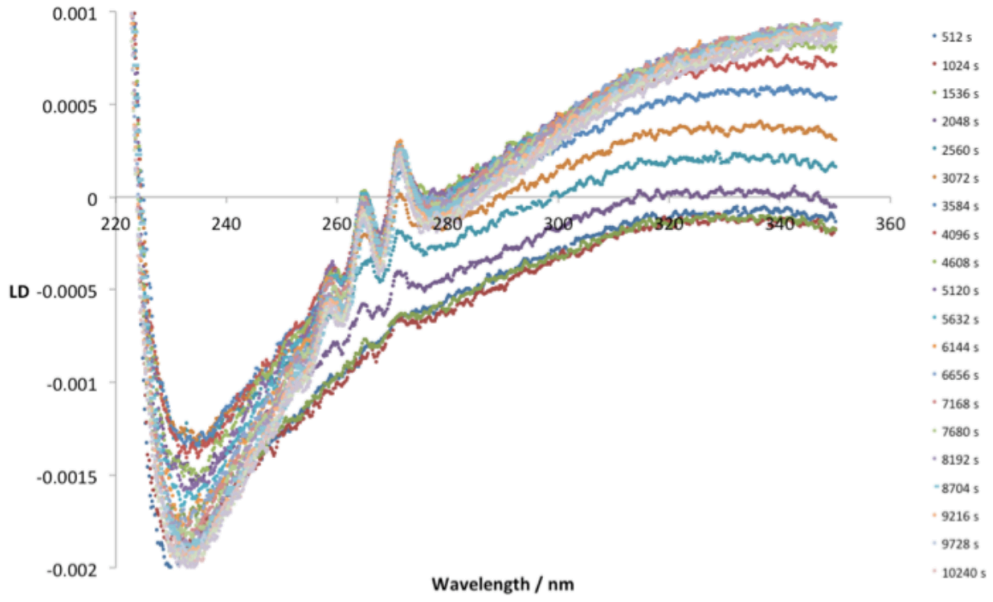

Figure 5.20 *The data from the same LD experiment as Figure 5.21, with the spinning switched on. This experiment followed the assembly of FF fibres at 40 °C for 4 hours at a 2 mg/ml concentration.*

The fact that baselines more or less equal spinning samples as soon as a signal appears suggests we have a process which does not begin with a large population of short fibres that grow to long ones, but one where once a fibre is initiated it rapidly becomes too long for the capillary geometry.

5.2.3.3 Solvent

The data may be irreproducible because the fibres start forming before the start of the experiment, during the initial heating stage. This would mean that each experiment could have a slightly different starting point. It is impossible to detect the small beginnings of fibres that may be present at time zero, so instead different solvents were investigated and compared for their ability to keep FF molecules separate. This solvent could then be used to dissolve FF to a high concentration at the start of the experiment and could then be diluted with water to initiate fibre formation. This would eliminate the possibility of an FF assembly being present at the start of an experiment, when we expect there to be no assembly.

HFIP is used in the literature,[3] as it is known to stop the FF from assembling into fibres. Three other similar solvents were used to compare to HFIP as well as water. These were trifluoroethanol (TFE), trifluoroacetic acid (TFA) and methanol (MeOH) (Figure 5.21).

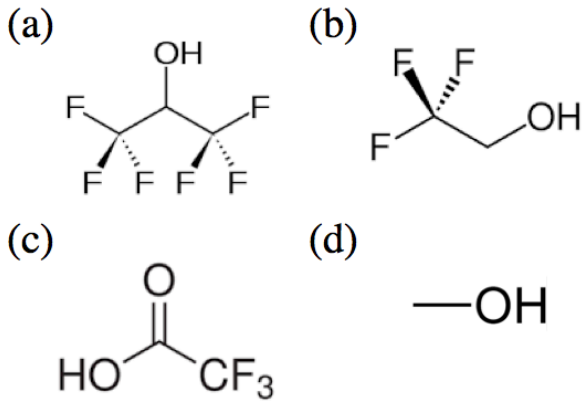

Figure 5.21 *The molecular structures of the solvents used: (a) HFIP, (b) TFE, (c) TFA and (d) MeOH.*

Absorbance spectroscopy was used to find the relative amounts of π-stacking between FF molecules in each solvent. A shift to higher wavelength indicates π-stacking, as this causes the excitation energy to decrease.[4] The spectra collected are shown in Figure 5.22. The peaks for FF can be seen with each solvent, but the shift is small, so the data for the three middle peaks were plotted as a bar chart in Figure 5.23. This shows that FF exhibits the least π-stacking in HFIP and the most in methanol, which is followed by water. This confirms that HFIP is an appropriate solvent for inhibiting the assembly of FF, and TFA and TFE are also better than water for this purpose.

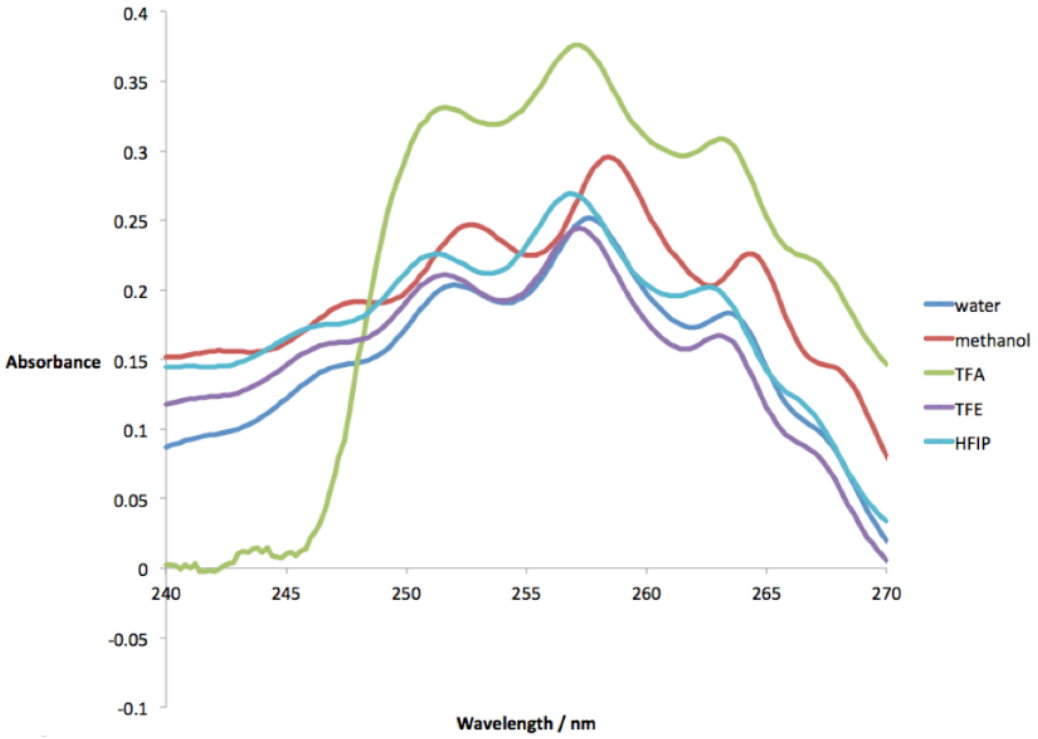

Figure 5.22 *The absorbance spectra for FF in water, methanol, TFA, TFE and HFIP. These measurements were taken at room temperature at a concentration of 0.2 mg/ml with a path length of 1 cm.*

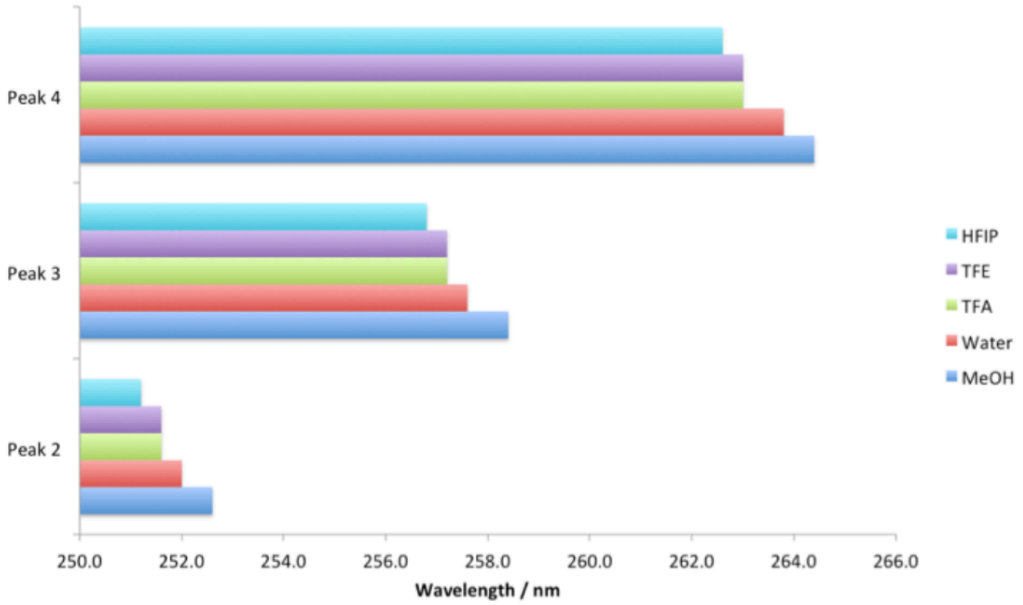

Figure 5.23 *The position of the absorbance peaks for FF in HFIP, TFE, TFA, water and methanol. These measurements were taken at room temperature at a concentration of 0.2 mg/ml with a path length of 1 cm.*

In order to perform the experiment described at the start of this section, a rapid injection LD system had to be used. This allows for two solutions to be mixed, in this case water and HFIP with FF dissolved in it, and LD measurements to be made immediately after this mixing. However, it was found that the solvents which showed the least π-stacking between FF molecules also damaged the plastic parts of the rapid injection LD system. Therefore, they could not be used in further experiments and no viable alternative to water or HFIP was found.

5.2.3.4 Intrinsic Variation in Onset Time

The experiment described at the start of this section was repeated several times, however the new Teflon Quartz capillary and rod were used and cleaned with nitric acid between experiments. The results from such an experiment are shown in Figure 5.24, and the area under the peaks is shown in Figure 5.25 for clarity. These data show clearly that no fibres were detected within the first 80 minutes of the experiment. When the fibres were detected there was a large increase in signal which was followed by a fluctuation. The work reported in Section 5.2.3.2 suggested that the fibres get stuck during the experiment as they grow to a length

which is comparable to the size of the capillary. It appears that in this experiment that point is reached at around 105 minutes, as this is the point at which the signal begins to fluctuate. Therefore, the data from this point onwards are unreliable, as the fibres can no longer become oriented. However, the data up to that point are reliable and this includes the time at which the fibres are first detected.

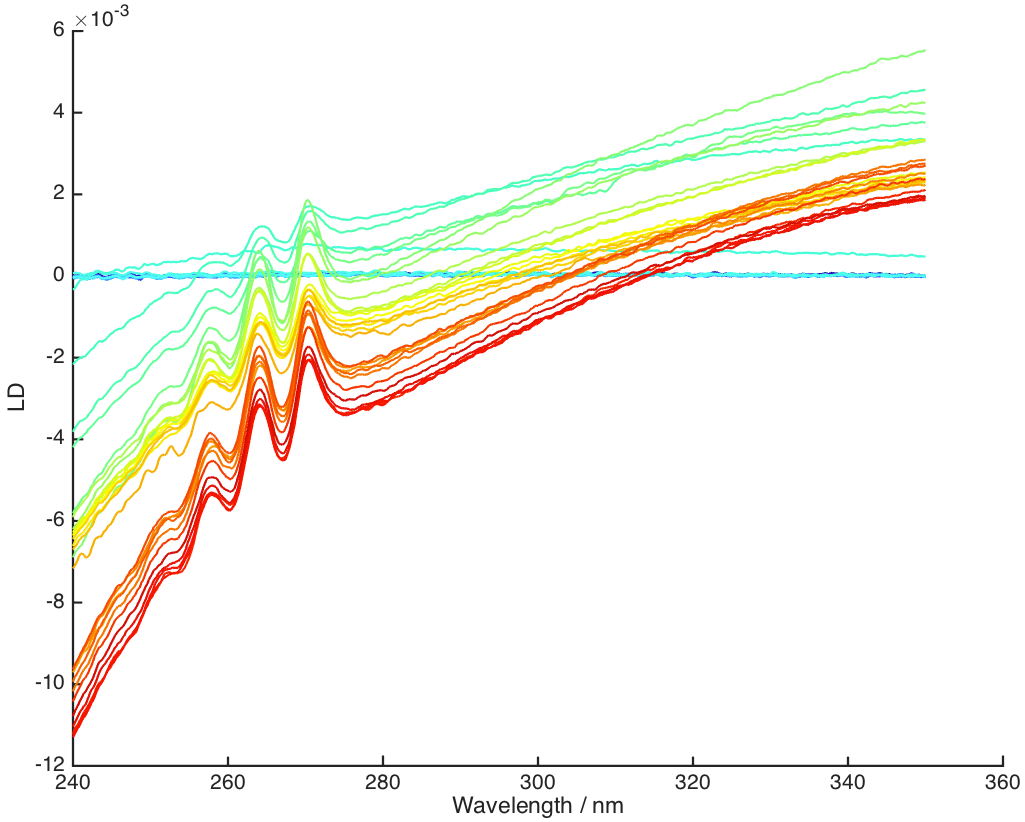

Figure 5.24 *The results of an LD experiment which monitors the kinetics of fibre formation at 40 °C. The blue spectra were taken at the start of the experiments and the red spectra, at the end. The experiment ran for 4 hours and the concentration of FF was 2 mg/ml.*

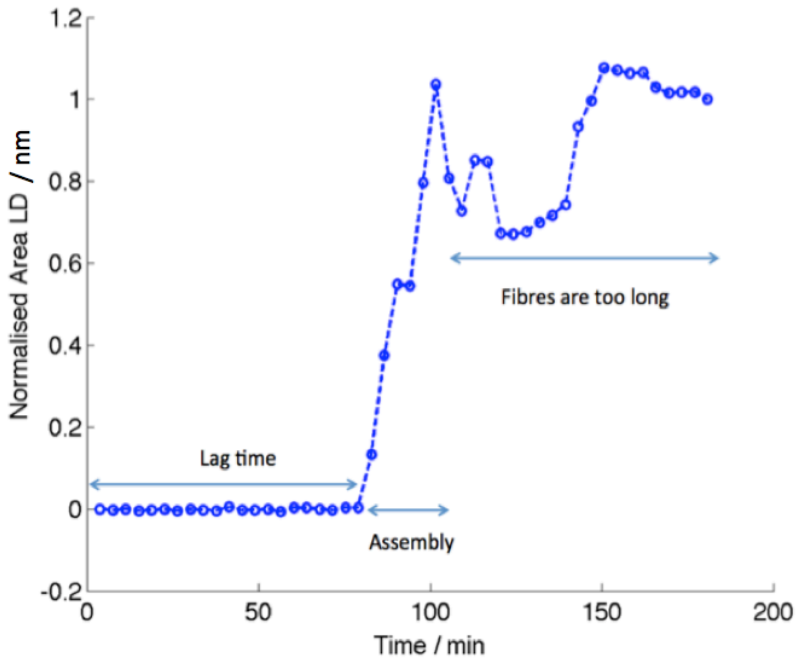

Figure 5.25 *The area under the peaks of the LD signal in figure 5.26. The fibres are detected at around 80 minutes in this experiment. The experiment ran for 4 hours at 40°C and the concentration of FF was 2 mg/ml.*

The same experiment (Figures 5.24 and 5.25) was repeated several times, one of which is shown in Figures 5.26 and 5.27. The fibres are first detected after 25 minutes in this instance, and by 80 minutes the signal has stopped increasing, indicating that the point has been reached where the fibres are long and get stuck in the capillary. This same pattern was found each time the experiment was performed, but with quantitatively different results. This illustrates the variability in the results which was still observed in these experiments, even when the clean Teflon-quartz capillary was used.

In order to quantify this variability, the time at which the fibres were first detected (the lag time) in each experiment was plotted in a histogram (Figure 5.28). This shows that the lag times follow a Gaussian distribution.

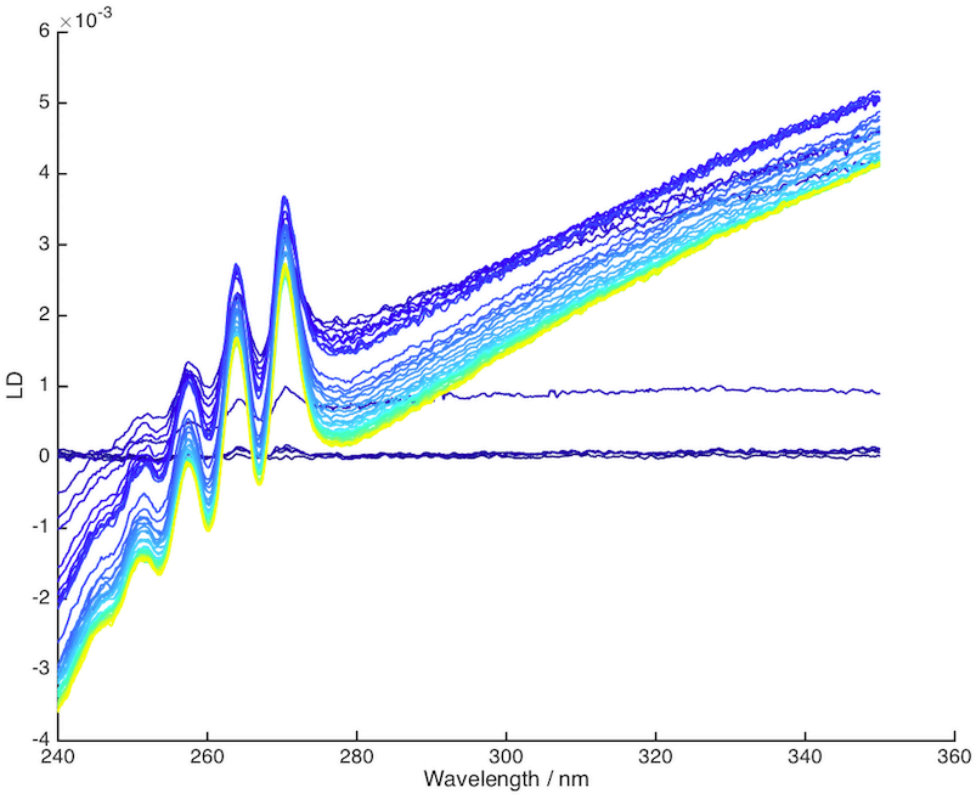

Figure 5.26 *The results of an LD experiment monitoring the kinetics of fibre formation at 40 °C. The blue spectra were taken at the start of the experiments and the yellow spectra, at the end. The experiment ran for 4 hours and the concentration of FF was 2 mg/ml.*

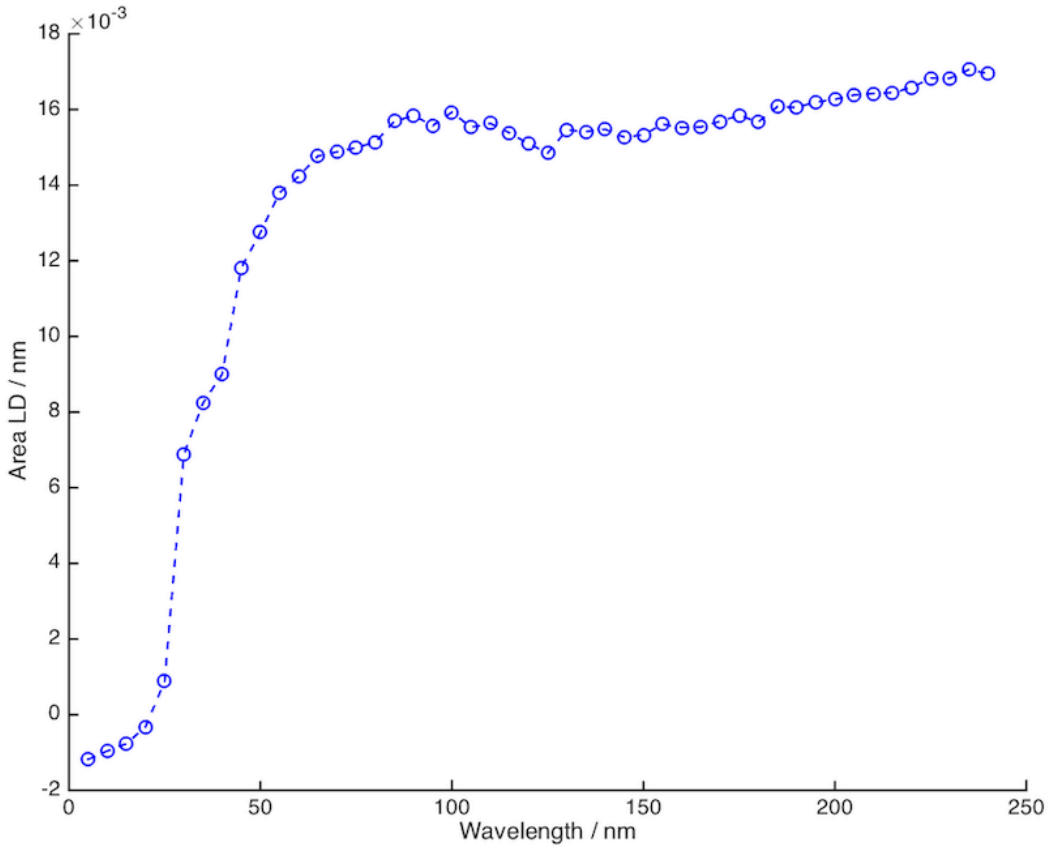

Figure 5.27 *The area under the peaks of the LD signal in the previous figure. The fibres are detected at around 25 minutes in this experiment. The experiment ran for 4 hours at 40°C and the concentration of FF was 2 mg/ml.*

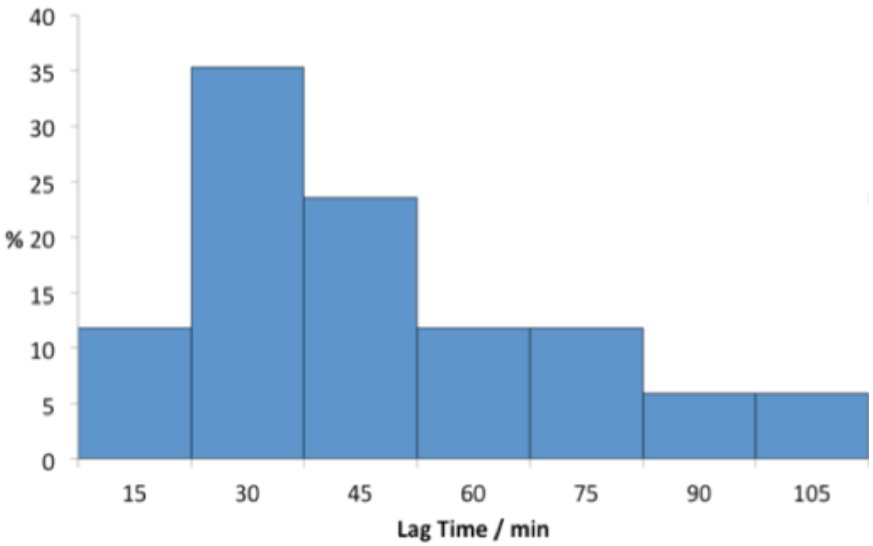

Figure 5.28 *The time taken for the LD signal to appear in 18 similar experiments (lag time). The experiments followed the assembly of FF into fibres for 4 hours at 40°C and the concentration of FF was 2 mg/ml.*

This lag time is in part due to the fact that the short fibres do not orient sufficiently to give an LD signal, however, the fact that it varies with the distribution in Figure 5.28 is indicative of nucleation-driven growth. This is because nucleation is a stochastic process, and in particular it has been shown to be Poisson-type.[5] The Poisson distribution describes a discrete random variable M and the probability ($P(M = m)$) that a number of events, m, occur in a given time interval, x, where λ is the rate at which the events occur.

$$P(M = m) = \frac{(\lambda x)^m e^{-\lambda x}}{m!} \tag{5.2}$$

In this case, m is the number of nucleation events that occur in a time interval x with a nucleation rate, λ. In order to explore the times associated with this Poisson process, we now consider time as a continuous random variable X. The cumulative distribution function (CDF) of the nucleation events as a function of time, $F(x)$, is described as follows.

$$F(x) = P(X \leq x) \tag{5.3}$$

$$F(x) = 1 - P(X > x) \tag{5.4}$$

The CDF is equal to the probability that at least one event has occurred up to and including the time interval x. We can find the probability, $P(X > x)$, by setting the number of nucleation events, M, equal to zero in the Poisson distribution (Equation 5.2).

$$P(X > x) = P(M = 0) \tag{5.5}$$

$$P(M = 0) = \frac{\lambda x^0 e^{-\lambda x}}{0!} \tag{5.6}$$

$$P(M = 0) = e^{-\lambda x} \tag{5.7}$$

This can now be substituted into the CDF (Equation 5.4).

$$F(x) = 1 - e^{-\lambda x} \tag{5.8}$$

This function describes the cumulative distribution of the probability for the time taken for a nucleation event to occur. It was noted by Jiang and Horst [6] that, in experiments, it is not possible to measure the time taken for a nucleation event to occur, but instead, the time it takes to detect that a nucleation event has occurred. In other words, the crystal must grow large enough to be detected, and therefore, we must introduce a growth period, t_g, into the equation. The total time, t, is the sum of the time for the nucleation event to occur, x, and the growth time, t_g.

$$t = x + t_g \tag{5.9}$$

We substitute this into Equation 5.8 to produce a modified cumulative distribution function for detecting a nucleation event.

$$F(t) = 1 - e^{-\lambda(t - t_g)} \tag{5.10}$$

This probability can be experimentally determined by performing a number of identical experiments, N, and plotting the fraction of experiments in which the product of nucleation has been detected versus time. This is given by the following equation.

$$F(t) = \frac{N^*}{N} \tag{5.11}$$

where N^* is the number of experiments in which the fibres have been detected. Once this data has been plotted, the growth time, t_g, can be extracted.

We can differentiate the CDF (Equation 5.10) to reach the probability density function for a nucleus to be detected at a particular time.

$$f(t) = \frac{dF(t)}{dt} = \frac{d}{dt}\left(1 - e^{-\lambda(t-t_g)}\right) \tag{5.12}$$

$$f(t) = \lambda e^{-\lambda(t-t_g)} \tag{5.13}$$

This is the distribution of probabilities for a nucleation event to be detected. It is the exponential distribution, shifted by a growth time, t_g. In the case of FF fibre growth being detected by LD, there are many fibres grown in each sample, of various widths and lengths, as opposed to a single crystal. Therefore, we do not expect to see one shifted exponential distribution, but several combined, to produce a distribution as shown in Figure 5.29 (b). This is similar to the data recorded for FF fibres shown in Figure 5.28, which shows that FF grows into fibres in a way that is consistent with nucleation driven assembly.

The data were also plotted in the form of Equation 5.10. This is shown in Figure 5.30 for the case of FF fibres measured by LD and it fits well with Equation 5.1 (shown in blue), with a root mean square error (RMSE) of 0.04. This shows that the data fits well to this theoretical model of nucleation driven growth. The nucleation rate was extracted from the fit and was found to be 0.03 (0.028, 0.035) min^{-1}. Typically the experiments are 4 hours long, and therefore this nucleation rate would only produce 7 fibres. This is much too low, as there are many more fibres than this at the end of an experiment as shown by microscopy in Chapter 3. Therefore primary nucleation cannot be the only method by which fibres grow. Secondary nucleation may be taking place which would dramatically increase the number of fibres present in a sample. Secondary nucleation requires that when the fibres are small, they easily break up. These pieces would then act as nuclei to seed the growth of several other fibres, and the nucleation rate does not include these fibres. Some evidence to support such a secondary nucleation hypothesis has been observed in SEM images. Figure 5.31 shows a fibre which has branched out into many fibres. One of these fibres has started to break off from the main fibre. If this structure was still in water, it is easy to see that it could snap off and grow separately. It is likely that the Couette

flow used in LD would contribute to the fragmentation of the early assemblies, facilitating the secondary nucleation of new fibres.[7]

The growth time of the fibres was 8 (6.3, 10.8) minutes, which in this case is the time taken for the fibres to grow larger than the diameter of the light beam (~1 mm). From microscopy data (Chapter 3) it is possible to see that the fibres grow at a speed of around 2 mm/hour at the start of the experiment which means they would be larger than the beam size within half an hour, which is consistent with a fibre growth time of 8 minutes.

A further source of variation in nucleation-driven assembly can come from the heterogenous nature of the mechanism. It is possible to have a system in which homogenous nucleation takes place, however this is uncommon. Homogenous nucleation happens in solution whereas heterogenous nucleation occurs at a surface which is in contact with the solution and is typically much quicker. Heterogenous nucleation often takes place at the surface of impurities in the solution. For example water can freeze in ice at high temperatures *via* heterogenous nucleation when impurities are present.[8]

In the case of FF, it is likely that the molecules nucleate on surfaces of impurities which may be present in solution or on the rod and capillary used in LD experiments. It is impossible to know the exact nature of these impurities, but there will be a variety of them and their surface is likely to be uneven and course. The rate of nucleation rate at a surface will depend on the ability of the FF nucleus assemble at it based on its local characteristics. This will vary within one surface if it is uneven and will therefore give rise to a variation in the nucleation and subsequent assembly of the fibres.[9]

(a)

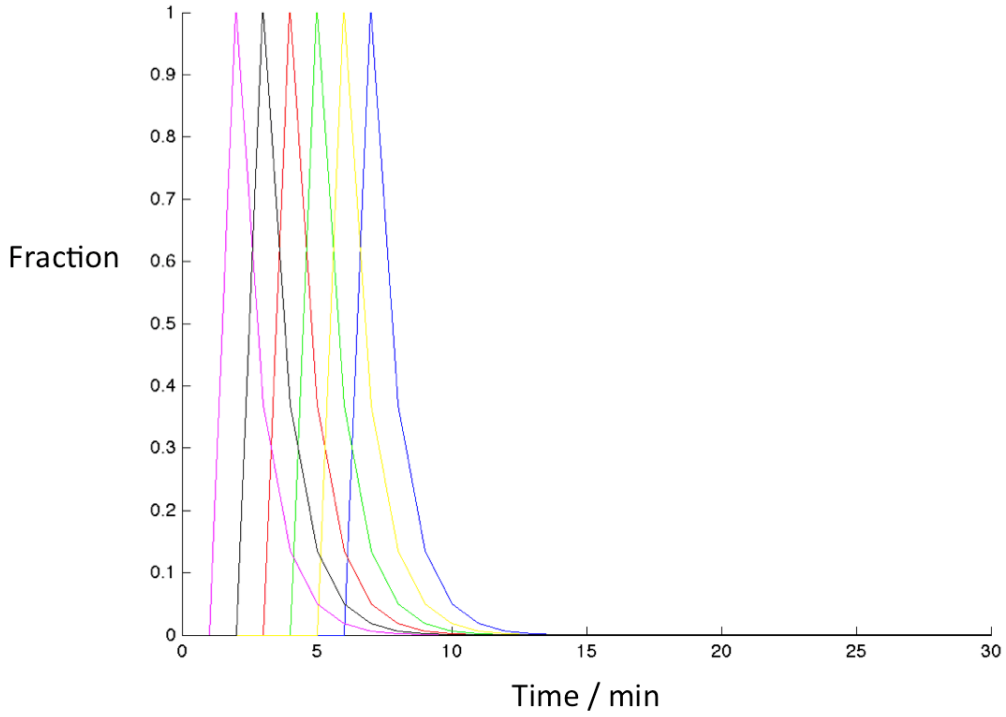

(b)

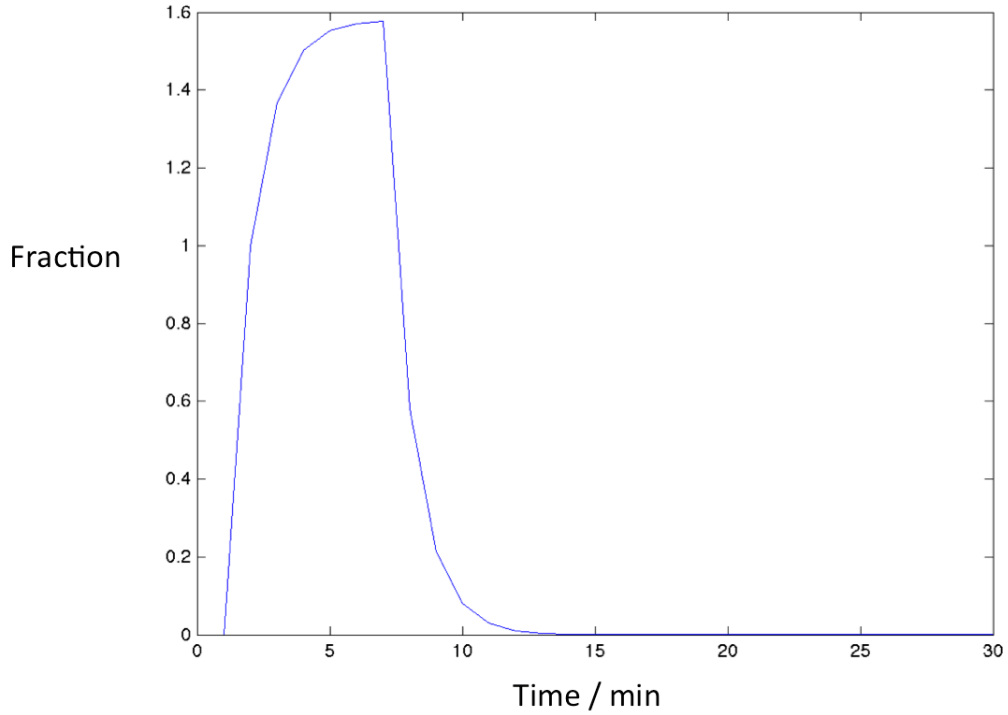

Figure 5.29 *(a) Several exponential distributions with different lag times. (b) The sum of the curves in (a).*

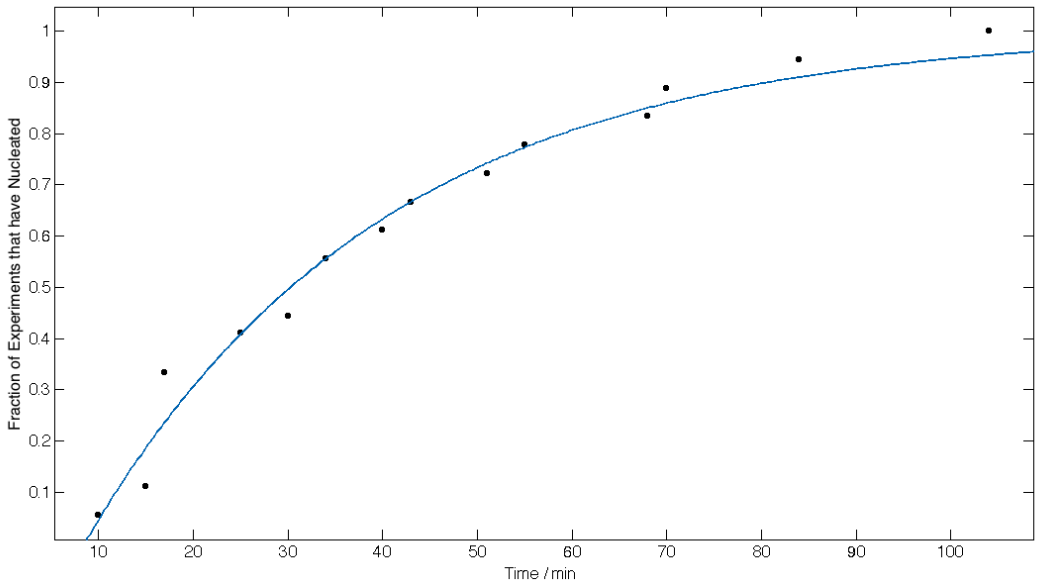

Figure 5.30 *The fraction of kinetics experiments that have detected fibres (as defined by the time at which the peaks are first detected) as a function of time. The blue line shows the fit to the cumulative distribution function. These kinetics experiments followed the assembly of FF fibres for 4 hours at 40°C and the concentration of FF was 2 mg/ml.*

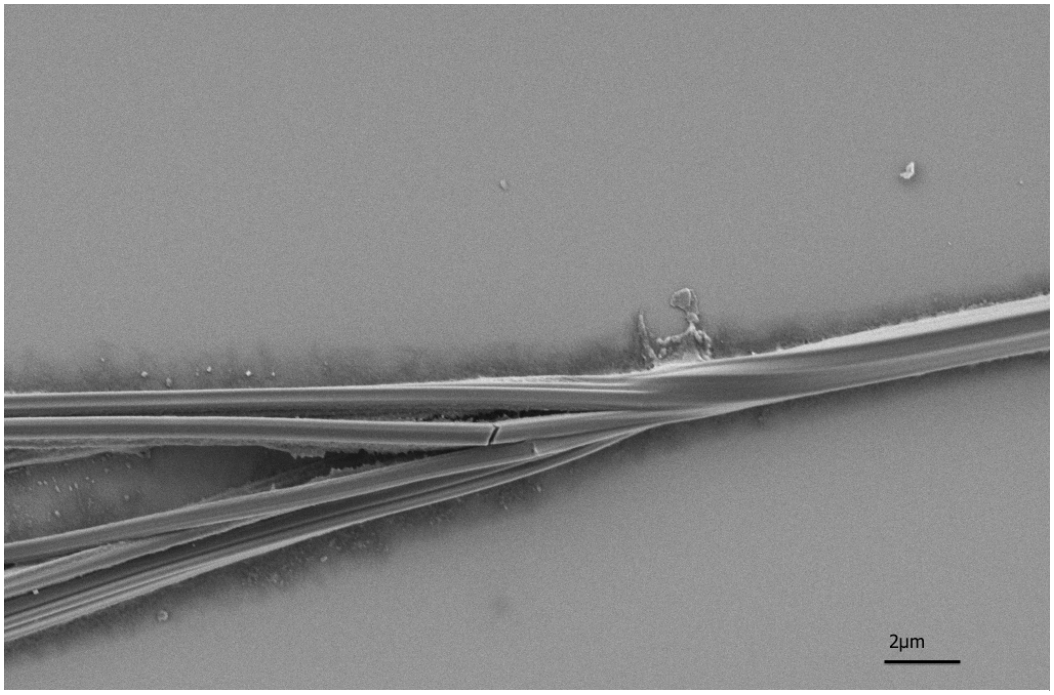

Figure 5.31 *A fibre, which has branched into many fibres. One of these fibres has started to break off. This shows that fibres may break up during their growth.*

5.2.4 LD with Aliquots Taken

In Section 3.5 an experiment is discussed in which an LD experiment was performed at 40 °C in order to monitor the kinetics of assembly of FF fibres. It is identical to the previous kinetics experiments in Section 5.2.3, except that at four times in the experiment, an aliquot was taken from the LD capillary. These aliquots were analysed by SEM. The aim of this experiment was to view the range of sizes of fibres present at different points in an experiment, and to correlate this with the LD signal. The results of the SEM imaging are shown in Section 3.5.

The LD results from this experiment are shown in Figures 5.32 and 5.33. It is clear that fibres are present as peaks occur 80 minutes into the experiment. However, this coincides with the time at which the second aliquot was taken, so it appears that the process of taking the aliquot interfered with the LD experiment. The third aliquot was taken at 160 minutes and at this point the signal dramatically decreased. This confirms that taking an aliquot impacts heavily on the LD experiment. This is because the rod must be removed from the

capillary and then the capillary must be removed from the instrument in order for the removal of a 10 μL drop to take place. The process of removing and replacing the rod has a large impact on the orientation of the fibres, and for the long fibres, this effect could be permanent, as the Couette flow is not sufficient to change it. It has already been shown that the fibres are likely to get stuck in between the rod and capillary as they grow to large sizes, and this supports the idea that moving the rod would permanently change the orientation of the fibres. Therefore, it is not possible to take aliquots from FF fibres whilst performing an LD experiment without affecting the signal.

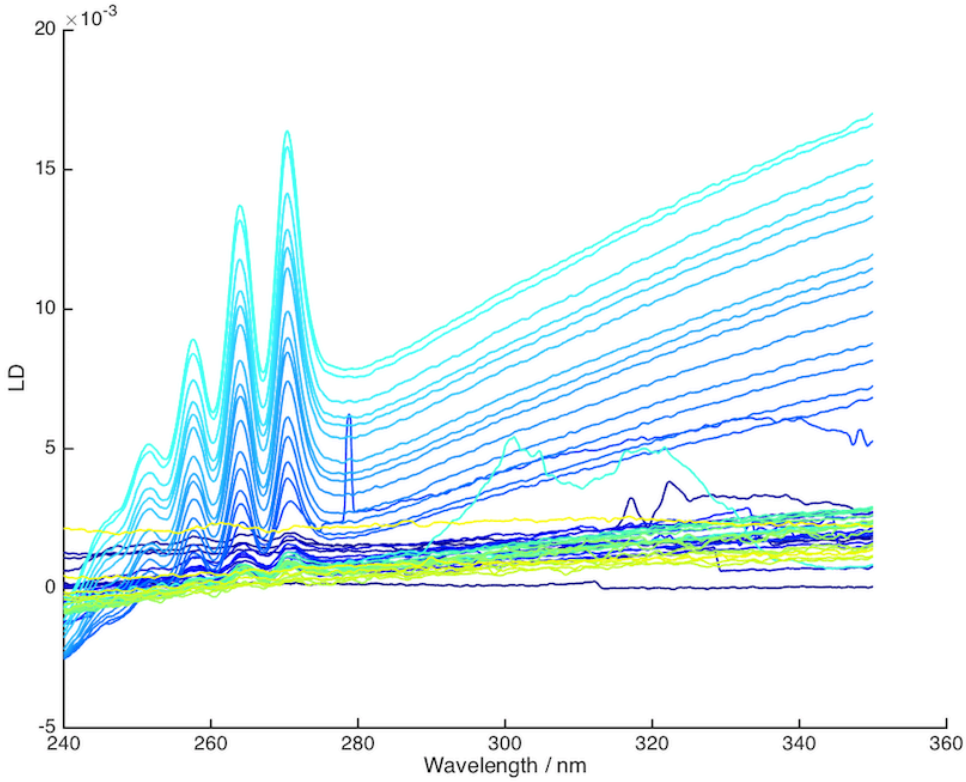

Figure 5.32 *The results of an LD experiment monitoring the kinetics of fibre formation at 40 °C for four hours at a concentration of 2 mg/ml. The blue spectra were taken at the start of the experiments and the yellow spectra, at the end.*

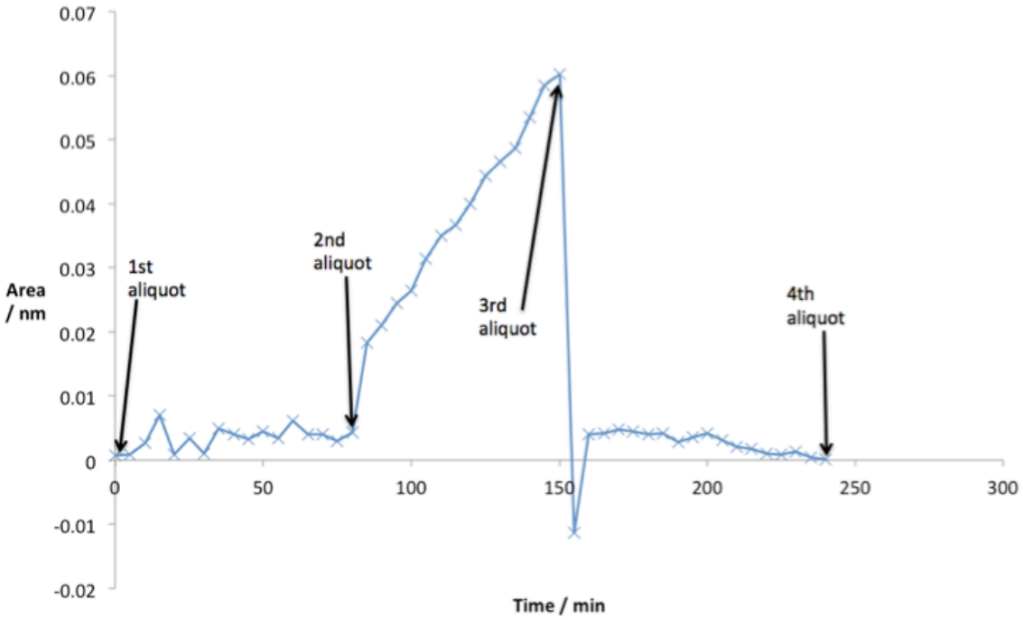

Figure 5.33 *The area under the peaks in the LD signal in the previous figure. This experiment follows the assembly of FF fibres in a 2 mg/ml solution at 40 °C for 4 hours. The signal is clearly affected by the removal on an aliquot of the reaction mixture.*

It is apparent that although Couette LD can provide useful information about the assembly of FF fibres, it cannot cover the whole process. Therefore, a different technique was used which is described in the next section.

5.3 Right Angle Light Scattering

The LD experiments showed that FF ultimately assembles into structures with a high aspect ratio. However, they miss the initial assembly because the low aspect ratio oligomers do not flow orient. Therefore, once it was established that fibres did form in spectroscopy experiments, we turned to right angle light scattering (RALS) which allowed for the whole assembly process to be detected, as even small aggregates can be revealed. RALS has previously been used to monitor the formation of various fibres including FtsZ fibres [10] and the nucleation-driven assembly of the bacterial actin MreB.[11] It is useful for these types of investigations because the RALS signal increases as the particle size increases. A large cuvette was used in these experiments (1 cm^2 cross sectional area) so that

the large FF fibres did not get stuck. The experimental setup was similar to that of the LD experiments; the sample was heated to 70 °C, transferred to the cuvette, cooled to 40 °C and then the measurement was started. However, a spectrofluorometer was used as this instrument allows for light scattered at 90 ° to be measured.

The time-dependent RALS signal for the self-assembly of fibres (Figure 5.34) shows that the assembly is fast, but variable from run to run, then progressively slows down. The similar shapes but different intital slopes of the repeats of this experiment support the nucleation-driven assembly hypothesis.

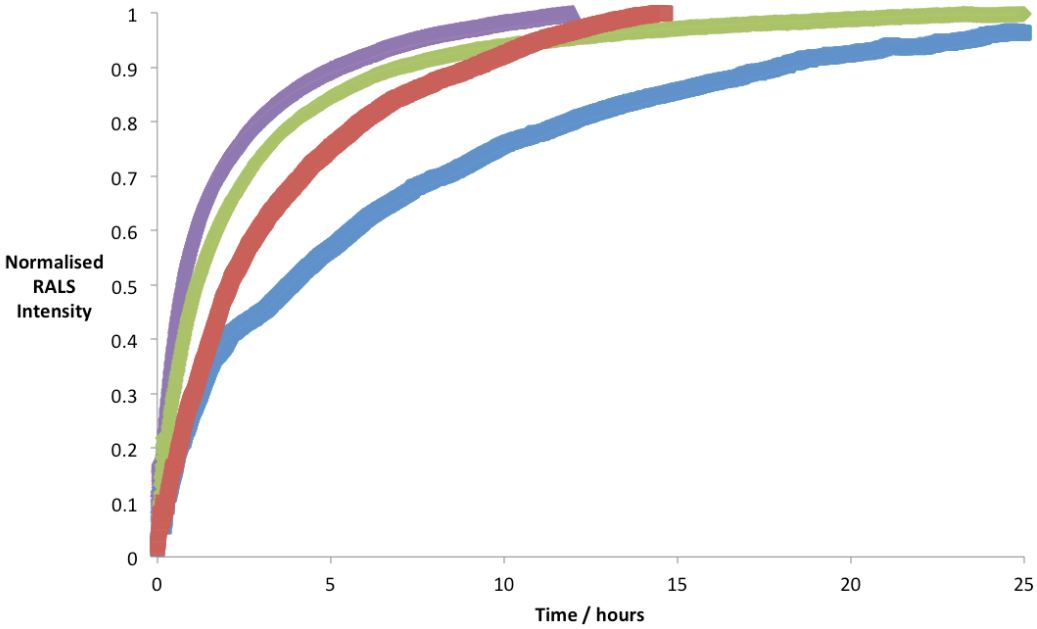

Figure 5.34 *RALS of 4 similar experiments of a 2 mg/ml FF solutions heated to 70 °C, cooled to 40°C using a Peltier cooling and heating system and then held at that temperature.*

Using RALS, we do not necessarily expect to see a lag period as we do with the LD experiments because RALS detects even small aggregates, which are too short for LD. Instead, we expect to see a variation in the gradient of the curve for the assembly, so that they will all reach the same intensity at different times. The variation in the times should be similar to the variation in lag time seen in the LD experiments.

After ~5 hours the growth becomes consistent with a first order reaction. This was found by calculating the natural log of the RALS intensity subtracted from the maximum RALS intensity, shown in Figure 5.35. During the first 5 hours, the reaction is quicker and the total assembly process continues for 24 hours.

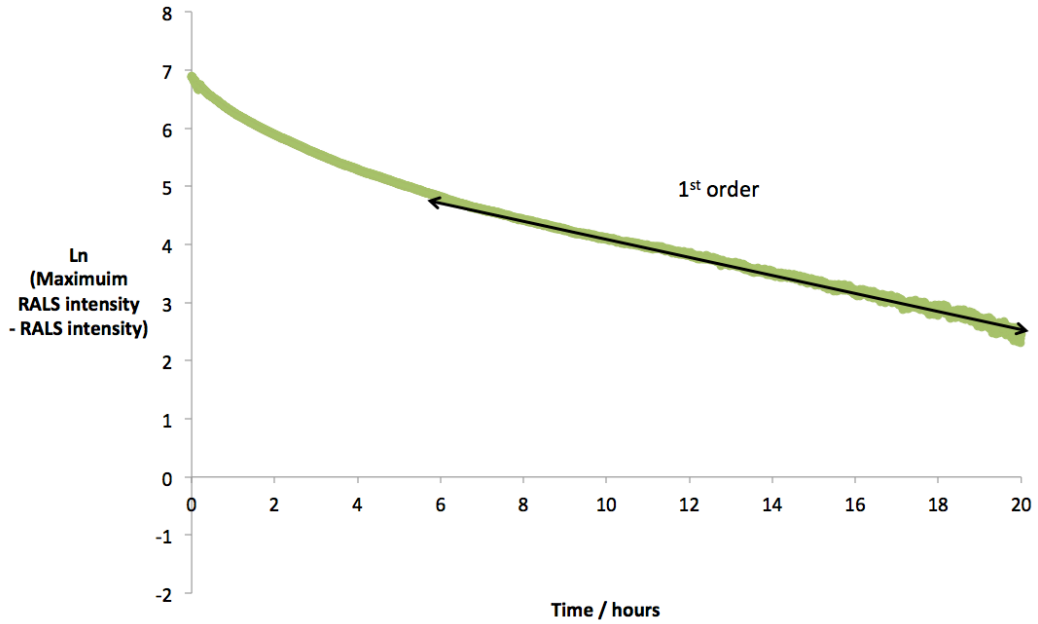

Figure 5.35 *The natural log of the RALS intensity subtracted from the maximum RALS intensity for the green data set in Figure 5.33. This experiment uses RALS to follow the assembly of a 2 mg/ml solution of FF which was heated to 70 °C, rapidly cooled and then held at 40°C. The linear part from 5 hours onwards indicates a 1st order reaction.*

Static light scattering is not only dependent on the volume of the scattering particle, but also its shape, and for a heterogeneous sample such as FF fibres, it is impossible to determine the size distribution from RALS data. First order growth is consistent with fibres growing by addition of single peptides, rather than continuous nucleation and new fibre growth.

It is now possible to compare the RALS data, which monitors the whole growth process and averages over many fibres, to the microscopy data, which gives information about the fibres size. Both experiments had identical conditions, so it is possible to correlate a certain time point in one experiment with the other. The

results from RALS and optical microscopy are overlaid in Figure 5.36. The length of the fibres, calculated from microscopy data increase in a similar manner to the RALS signal. This suggests that the main contribution to the RALS signal is the length of the fibres. It is also evident from the microscopy that the width of the fibre does not vary much during the experiment, so cannot be the cause for the RALS signal to change. This allows us to conclude that the RALS data shows that the length of individual fibres grows in accordance with a first order reaction.

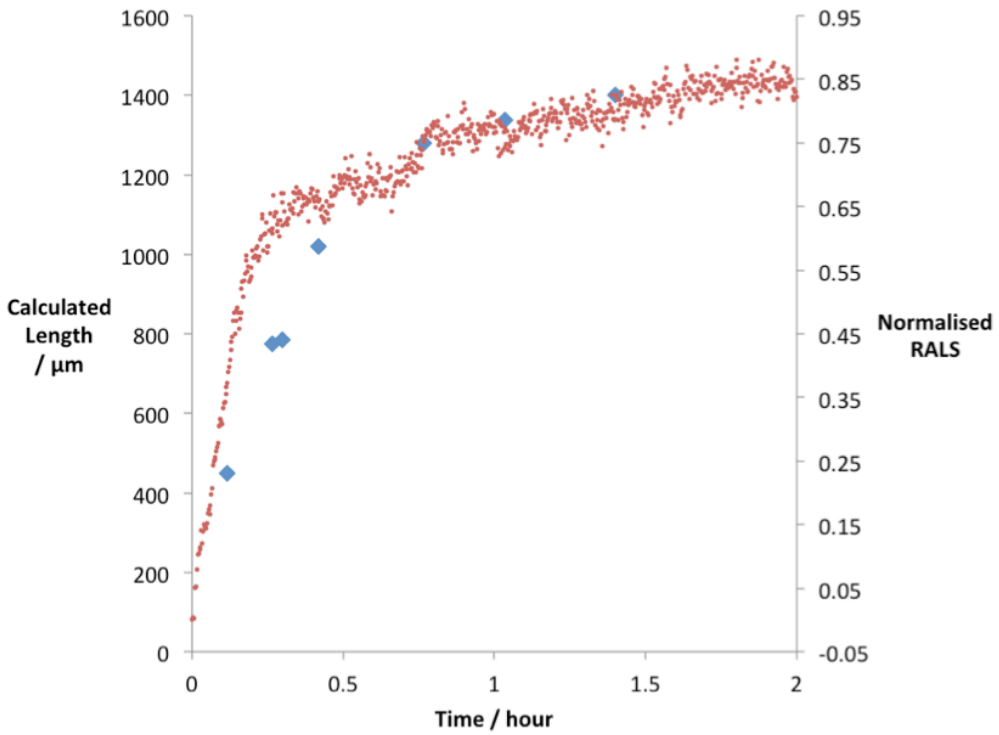

Figure 5.36 *Data from fibre assembly at 40 °C measured by right angle light scattering (from Figure 5.34) are shown in red overlaid with calculated lengths from microscopy (from Figure 3.25) are shown in blue.*

5.4 Investigation into the Reason for the Decrease in Growth Speed of FF Fibres using Absorbance Spectroscopy

It was evident in Figure 5.36 that the fibre growth was very fast at the start and then slowed down over time. A reason for this could be that the available

peptides are depleted as more fibres are made. In order to investigate this we looked at the concentration of available peptides in the solution during assembly using absorbance spectroscopy.

In order to check whether or not peptide depletion was a factor in the dramatic decrease in growth speed, absorbance spectroscopy of the FF peptides and small oligomers in solution during the assembly process was performed. Absorbance spectroscopy can be used to measure the absolute concentration of chromophores in a solution. The assembly was monitored using absorbance spectroscopy, and between each time point a 1 μm filter was used to remove fibres larger than 1 μm, so that only the concentration of monomers and small oligomers was measured. The FF solution was heated to 70 °C for 20 minutes in an oil bath and then transferred to a 1 cm x 1 cm cuvette in the spectrometer where it was cooled to 40 °C. A spectrum was measured every 30 minutes and the sample was passed through a warm 1 μm filter just before each spectrum measurement (Figure 5.37). The extinction coefficient was used to calculate the concentration of FF in solution from the absorbance intensity after a subtraction was done to eliminate the scattering contribution to the signal.

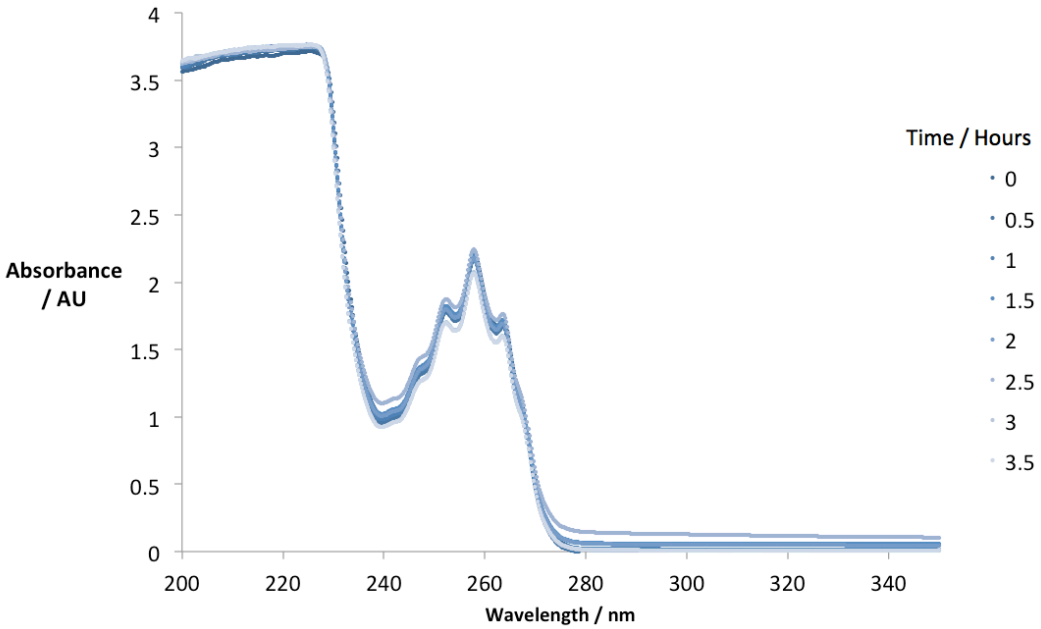

Figure 5.37 *The absorbance spectrum over 3.5 hours of FF assembling at 40 °C at a concentration of 2 mg/ml in a cuvette with a 1 cm path length.*

The intensity of the absorbance peaks was used to calculate the concentrations of the FF solution. The percentage concentration of monomers and small oligomers is shown in Figure 5.38. These data suggest that the concentration of monomeric and oligomeric FF is not decreasing in the same manner as the growth speed is increasing. This means that the decrease in growth speed is not because of dipeptide depletion, but must be intrinsic to this system.

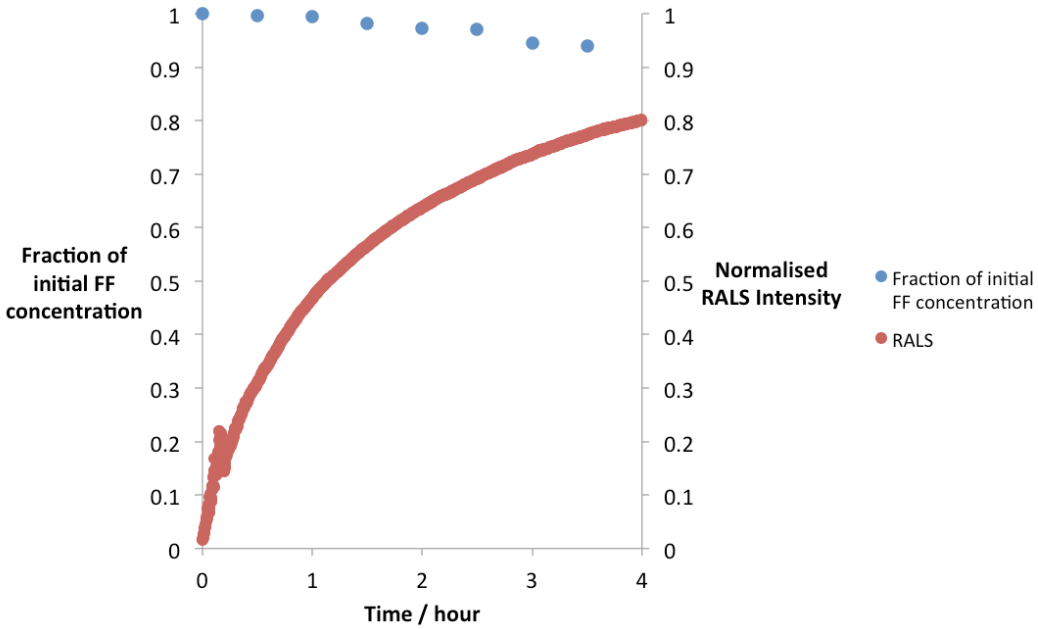

Figure 5.38 *Concentration of monomeric and oligomeric diphenylalanine as measured by absorbance spectroscopy during the assembly of the fibres overlaid with the right angle light scattering signal of FF assembling into fibres. The concentration data is from the results shown in Figure 5.37, where the assembly of FF was monitored using absorption spectroscopy, with fibres filtered from the sample before each measurement. The RALS data comes from Figure 5.34 and shows the FF assembly over time. Both experiments were done at 40 °C with a concentration of 2 mg/ml of FF.*

5.5 Conclusion

This work has shown for the first time the spectroscopic properties of FF and used them to learn about the mechanism by which the fibres assemble. LD can be

coupled with RALS to monitor this whole process under a variety of conditions, and this methodology can be applied to other rod-shaped systems.

LD has revealed quantitatively the nature of the temperature dependence of this self-assembly process. These experiments showed that the fibres assembly and disassembly is different. During the assembly process there is no sign of the fibres for the first 30 °C of cooling from 70 °C. The signal then appears, at around 40 °C and increases dramatically until the cooling has finished at 20 °C. When the sample is then heated up, the fibres start to disassemble immediately and do so in a continuous fashion for the remainder of the experiment. This suggests that the fibres do not start to assemble until the solution reaches a supersaturation level, at which point they assemble quickly. At the supersaturation point, crystal nuclei are able to form. These nuclei seed the growth of fibres which are then detected by LD. Therefore we can conclude that this supersaturation point is reached before 40 °C. Conversely, the disassembly is a steady process as it is not affected by nucleation.

The nucleation-driven assembly mechanism is further confirmed by LD experiments monitoring the kinetics of assembly of FF fibres. These experiments revealed that there was a period of time in which the fibres did not assemble and then they grew quickly. The LD data also showed a variation in onset time which fitted mathematically with nucleation-driven assembly (Figure 5.30). The low nucleation rate extracted from this fit, coupled with evidence from SEM images suggests that secondary nucleation is taking place.

The LD method was improved in several ways in order to facilitate the problematic fibres. A new Teflon-quartz capillary and rod with removable parts were designed and built. They were designed to allow for a more thorough cleaning to take place than has been possible before, and in this case they prevented FF remnants from previous experiments from seeding in subsequent measurements.

A new sequencer was also designed and built. This allowed for an automated background measurement to be taken for each individual spectrum when a series of spectra were being taken. Previously the background measurement taken at the start of the experiment had to be used for all subsequent spectra, but it is not always adequate. This is true for many systems, and particularly ones that have a dramatic change in size as this will cause the light scattering to change, which affects the LD spectrum.

Although LD revealed the nucleation driven nature of FF assembly and the nature of its temperature dependence, it was not capable of following the entirety of the growth process. Therefore, once LD had confirmed the presence of fibres, RALS was used to record the whole self-assembly period. When this RALS experiment was repeated it revealed a variation in the speed of assembly at the start of the measurement. This is consistent with the variation in onset time observed with LD and indeed, nucleation-driven growth. Further analysis of RALS data revealed that the fibres grow in a manner consistent with first order growth after the first 5 hours.

We are able to conclude that the FF peptides grow by nucleation-driven assembly in order to form fibres. This is achieved by a solution containing FF becoming supersaturated. Once this point has been reached, the fibres can nucleate and grow quickly. Then after 5 hours, the growth settles into a first order process, which is consistent with one peptide attaching to a fibre at a time, as opposed to a group adding to a fibre.

5.6 Future Work

It has been possible to ascertain that FF fibres grow by a nucleation driven assembly mechanism. However, it may be feasible to find more information on the initial assembly period by using CD spectroscopy. This is a technique similar in experimental setup to linear dichroism, except that circularly polarized light is used instead of linear and no alignment is required. This allows for the secondary structure of proteins to be ascertained. FF fibres have a β-sheet secondary structure, so they should produce a CD signal and the single petides will not. As

alignment is not necessary a standard 1 cm × 1 cm cuvette can be used and so there will be no issues with size as in LD.

Following on from the absorbance experiment in Section 5.4 of this chapter, it is possible to perform a definitive experiment to determine whether or not diffusion limited growth is taking place. This experiment could be performed in a similar manner, where the assembly of FF is monitored over time by measuring the absorption spectra. However, instead of filtering the solution at different time points, extra FF could be added during the experiments. If this made no difference to the kinetics of the experiment, it would determine that surface limited growth is taking place. However, if the growth rate ceased to slow down as in other experiments, it would be possible to conclude the growth is diffusion limited.

References

[1] Mikati, N., Nordh, Jerker, & Nordén, B. (1987). Scattering anisotropy of partially oriented samples: Turbidity Flow Linear Dichroism (Conservative Dichroism) of Rod-Shaped Macromolecules. *American Chemical Society. 23,* 6048-6055.

[2] Vogel, W. (1985). Chemistry of Glass. *American Ceramic Society.*

[3] Reches, M. & Gazit, E., (2003). Casting metal nanowires within discrete self-assembled peptide nanotubes. *Science, 300*, 625-627.

[4] Brédas, J. (1998). Conjugated oligomers, polymers and dendrimers: from polyacetylene to DNA. *Proceedings of the Fourth International Francqui Symposium*. 21-23.

[5] Barlow, T.W., & Haymet, A.D.J. (1994). ALTA: An automated lag-time apparatus for studying the nucleation of supercooled liquids. *Review of Scientific Instruments, 66*, 2996.

[6] Jiang, S., & ter Horst, J. H. (2011). Crystal nucleation rates from probability distributions of induction times. *Crystal Growth and Design, 11*, 256-261.

[7] Serra, T. & Casamitjana, X. (1998). Modelling the Aggregation and Break -up of Fractal Aggregates in a Shear Flow. *Applied Scientific Research, 59,* 255 -268.

[8] Pruppacher, H. R. & Klett, J. D. (1978). Microphysics of Clouds and Precipitation. *Reidal Publishing, Dordrecht.*

[9] Sear, R. P. (2014). Quantitaive Studies of Crystal Nucleation at Constant Supersaturation: Experimental Data and Models. *CrystEngComm, 16,* 6506-6522.

[10] Marrington, R., Small, E., Rodger, A., Dafforn, T.R., & Addinall, S. (2004). FtsZ fibre bundling is triggered by a calcium-induced conformational change in bound GTP. *J. Biol. Chem., 279*, 48821-48829.

[11] Mayer, J. A., & Amann, K. J. (2009). Assembly properties of the *Bacillus subtilis* actin, MreB. *Cell Motility and the Cytoskeleton, 66,* 109-118.

Chapter 6

Summary and Conclusions

6 Summary and Conclusions

6.1 Summary

6.1.1 Morphology of Fibres

Previous work has shown FF fibres to be heterogeneous,[1] so initial experiments were performed to quantify their size distribution. By naked eye it was apparent that the fibres were millimetres long. Images were taken of dried fibres by SEM and in water by optical microscopy. It was impossible to assess the full extent of their elongation as they extended beyond the field of view of the microscopes, yet were too small to measure accurately by eye. With an optical microscope the diameters of the largest fibres were accessible. SEM was used in order to view the width of the smaller fibres. These images showed the extent of the polydispersity of a sample of FF. Fibre diameters spanned from the nanometre to the micrometre range, demonstrating that they are indeed heterogeneous with an approximately Poisson distribution. The fibres are mostly hexagonal and hollow, however, we observed that others are closed over at the ends. This suggests that the fibres do not simply curl up from a flat sheet into a tube as suggested by Reches and Gazit, as they are not all hollow, however, it does not entirely eliminate this possibility.[2]

In order to investigate the reason for the high aspect ratio of the fibres, molecular dynamics simulations were performed on small FF assemblies based on the available crystal structure. We first tested our simulation method on an infinite crystal system of FF. This proved to be stable, demonstrating that the CHARMM27 force field was a suitable choice for FF. In order to probe independently lateral and axial growth we then chose two sets of assemblies: the first set had 4-hexagonal cylinder assemblies of varying depths, and the second set had 3-layer assemblies of differing widths.

The first set of structures simulated varied from 1 to 6 layers and all other dimensions were kept constant. The movement of the molecules in these simulations was quantified using the RMSD of the peptide atoms along the

simulation trajectory. This parameter showed that the molecules in structure 1 (Figure 4.3 (a) and (c)) completely abandoned their original layout and moved into a disordered state. However, for structures 2–6, the molecules retained their original assembly with small rearrangements at the surfaces.

Next, the lateral extension of an assembly of FF molecules was varied and the number of layers kept constant at 3 layers (Figure 4.3 (b) and (d)). A visual inspection of the simulations indicated that all of the structures had a similar level of stability. This was confirmed by the RMSDs which were similar for structures A to E.

This is consistent with the large aspect ratio observed in the fibres. The difference in increase in stability obtained in these two sets of simulations demonstrates the preference for a peptide to adsorb on to the end of a fibre rather than on to the side. The layers of molecules in the FF fibres are held together by hydrogen bonding and electrostatic interactions between the termini of the peptides. These bonds are stronger than the three-dimensional stacking that keeps the hexagonal cylinders together laterally.[1] This is in agreement with the molecules preferentially adsorbing onto the ends of a structure so they can partake in electrostatic interactions rather than the relatively weak lateral stacking. This difference results in the remarkably high aspect ratio observed in the fibres. Although atomistic simulations have previously been performed on FF, this is the first time hundreds have been used atomistically, leading to new insights into their shape.[3,4,5]

6.1.2 Assembly of the Fibres

In order to investigate the assembly of FF fibres computationally, it was necessary to employ metadynamics. It was shown that this method can successfully replicate atomistic peptides adsorbing onto an assembly of FF molecules. Two adsorption states were found with the lowest energy state 3 Å from the surface. An adsorption energy of around 10 kT was found for a FF adsorbing onto and assembly of the same molecules. This shows that it is a very stable state, and therefore indicates that the assembly is not limited by surface interactions, but instead by diffusion. The next step would be to do a similar set of simulations but look at adsorption onto the side of the nucleus rather than the

top to compare the adsorption energy. It would also be possible to perform further simulations to use rates of adsorption and desorption obtained from metadynamics runs to construct a Monte Carlo simulation to simulate FF assembly on a larger scale.

FF fibres assemble when they are cooled according to the Song method; therefore the stability of fibres is clearly a function of temperature. This is because the growth of fibres is initiated by supersaturation of the solution, and supersaturation depends on temperature, and can be increased by cooling. We investigated the temperature dependence of fibre formation and stability by spectroscopic methods as it shows a precise real-time response to any temperature variation and allows us to analyse the fibres *in situ*. This eliminates the need to remove them from solution for analysis, which has several practical disadvantages and can change their characteristics.

We chose to use flow LD as the first spectroscopic technique because it requires molecules to be aligned in order to detect them. In this case FF fibres align in Couette flow whereas dipeptides and small oligomers do not. This means that it can be used to monitor the assembly of fibres without any background peptide signal. Although there are size limitations with our LD set up due to the annular gap and circumference of the Couette cell, we were able to use it to monitor fibres shorter than ~1 mm in the early stages of assembly. The peaks observed with FF in LD are characteristic of phenylalanine and correspond to π-π^* transitions in the aromatic part of the molecule. As the signal is relatively small, it was necessary to develop some new methods to collect reliable data.

The data from these heating and cooling experiments showed that the fibres had become long enough to align in shear flow by the time the sample was cooled to 40 °C. When the solution was heated back up, the signal decreased, which shows that the fibres do disassemble upon heating. By the time it reached 70 °C the signal was absent. These experiments also showed that there is a clear difference between the formation and dissolution for these fibres. We found that the fibres do not assemble at high temperatures but once they reach a temperature where they can start to assemble they form quickly. Conversely the dissolution is a

steadier process. This suggests that a nucleation-driven assembly is taking place with nucleation happening by supersaturation, which is achieved by heating a sample to 70 °C to dissolve the peptide and then cooling it down. With FF, the supersaturation point is reached by 40 °C when a 2 mg/ml concentration is used, where we observe a sharp increase in signal. However, there is no such equivalent for the disassembly process so there is a steady decrease in signal throughout the cooling period.

Next we investigated the kinetics of assembly at a constant temperature, using LD to monitor the assembly process at 40 °C. This experiment was repeated many times and the same pattern was seen, with different quantitative results. Many possible sources of this quantitative variation were investigated, and in the process the LD method was improved for investigating assembling fibres. The improvement that contributed to the investigation into FF fibres was the development of a new Teflon-quartz capillary which allowed for thorough cleaning to take place between experiments. However, a new device was also developed which can be used on other systems to investigate the kinetics of assembly with an automated background spectrum for each measurement. This device is called a sequencer and is a separate unit which can be plugged into the instrument. This allows for each spectrum in a kinetics run to have the scattering component eliminated at the experimental stage, rather than in the data processing, which will increase its accuracy.

We know that the maximum size of fibres that can fit in the LD cell is ~1 mm so we hypothesize that the fluctuation in signal towards the end of the experiment is caused by fibres getting stuck in the Couette cell as their length becomes comparable to the size of the LD capillary, so only the first 100 or so minutes is reliable. (Once the fibres get stuck they cannot align in Couette flow and therefore their orientation will not be consistent and so the LD signal is unreliable.)

Repeat experiments showed different times to initiation. These lag times had a Poisson distribution which is indicative of nucleation-driven assembly.[6] The waiting times associated with Poisson events are exponentially distributed. Jiang and Horst [7] show that in experiments where there is a delay in detection of

nucleation, due to the crystal needing time to grow large enough to be detected, a shifted exponential distribution is seen. In the case of multiple nucleation events and multiple fibres, we see several combined exponentials which is consistent with our data.

The work of Jiang and Horst [7] shows that the distribution of lag times detected for a single crystal has a cumulative distribution function (CDF) given by Equation 5.10. This can be determined experimentally by plotting the fraction of events which have nucleated versus time. This fits well with the model of Jiang and Horst which shows that our data are consistent with this theoretical model of nucleation driven growth. The time it takes for the fibres to grow large enough to be detected (the growth time) was extracted from this fit and was found to be ~8 minutes. From microscopy data (Section 2.4.3) it is possible to see that the fibres grow at a speed of around 2 mm/hour at the start of the experiment which means they would be larger than the beams size within half an hour.

The nucleation rate was extracted from the fit and was 0.03 (0.028, 0.035) min^{-1} (95 % confidence interval). This is too low to account for all the fibres present in a sample at the end of an experiment, but is consistent with secondary nucleation taking place. Secondary nucleation occurs when a fibre breaks and the pieces seed the growth of new fibres. This is common in the early stages of crystal growth and would dramatically increase the number of fibres present, as each broken fibre can spawn many new ones. Further evidence for secondary nucleation was observed with the SEM, where branched fibres were found. The branching fibres had started to break off, and it is likely that if they were still in solution they would have done so completely and partaken in secondary nucleation.

The LD experiments show that FF ultimately assembled into structures with high aspect ratios. However, they miss the initial assembly because the low aspect ratio oligomers do not flow orient. Therefore, once it was established that fibres did form in the spectroscopy experiments, we turned to right angle light scattering (RALS) which allowed the whole assembly process to be detected, as even small aggregates can be revealed with this technique. The time-dependent RALS signal for the self-assembly of fibres showed that the assembly was very

fast (but variable from run to run) then progressively slowed down. The similar shapes but different initial slopes of the repeats of this experiment support the nucleation–driven assembly hypothesis.

Using RALS, we did not expect to see a lag period as we did with the LD experiments because RALS detects small aggregates which are too short for LD. Instead, if the above discussion is correct we expect to see a variation in the gradient of the curve for the assembly, with different experiments reaching the same intensity at different times. The variation in the times should be similar to the variation in lag time seen in the LD experiments, which is indeed the case.

After ~5 hours the growth became consistent with a first order reaction, prior to that it was quicker. This is in accord with initial primary and then secondary nucleation taking place until assembly rather than nucleation dominates. The total assembly process continued for 24 hours. The first order growth is consistent with a comparatively small number of fibres growing by addition of single peptides rather than continuous nucleation and new fibre growth.

LD and RALS are techniques that average over the whole sample. In order to see what was happening at a single fibre level, we used a widefield optical microscope to observe individual fibres growing. The sample was in solution and held at 40 °C under conditions similar to the spectroscopy experiments to allow for *in situ* analysis of the fibres assembly. It was possible to detect fibres from around 5 minutes into the experiment, where the start is defined as the time that the fibres were cooled to 40 °C. It was not possible to measure the full length of fibres as they were too long for the field of view of the microscope, however, from a series of images it was possible to measure the speed of growth. The product of the speed of growth and the time point in the experiment can be used to estimate the length of fibres, which can be directly compared with the first few hours of the RALS data. The RALS data correlate well with the estimate of the fibre lengths measured from the optical microscope, suggesting that the main contribution to the RALS signal is the length of the fibres (at least once they are long enough to be viewed under the microscope). This means that the RALS data show that the lengths of individual fibres are growing in accordance with a first order reaction.

It was evident that the signal increase was very fast at the start and then slowed down over time. A reason for this could be that the available peptides are depleted as more fibres are made and the growth becomes limited by the peptide concentration. In order to investigate this we looked at the concentration of available peptides in the solution during assembly using absorbance spectroscopy. It is apparent that the FF concentration used in these experiments remained high so it is not the case that concentration limits fibre growth.

Microscopy also allowed for nucleation sites to be seen which had several fibres growing radially outwards from them. This supports the linear dichroism data which suggests nucleation driven growth is taking place in the self-assembly of FF fibres.

6.2 Conclusions

The aim of this work was to better understand the growth of FF fibres. This is important for the understanding of the self-assembly of the amyloid-β peptide *in vivo*. It can also contribute to the ability to control the assembly and therefore the size of the fibres which can be used for a variety of biological and technological applications. A range of complementary experiments and calculations have been performed to that end. SEM images show the hexagonal, and sometimes hollow nature of FF fibres with a large range of widths that are present in a single sample. Fibres range from hundreds of nanometres in diameter to tens of microns and their length can go up to millimetres. The SEM images also illustrate closed over ends on some of the fibres which suggests that they do not first assemble into a sheet and then curl up into a tube, as has previously been hypothesized.[2]

The SEM images demonstrated the high aspect ratio of the fibres, and the MD simulations gave an insight into the reason for this. MD showed that the FF assemblies become much more stable if molecules are added to the top than if they are added to the sides. This shows that the interactions between layers of the fibres are much more important in contributing to a structure's stability than the lateral interactions. However, the lateral interactions are stabilising so if a 'short fat' structure grows early in the process, it continues to elongate resulting in the final width distribution observed, with any one fibre of constant width. Thus, the

difference in increase in stability obtained in these two types of MD experiments is consistent both with the range of widths and with the high aspect ratios of the fibres observed. It was also possible to extract and adsorption energy for a peptide on the surface of a nucleus of FF molecules, which showed a strong binding, and therefore indicated that diffusion limited growth takes place.

It was possible to study the mechanism of growth of the fibres using spectroscopy and microscopy. LD experiments showed that 40 °C is an important temperature in the onset of fibre formation. It was also demonstrated that, in contrast to previous work, the fibres dissolved as the solution was heated back up to 70 °C.[8] The difference between assembly and disassembly as a function of temperature is consistent with nucleation driven growth as is the LD kinetic data at 40 °C which showed a distribution of lag times. This was supported by optical microscopy which allowed direct visualisation of fibres growing from nucleation points, and RALS, which again showed variation. This is the first time to our knowledge that the kinetics of the fibres has been quantitatively measured and the mechanism determined.

The kinetics of the process is complex initially, and involves the formation of nuclei upon supersaturation of the reaction mixture. We hypothesize that early fibres break up and seed further fibres to grow. However, later the RALS becomes first order, which is consistent with linear growth of the fibres. This was shown by the microscopy data which measured the speed of growth of the fibre lengths, to show that individual fibres grow very quickly at first and then slow down dramatically within the first few hours. It is also evident from the microscopy that the width of a fibre does not change quickly during an experiment, which again is consistent with an initial complex lateral and elongation nucleation process to establish the starting point for the linear growth phase. The growth then slows down as it is limited by diffusion of the FF molecules.

It has been possible to extract meaningful data from a heterogeneous system with a low signal, and to quantitatively characterise the growth of FF fibres, using a combination of theoretical, spectroscopic and microscopy techniques. During this process several improvements have been made to the LD method. A new

capillary was designed to allow for thorough cleaning, which has now been used for several other systems within the biophysical chemistry laboratory, such as DNA and FtsZ polymerisation. A new sequencer was built which switches the spinning of the LD capillary on and off so that an automatic background spectrum can be measured for every measurement. These improvements to the LD method can be coupled with the molecular and metadynamics methods shown in this work, and electron and optical microscopy to investigate the assembly of many other rod-like systems, which cannot always be studied with standard laboratory techniques.

References

[1] Görbitz, C.H. (2006). The structure of nanotubes formed by diphenylalanine, the core recognition motif of Alzheimer's β-amyloid polypeptide. *Chem. Commun., 22,* 2332-2334.

[2] Reches, M. & Gazit, E. (2004). Formation of Closed-Cage Nanostructures by Self-Assembly of Aromatic Dipeptides. *Nanoletters, 4,* 581-585.

[3] Jeon, J., Mills, C. E. & Shell, M. S. (2013). Molecular Insights in Diphenylalanine Assembly: All-Atom Simulations of Oligomerization. *J. Phys. Chem. B, 117,* 3935-3943.

[4] Tamamis, P. *et al.* (2009). Self-Assembly of Phenylalanine Oligopeptides: Insights from Experiments and Simulations. *Biophysical Journal, 96.* 5020-5029

[5] Rissanou, A. N, Georgilis, E., Kasotakis, E., Mitraki, A. & Harmandaris, V. (2013). Effect of Solvent on the Self-Assembly of Dialanine and Diphenylalanine Peptides. *J. Phys. Chem. B, 117(5),* 3962-3975.

[6] Barlow, T.W., & Haymet, A.D.J. (1994) ALTA: An automated lag-time apparatus for studying the nucleation of supercooled liquids. *Review of Scientific Instruments, 66*, 2996.

[7] Jiang, S., & Horst, J. H. (2011). Crystal nucleation rates from probability distributions of induction times. *Crystal Growth and Design, 11*, 256-261.

[8] Sedman, V. L., Adler-Abramovich, L., Allen, S., Gazit, E. & Tendler, S. J. B. (2006). Direct Observation of the Release of Phenylalanine from Diphenylalanine Nanotubes. *J. Am. Chem. Soc., 128,* 6903-6908.